WA-RD 91.1

Diagnosis and Prediction of Precipitation in Regions of Complex Terrain

Final Report

June 1986

Washington State Department of Transportation
Planning, Research and Public Transportation Division

WASHINGTON STATE DEPARTMENT OF TRANSPORTATION

TECHNICAL REPORT STANDARD TITLE PAGE

1 REPORT NO	2. GOVERNMENT ACCESSION NO	3 RECIPIENT'S CATALOG NO.
WA-RD-91.1		

4 TITLE AND SUBTITLE	5 REPORT DATE
DIAGNOSIS AND PREDICTION OF PRECIPITATION IN REGIONS OF COMPLEX TERRAIN	June 1986
	6 PERFORMING ORGANIZATION CODE
7 AUTHOR(S)	8. PERFORMING ORGANIZATION REPORT NO
Pamela Speers, Clifford F. Mass	
9 PERFORMING ORGANIZATION NAME AND ADDRESS University of Washington Department of Atmospheris Sciences Seattle, WA 98195	10 WORK UNIT NO.
	11. CONTRACT OR GRANT NO Y-2811, Task 8
12 SPONSORING AGENCY NAME AND ADDRESS Washington State Department of Transportation Transportation Building Olympia, Wa 98504	13 TYPE OF REPORT AN PERIOD COVERED Final report
	14. SPONSORING AGENCY CODE

15. SUPPLEMENTARY NOTES

Conducted in cooperation with U.S. Department of Transportation, Federal Highway Administration

16 ABSTRACT

This research has attempted to determine the distribution of precipitation in the complex terrain of Washington State. The first part of this report examines the precipitation distribution for various large scale wind directions. It is found that there are meaningful shifts in the precipitation pattern as the large scale wind changes direction and that knowledge of this behavior can be useful for operational applications. The second section presents a simple numerical model of precipitation in complex terrain. Although the results are not perfect by any means, they can usefully indicate the variation of precipitation in the mountains of our area. However, such a model requires at least a minicomputer to run it.

17 KEY WORDS	18 DISTRIBUTION STATEMENT

19. SECURITY CLASSIF (of this report)	20. SECURITY CLASSIF. (of this page)	21 NO. OF PAGES	22. PRICE
Unclassified	Unclassified	166	

DOT FORM 310-022 (11 86) -1216 S 3

Diagnosis and Prediction of Precipitation in Regions of Complex Terrain

by
Pamela Speers and Clifford F. Mass

Washington State Department of Transportation Center
Department of Atmospheric Sciences
University of Washington
Seattle, Washington

WSDOT Technical Monitor:
G. Scott Rutherford
University of Washington

Final Report
Research Project Y-2811
Task 8

Prepared for
Washington State Department of Transportation
and in cooperation with
U.S. Department of Transportation
Federal Highway Administration

June 1986

TABLE OF CONTENTS

TABLE OF CONTENTS (Continued)

LIST OF FIGURES

LIST OF FIGURES (Continued)

LIST OF FIGURES (Continued)

LIST OF FIGURES (Continued)

LIST OF TABLES

EXECUTIVE SUMMARY

This project analyzed a series of mean hourly precipitation pattern maps that were produced from hourly precipitation data for the months November through March of 1977 through 1981 for eight Hoquiam surface wind directions and separately for eight Quillayute 850 millibarn (mb) wind directions. Precipitation pattern maps were also produced for Hoquiam surface winds greater than or equal to 15 knots (kts) and for Quillayute 850 mb winds greater than or equal to 25 kts. The analyses produced several general conclusions.

1. Most precipitation occurs during southerly, southwesterly, and westerly winds at the surface and 850 mb level.
2. The Olympic Mountains receive more precipitation than the Cascade Mountains for surface and 850 mb southerly and southwesterly winds, whereas the Cascades receive more precipitation than the Olympics for westerly and northwesterly wind directions.
3. The magnitude of precipitation for Hoquiam surface winds greater than or equal to 15 kts and Quillayute 850 mb winds greater than or equal to 25 kts is generally 1.5 to three times higher

than for precipitation rates averaged for all wind speeds.

4. The analysis of precipitation sites on the Olympic Peninsula indicates that the rain shadow in the lee of the Olympics moves in response to shifts in wind direction. Mount Rainier and Mount Baker also produce a rain shadow in their lee.

5. The Skykomish/Stevens Pass analysis for southwesterly to northwesterly winds indicates that more precipitation falls over the foothills near Skykomish than at Stevens Pass at the Cascade Crest.

An orographic precipitation model addition to the Mass and Dempsey (1985) wind model was developed in Chapter 2. The model employed a simple precipitation parameterization scheme with condensation proportional to vertical velocity. Vertical velocity was composed of three elements: (1) the vertical component of the surface winds from the Mass-Dempsey model, (2) convergence vertical velocity, again from the wind model, and (3) the vertical velocity from a separate large scale wind field imposed on the terrain. The precipitation parameterization assumed a constant precipitation efficiency with the remaining condensate carried to the next grid point downstream. For southwesterly to northwesterly wind cases, the saturated mixing ratio was

assumed to decrease linearly by 30 percent from the coast to the eastern boundary of the domain.

Two case studies were presented. The model duplicated the precipitation field for the November 7th southwesterly flow fairly well; however, the model underpredicted precipitation on the south and southeast slopes of the Olympic Mountains. The Mass-Dempsey model surface winds are deflected around the Olympics in response to adiabatic cooling and the associated pressure increase as the airflow initially moves upslope. As a result, there is very little slope induced vertical velocity contribution from the surface winds. Additionally, divergence of the surface winds on the windward slopes results in a negative vertical velocity component. Upslope winds can be increased on the south and southeast slopes of the Olympics by decreasing the stability of the lapse rate used to initialize the wind model; however, this solution also decreases channeling and blocking, which are positive features of the model. Elsewhere in Washington State, the model adequately duplicated the observed precipitation. For nine sites in widely varying terrain, the model accurately predicted precipitation at six sites. Model precipitation was 50 percent too high for two sites and 15 percent too low for one site.

The model qualitatively reproduced the November 14th convergence precipitation that extended from Puget Sound to the Cascades as well as the precipitation areas near Mount

Rainier, Mount St. Helens and Mount Hood; however, the model indicated more areas with precipitation than did the observations and the model's position of the convergence precipitation was north of the observed position. A more important problem with the Mass-Dempsey model surface wind field occurred to the northeast of the Olympic Mountains and Vancouver Island where the model produced very strong downslope winds that converged with winds channeled through the Strain of Juan de Fuca and through Georgia Strait. There is not an easy way to decrease the strong downslope winds in these areas while maintaining the lines of convergence across Puget Sound and southern Georgia Strait. The convergence in Puget Sound is influenced by a three-dimensional eddy in the lee of the Olympics that the wind model is unable to resolve.

A model run for a 'typical' northwesterly flow was also presented. The input parameters were determined by averaging the specific parameters from several northwest wind cases during the winter of 1985-86. The precipitation patterns were qualitatively similar to the precipitation for the November 14th convergence zone; however, the convergence precipitation across Puget Sound and in southern Georgia Strait was heavier and more sharply defined for the general case.

In conclusion, the precipitation model does remarkably well given the simple precipitation parameterization that

is used. Most of the significant deviations from observations can be attributed to errors with the wind model. The current version of the model may be a useful predictive tool for relatively two dimensional flow patterns; however, the model is not expected to do well in cases with significant three-dimensional structure because it cannot resolve three-dimensional variations of pressure and wind or moisture. The use of a three-dimensional wind model might significantly improve model results; however, three-dimensional wind models are currently too expensive to run on an operational basis. This research suggests that it may be possible to adequately model precipitation in complex terrain with simple precipitation parameterizations if a suitable wind model is employed. As computers become faster, it may be feasible to base a simple precipitation model on a three-dimensional wind model.

INTRODUCTION

Determining the variation of precipitation in the mountains of western Washington State is an important problem for professionals responsible for mountain weather and avalanche forecasts, and for those who must apply site-specific precipitation forecasts to ski areas, highways, or backcountry regions. At present, forecasts of precipitation amounts in the Washington Cascades and Olympics are based on forecasters' experience in estimating the amount of precipitation that a synoptic event will produce. Computer generated quantitative precipitation forecasts are available twice daily for Seattle from the LFM(Limited Fine Mesh) and NGM(Nested grid) models; however, these forecast amounts are not easily applied to mountain locations because mesoscale complex terrain, which the models can't resolve, results in widely varying precipitation amounts. Furthermore, even on a synoptic scale the model precipitation forecasts demonstrate only moderate skill.

The objective of this project is to document the precipitation patterns that are produced by different large scale wind directions and to improve orographic pre.ipitation forecasts. Two separate methods are used

in the study. Chapter 1 presents and analyzes a series of precipitation pattern maps for western Washington State which are based on hourly precipitation records from five winters. These maps correlate precipitation with large scale wind direction as represented by Hoquiam surface wind direction, and separately by Quillayute 850 mb wind direction. Chapter 2 presents a simple orographic precipitation model based on a windflow model developed at the University of Washington (Mass and Dempsey, 1985).

Chapter 1. ANALYSIS OF PRECIPITATION PATTERNS FOR WESTERN WASHINGTON STATE

1.1. GEOGRAPHY

Western Washington (Fig. 1.1) is characterized by two rugged mountain ranges, the Coast Range and the Cascade Mountains, which are separated by Puget Sound. The most pronounced portion of the Coast Range, the Olympic Mountains, are located 35 miles east of the Pacific coast and extend above 7000 feet. The Strait of Juan de Fuca lies to the north of the Olympic Peninsula, and the Chehalis Gap is found to the south. The Cascades, located approximately 145 miles from the Pacific Ocean, run from the Canadian border south into Oregon. A chain of volcanic peaks, with elevations ranging from 7000 feet to over 14000 feet (Mt Rainier), run in a N-S line on the west side of the Cascade crest which ranges from 4000 feet to 9000 feet. There are several mountain passes (e.g. Snoqualmie Pass, Stevens Pass) crossing the Cascade Range in Washington. East of the Cascade Mountains lies a plateau that is about 3000 feet in elevation.

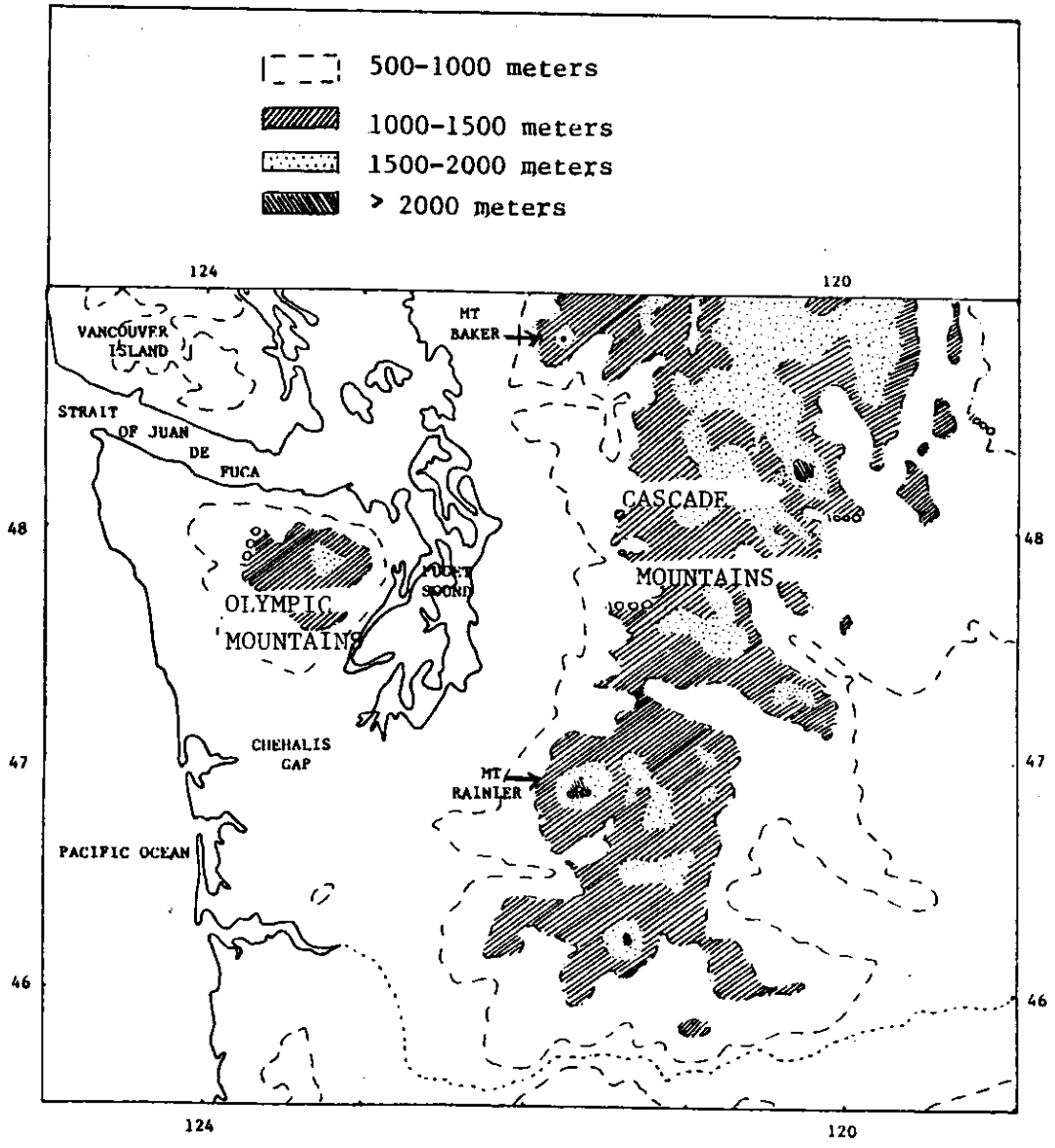

Figure 1.1 Map of western Washington with major geographic features.

1.2. LITERATURE REVIEW

Numerous authors have investigated the influence of topography on precipitation. For example, Spreen (1947) attributed 88% of the variance of the distribution of winter orographic precipitation to station elevation and orientation, maximum slope of the land within a five mile radius of the station and the exposure of the station to incoming storms. Bergeron (1965) found that hills 50 meters above the surrounding terrain could increase short term precipitation (over 12 hours) 2-3 times. Orographic lifting of 50 meters could not alone account for such a marked increase in precipitation. Instead, he suggested that orographic lifting produced cap (feeder) clouds over the hills. Rain from a frontal system (seeder clouds) falling through the cap clouds collect cloud droplets, which in turn enhance precipitation.

There have been a considerable number of studies of the effects of orography on precipitation in the Pacific Northwest. Schermerhorn (1967) investigated the influence of topography and latitude on precipitation in western Washington state. He considered only southwest flow into the region since most precipitation in Washington State is associated with flow approaching from this direction.

Schermerhorn used three terrain indices; station elevation, a general elevation term involving the elevation of terrain up to 4 miles away in the SW quadrant and up to 10 miles away in the NE quadrant from the station, and the elevation of upwind terrain barriers. He also used a factor for latitude which assumes a decreasing north-south gradient of precipitation from the Canadian border to California of 8% per 1 degree of latitude. He found that most of the variation in precipitation can be explained by the three terrain indices.

Storr and Ferguson (1972) analyzed precipitation data gathered from ten instrument sites situated on two parallel lines across the Beaufort Range, which runs NW to SE on Vancouver Island. They concluded that during May to September, when the mean 850 mb winds are from the WSW, the relative decrease in precipitation on the leeward slope was larger than the increase in precipitation on the windward slope. The variation in precipitation between adjacent sites at the same elevation pointed to the significance of local variations in slope, aspect and site exposure. A second precipitation network in the Okanogan Basin in British Columbia provided data for a regression analysis of 6 independent physiographic parameters to determine the

correlation between precipitation and the individual parameters. The highest correlations occurred with station elevation and the distance along the 850 mb level wind flow direction from the Pacific Coast Range to the precipitation measurement site.

Rasmussen and Tangborn (1976) found a very poor correlation between precipitation and station altitude in the north Cascades of Washington State. There was an improved correlation when the topographic mean altitude for a 200 square kilometer area centered at the measurement site was used. They noted that the wettest area within their study region lay in the Sultan River drainage in the foothills of the Cascades east of the city of Everett. They also noted that both the Stevens Pass and Snoqualmie Pass gauges measured too little precipitation to account for the runoff from these areas. This may be explained by inefficient gauge catchment during strong winds when some snow blows across the gauge instead of falling vertically into it.

The Bonneville Power Administration set up the Portland Oregon Mesoscale Precipitation (POMP) Network in 1969 with approximately 100 volunteer observers recording monthly precipitation totals. In 1981, the network began taking daily precipitation reports. Wantz, Feris, and Larsen (1983) summarized the topographic influence on

precipitation within the 2500 square miles covered by the POMP network. They noted that topography does not appear to influence the precipitation distribution for pre-warm frontal synoptic conditions, when drainage down the Columbia River forms a dome of cold air over the network area.

Mark Albright (personal communication) at the University of Washington has recently set up a rain gauge network in the Seattle area with volunteer observers taking daily precipitation measurements. To date, his emphasis has been in determining monthly precipitation patterns, and on the precipitation distribution during Puget Sound convergence zone events. He has found that the convergence zone rain maximum is in a very narrow zone.

The position of maximum precipitation relative to the crests of mountains is discussed in several papers. Sarker (1967) found that the maximum rainfall over the western Ghats occured 10-20 km upwind of mountain crests. Peck and Brown (1962) found no evidence that precipitation decreased at higher elevations in the Intermountain West. They suggested that a decrease in precipitation at higher elevations found by other researchers may result from poor gauge catchment during strong winds.

Several papers relate precipitation distribution to synoptic weather conditions or to wind direction. Elliott and Shaffer (1962) found that the orographic enhancement of precipitation in the San Gabriel Mountains in California depends on the stability of the atmosphere. During very stable conditions, or when the wind blew parallel to the mountain range, the mountains received less precipitation than the plains. In contrast, during unstable atmospheric conditions, orographic lifting was enhanced, and the mountains received more precipitation than the coastal plains. Wilson and Atwater (1972) analyzed precipitation data gathered over a 2 year period from 136 stations in Connecticut. As would be expected, the maximum precipitation fell on the windward side of hills; however, during many storms the maximum precipitation occured over the initial windward rise of the hills and not along the hill crests. They found that in areas of minimal relief (75-150 meters in elevation), total rainfall could vary as much as 20-30% for stations 8 or more km apart, with the precipitation patterns repeated from storm to storm. Dunn (1982) related winter precipitation at nine sites in the Wasatch Mountains of northern Utah to the 850 mb and 700 mb level wind directions measured from the Salt Lake City radiosonde. He concluded that precipitation maxima at all nine sites

occured when orographic lifting and wind flow channeling were maximum.

1.3. DATA AND METHODS

Although precipitation patterns can be determined by using historical precipitation data averaged over months or seasons, this information lends little insight into the complex precipitation patterns that result from different synoptic weather conditions. In this study, precipitation is related to regional flow patterns, since orographic precipitation at any given location is related to the direction and speed of the airflow approaching the topography.

Two independent approaches have been taken to represent the large scale airflow. In the first, the large scale wind is represented by the surface wind along the Pacific coast, where airflow is relatively unaffected by the complex terrain of the region. In the second, the 850 mb wind direction from the Quillayute, Washington radiosonde sounding is used to represent the large scale flow.

Hoquiam, an hourly reporting station on the coast, has been found to be a representative coastal wind station. Hourly wind records for Hoquiam for December through March of 1977 through 1981 were grouped into eight wind direction categories (see Table 1.1).

TABLE 1.1 Cardinal names and corresponding numerical wind direction groupings used in Chapter 1.

DIRECTION	DEGREES
NE	025-064
E	065-114
SE	115-154
S	155-204
SW	205-244
W	245-294
NW	295-334
N	335-024

Composite precipitation pattern maps were produced for each of the eight wind direction groups by calculating mean precipitation rates for the hours when the wind was in each direction category.

There are potential problems with correlating orographic precipitation with coastal surface wind observations. Although Hoquiam winds generally are representative of the large scale surface flow approaching the coast, they may differ from the mesoscale low level flow in the Washington Cascades and Olympics. Figure 1.2 compares Stevens Pass and Hoquiam surface wind directions for two weeks in February 1984. In general, wind directions at the two sites are similar. A problem may arise when precipitation at high elevation sites is correlated with Hoquiam surface wind direction. At high elevations, where winds become increasingly geostrophic, the wind direction generally follows the 850 mb or 700 mb flow. The direction and speed with which this air approaches the mountains may not closely correspond to Hoquiam's surface winds, which often are highly ageostrophic. However, in western Washington, where precipitation forecasting is generally for low elevation sites, the use of Hoquiam surface wind direction may be an adequate measure.

The second method for representing the large scale

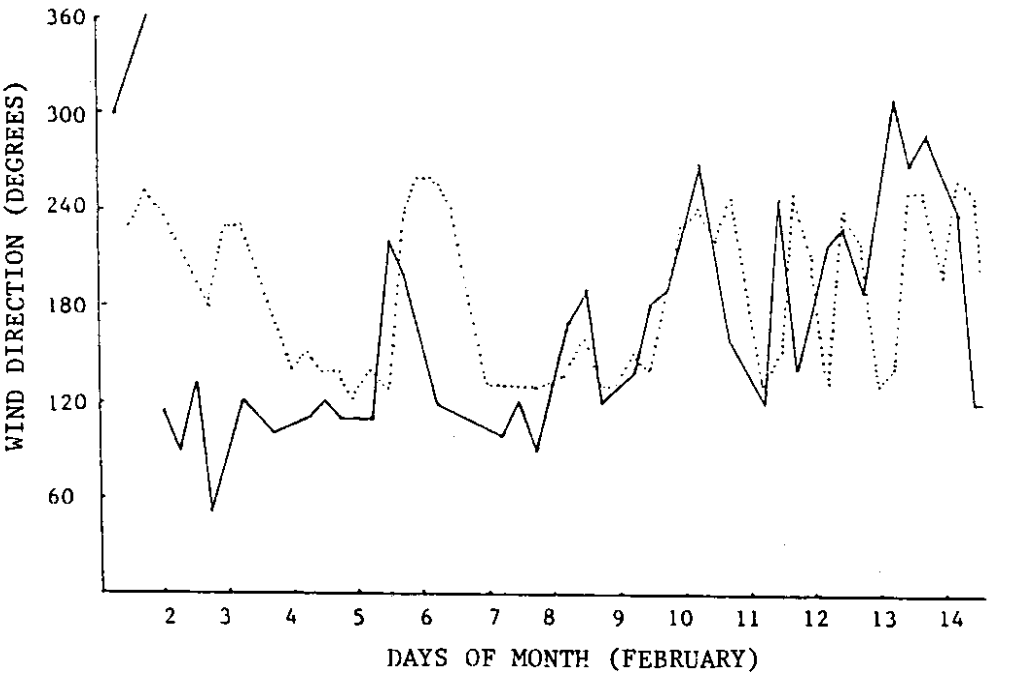

Figure 1.2 Time series of surface wind directions for Hoquiam (—) and Stevens Pass (·····) for a two week period in February 1984.

airflow uses the 850 mb level winds from the Quillayute, Washington radiosonde. Quillayute, located 12 miles inland from Washington's Pacific coast, is the most representative upper air site available for free air winds approaching Washington from the ocean. The 850 mb winds were chosen because this pressure level is the lowest mandatory wind measurement and also corresponds to the elevation of many of the avalanche starting zones that affect highways and ski areas.

Twice daily 850 mb level winds for Quillayute for the months December through March of 1977 through 1981 were grouped into the eight wind direction categories delineated in Table 1. In this study it is assumed that 850 mb level winds change direction slowly, as compared to surface wind direction. Precipitation data for the time period from 3 hours before to 3 hours after a sounding was used. If consecutive sounding measurements fell into the same wind direction category, precipitation data for the entire period between soundings was also used. Precipitation pattern maps were produced by averaging the precipitation rates for each of the eight wind direction categories.

The empirical study of orographic precipitation in western Washington is complicated by several factors. First, there are a limited number of precipitation gauges

at higher elevations in the Washington Cascade and Olympic Mountains. Second, at locations with more than one precipitation gauge (for example, Stevens Pass), a wide range of water equivalency values have been measured (Marriott and Moore, 1984; Krimmel and Tangborn, unpublished). This range may result from variations produced by local topography, poor gauge placement, or differences inherent in the use of a variety of measuring devices or methods. The effects of local topography on precipitation measurements are difficult to quantify. Small scale convergence, channeling, or blocking produce precipitation variations within short distances. Additionally, precipitation catchment efficiency may vary with wind direction and speed, depending on gauge placement. In this study we will not directly address these two problems. This study uses 69 Fisher-Porter weighing bucket gauges maintained by the National Weather Service at elevations from sea level up to 4150 feet. The locations of the gauges are shown in Figure A.1. (refer to Appendix A). Table A.1. also gives the names and elevations of the gauge sites. Undoubtedly, a denser network of gauges would produce more detailed precipitation patterns and improve the quality of this study.

1.4. RESULTS

Precipitation pattern maps corresponding to the eight wind direction groupings for Hoquiam surface winds, and separately, for the eight wind direction groupings for Quillayute 850 mb winds, are presented in Figures 1.3 and 1.4 respectively. Detailed copies of the precipitation pattern maps showing the precipitation rates at individual gauge sites are presented in Appendix B. Precipitation quantities in Figures 1.3 and 1.4 are given in inches/hour, with a contour interval of .01 inches/hour indicated by solid lines. On maps with light precipitation, .005 inch/hour and .002 inch/hour contour lines are also included.

A general discussion of the precipitation patterns in Figures 1.3 and 1.4 follows. Refer to Appendix A for the locations of sites referred to in this discussion. In Figure 1.3, the precipitation pattern map for NE winds exhibits very light precipitation throughout western Washington. The areas receiving the heaviest precipitation include the Olympic Mountains, the Coastal Mountains in SW Washington, the Mt St. Helens and Mt Rainier areas, and Snoqualmie Pass. The E wind map also demonstrates very light precipitation, with little

HOQUIAM SURFACE WIND PRECIPITATION PATTERN MAPS

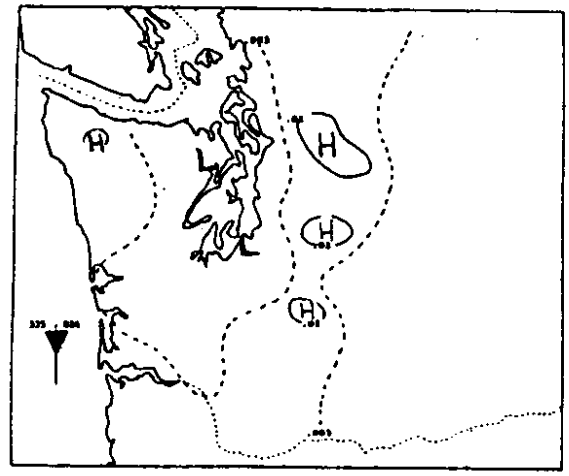

NORTH
1205 HOURS

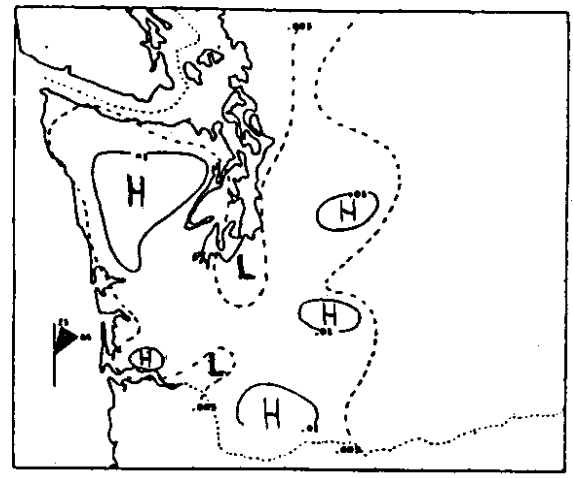

NORTHEAST
828 HOURS

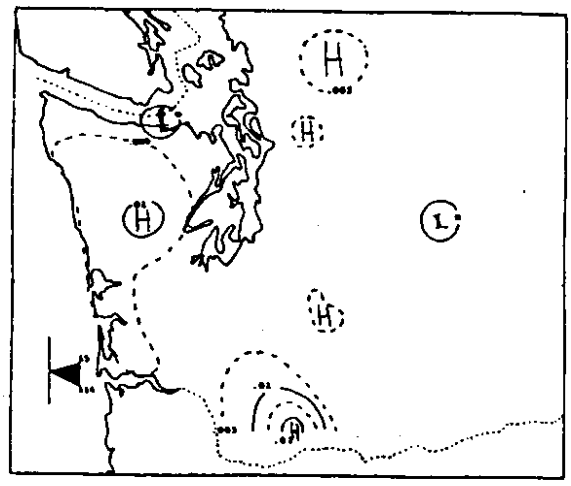

EAST
1384 HOURS

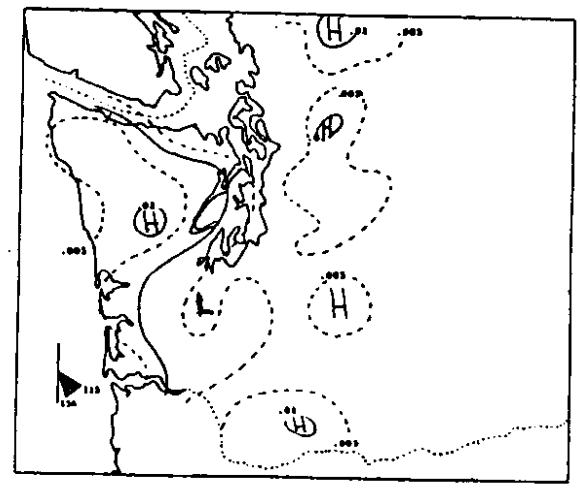

SOUTHEAST
1390 HOURS

Figure 1.3 Mean hourly precipitation pattern maps for Hoquiam surface winds. The wind direction is shown by the shaded region of the compass and is indicated below each map. The solid line contour interval is .01 inches of water equivalent per hour. Dashed line contours are drawn for .005 inch intervals.

HOQUIAM SURFACE WIND PRECIPITATION PATTERN MAPS

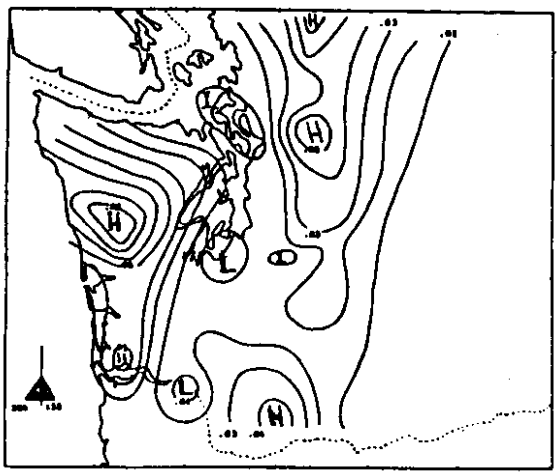

SOUTH
350 HOURS

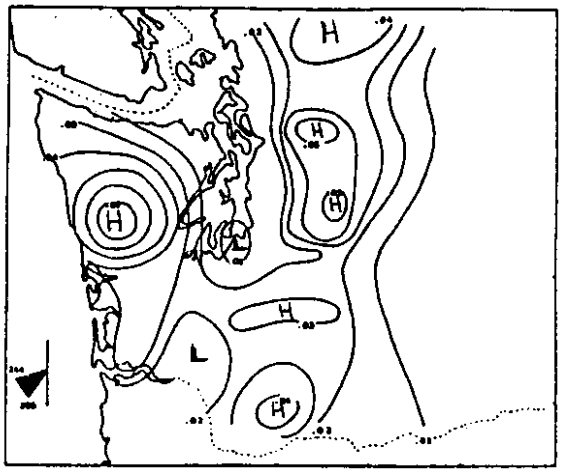

SOUTHWEST
1207 HOURS

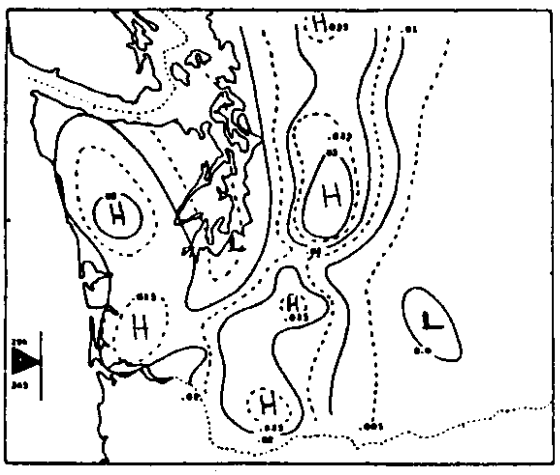

WEST
1455 HOURS

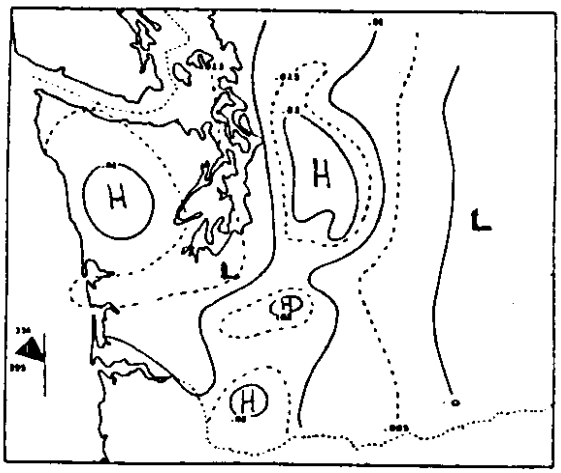

NORTHWEST
859 HOURS

Figure 1.3 (continued)

QUILLAYUTE 850 MB WIND PRECIPITATION PATTERN MAPS

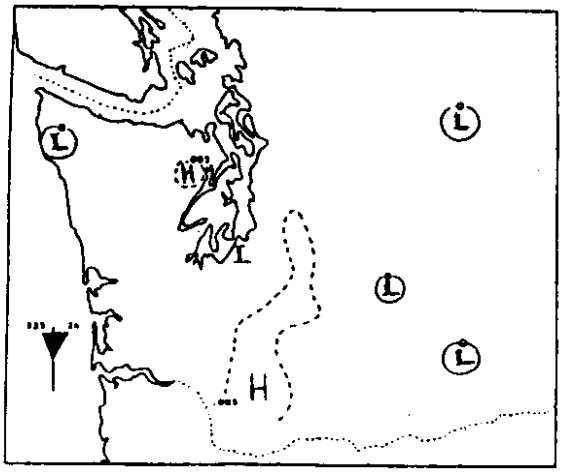

NORTH
664 HOURS

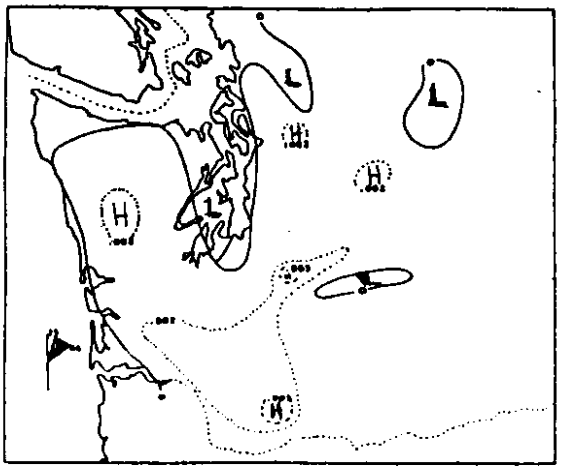

NORTHEAST
230 HOURS

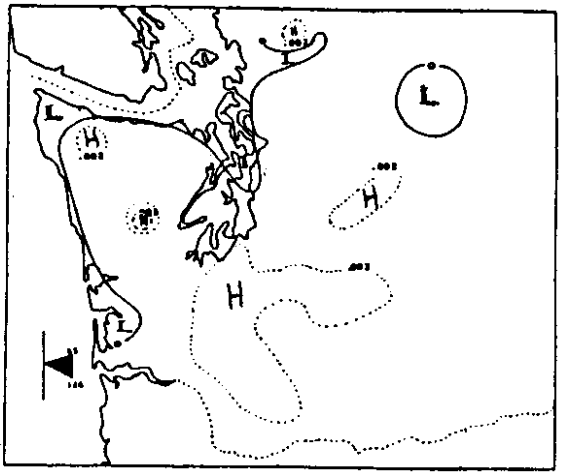

EAST
355 HOURS

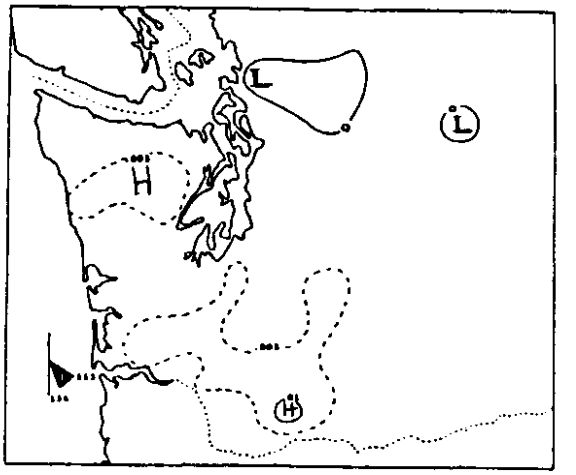

SOUTHEAST
350 HOURS

Figure 1.4 Mean hourly precipitation pattern maps for Quillayute 850 mb winds. The wind direction is shown by the shaded region of the compass and is indicated below each map. The solid line contour interval is .01 inches of water equivalent per hour. Dashed line contours are drawn for .005 inch intervals. Dotted line contours indicate .002 inch intervals.

QUILLAYUTE 850 MB WIND PRECIPITATION PATTERN MAPS

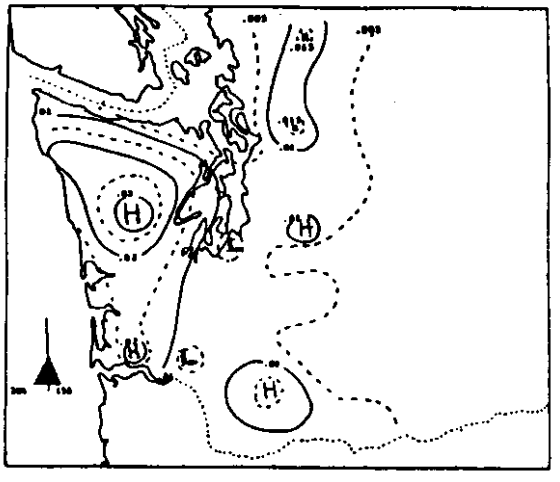

SOUTH
3274 HOURS

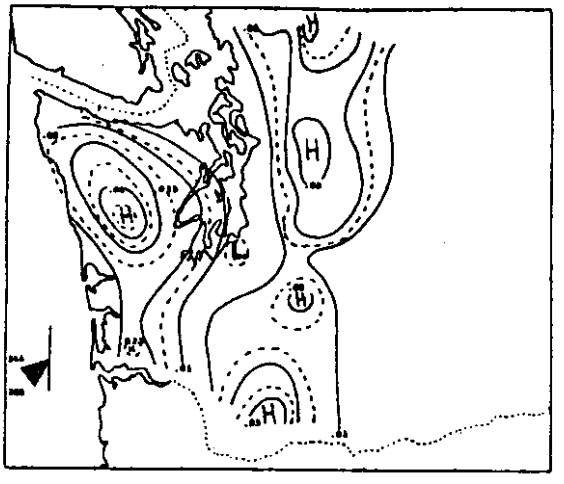

SOUTHWEST
1577 HOURS

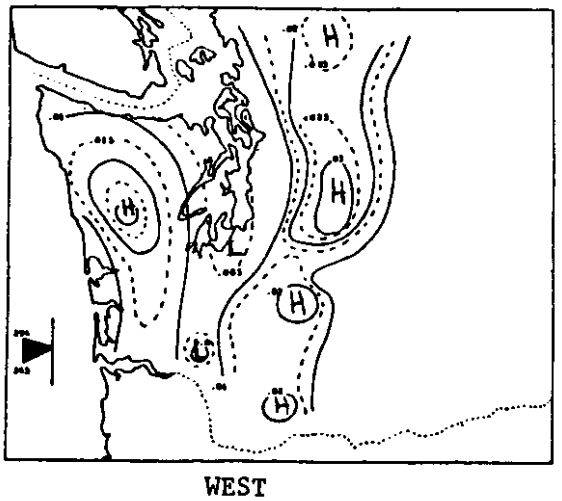

WEST
1677 HOURS

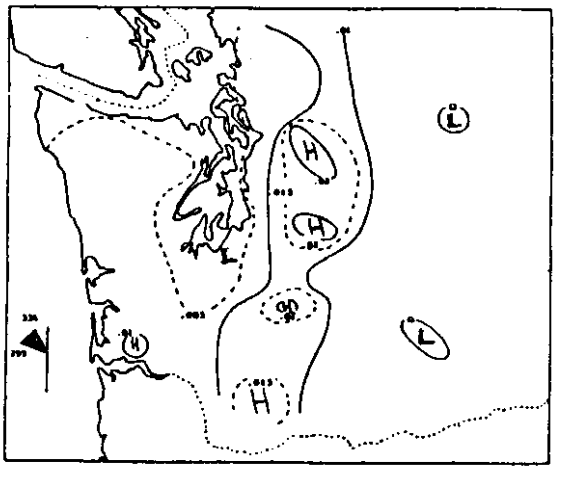

NORTHWEST
751 HOURS

Figure 1.4 (continued)

definition to the precipitation pattern in the Washington Cascades from Mt Rainier north. The areas of heaviest precipitation are centered at Carson Fish Hatchery in the southern Washington Cascades, and at Camp Grisdale in the Olympics. On the SE wind map, although precipitation continues to be light, the areas with heaviest precipitation extend from the Olympic Mountains south along the coast to Oregon, and generally along the Cascades from Mt Baker to Mt St. Helens. On the S wind map, precipitation rates increase significantly, with well defined areas of heavy precipitation on the south side of the Olympics, at Mt Baker, Silverton and Verlot, and at Carson Fish Hatchery. Areas of minimum precipitation occur in northern and southern Puget Sound and near Longview. High precipitation rates are also observed on the SW wind map. The Olympics continue to exhibit heavier precipitation than the Cascades; however, the distribution of precipitation in the Olympics has shifted, with Quinalt Ranger Station receiving the heaviest precipitation. In the Cascades, the precipitation maximum near Mt Baker extends east to Diablo Dam. Silverton, Verlot, and Mt St. Helens continue to experience heavy precipitation; however, on the SW wind map a new area of heavy precipitation extends from Skykomish south to Snoqualmie Pass. On the W wind map,

the intensity of precipitation has decreased with well defined areas of maximum precipitation in the Olympics, from Skykomish south to Stampede Pass, and around Mt Baker, Mt Rainier and Mt St. Helens. A precipitation minimum extends southeast from Port Angeles thru western Puget Sound. On the NW wind map, precipitation rates continue to decrease, with the heaviest precipitation in a broad region of the Cascades from Verlot south to Stampede Pass, Mt Rainier and Mt St. Helens. A lesser precipitation maximum exists over the Olympics. A rainshadow, suggested by a precipitation minimum, extends along the east and south sides of the Olympics. The N wind map exhibits very light precipitation, with relatively heavy precipitation on the NW side of the Olympics and in pockets along the Cascades centered at Mt Rainier, Snoqualmie Pass, and from Verlot SE to Stevens Pass.

The precipitation pattern maps based on 850 mb winds (Fig. 1.4) are similar to the corresponding surface maps (Fig. 1.3) with the areas of heaviest precipitation generally located over the southern Olympic Mountains, Mt Baker, the central Cascade Mountains from Silverton and Verlot south to Stampede Pass, and Mt Rainier and Mt St. Helens. Precipitation minima exist from Puget Sound south to Longview and east of the Cascade Mountains. The

Olympic Mountains receive 1.5 to 2 times more precipitation than the Cascades for S and SW 850 mb winds, while during W and NW 850 mb winds, the Cascades receive up to twice as much precipitation as the Olympic Mountains. The S, SW, W and NW 850 mb precipitation pattern maps present the most interesting contrast to the surface wind maps. The surface S and SW wind maps have precipitation that is 1.5-3 times heavier than the S and SW 850 mb maps. In contrast, the precipitation rates on the surface and 850 mb W and NW maps are similar.

Precipitation pattern maps corresponding to Hoquiam surface winds greater than or equal to 15 kts are presented in Figure 1.5. Only SE, S, SW and W maps were constructed since the remaining wind direction categories contained too few hours to produce statistically valid mean precipitation maps. Additionally, precipitation rates were too light to be of interest. The general precipitation patterns in Figure 1.5 are nearly identical to the patterns for the corresponding maps from all wind speeds (Fig. 1.3); however, the magnitude of precipitation is significantly higher (on the order of 2:1).

Precipitation pattern maps for 850 mb winds of 25 kts or greater were produced for S, SW, W and NW wind directions (Fig. 1.6). The remaining four wind direction

HOQUIAM SURFACE WIND PRECIPITATION PATTERN MAPS (WIND SPEED ≥ 15 KTS)

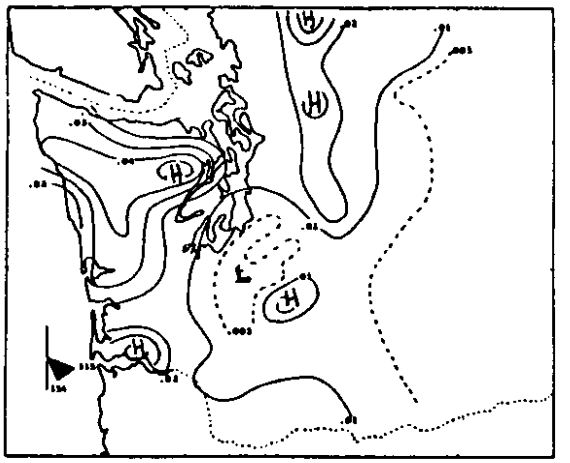

SOUTHEAST
102 HOURS

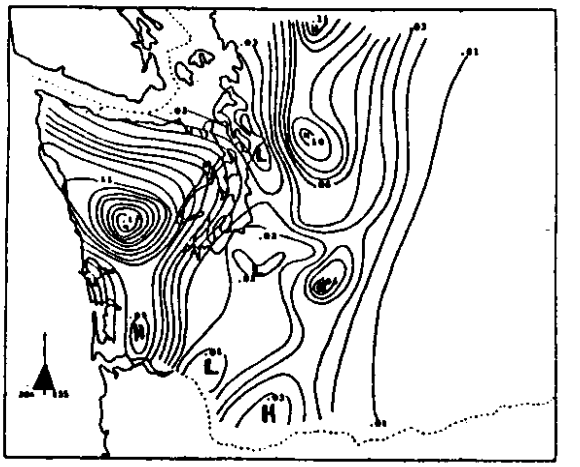

SOUTH
257 HOURS

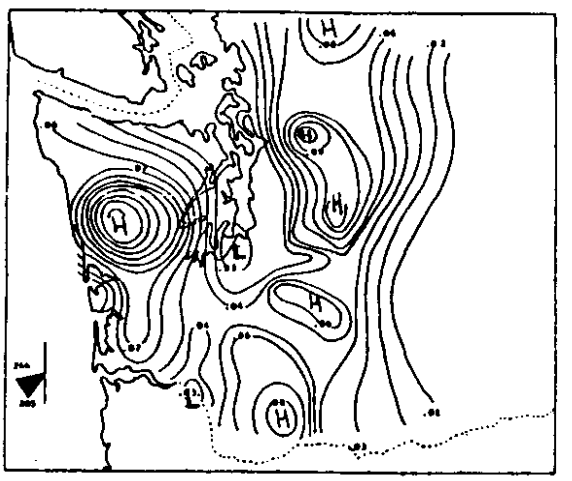

SOUTHWEST
386 HOURS

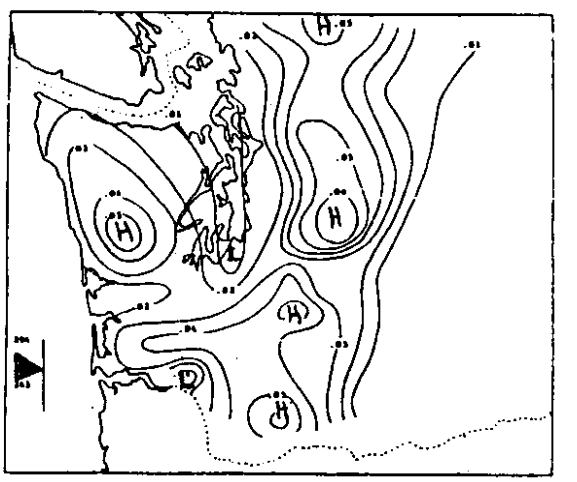

WEST
308 HOURS

Figure 1.5 Mean hourly precipitation pattern maps for Hoquiam surface wind speeds greater than or equal to 15 kts. The wind direction is shown by the shaded region of the compass and is indicated below each map. The solid line contour interval is .01 inches of water equivalent per hour. Dashed line contours are drawn for .005 inch intervals.

QUILLAYUTE 850 MB WIND PRECIPITATION PATTERN MAPS (WIND SPEED ≥ 25 KTS)

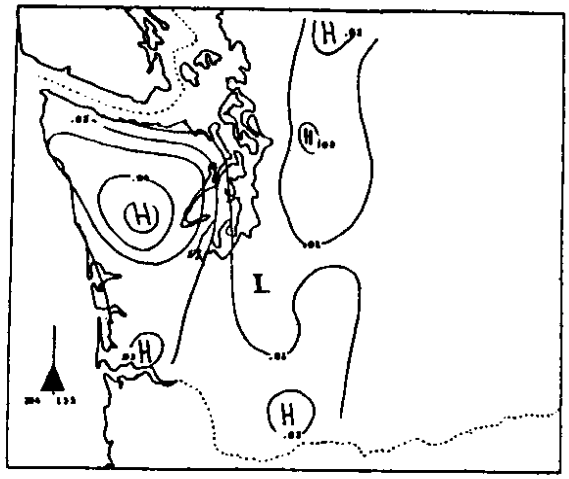

SOUTH
1367 HOURS

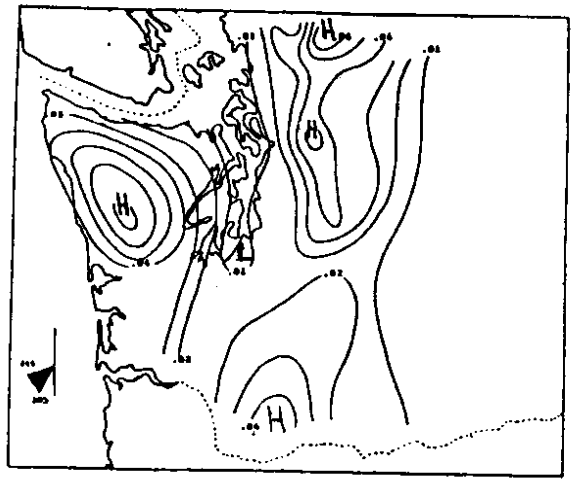

SOUTHWEST
810 HOURS

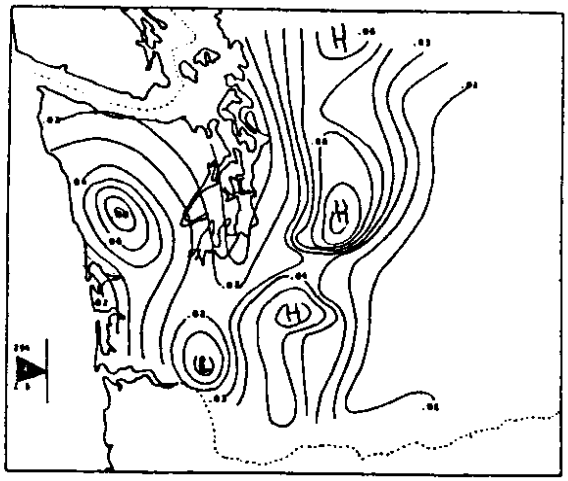

WEST
438 HOURS

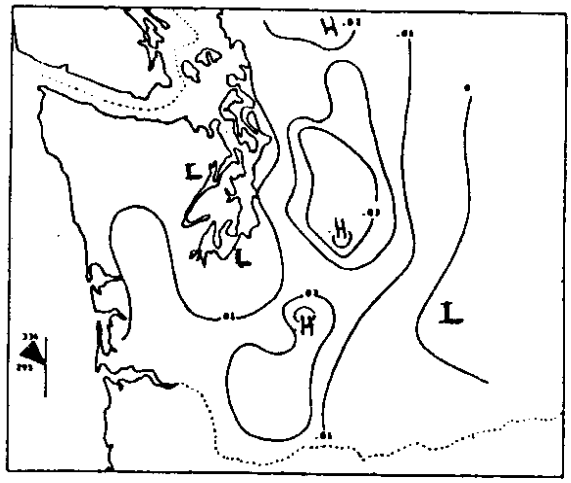

NORTHWEST
223 HOURS

Figure 1.6 Mean hourly precipitation pattern maps for Quillayute 850 mb wind speeds greater than or equal to 25 kts. The wind direction is shown by the shaded region of the compass and is indicated below each map. The solid line contour interval is .01 inches of water equivalent per hour. Dashed line contours are drawn for .005 inch intervals.

categories did not contain a sufficient number of hours to be included. Precipitation rates in Figure 1.6 are generally 1.5-3 times heavier than on the 850 mb series that includes all wind speeds (Fig. 1.4). The heaviest precipitation rates in Figure 1.4 occur during SW winds, whereas, the heaviest precipitation rates for winds greater than or equal to 25 kts occur during W winds.

An analysis of the precipitation pattern maps in Figures 1.3 through 1.6 produces several general conclusions. 1) The highest hourly precipitation rates generally occur when surface and 850 mb winds blow from the S and SW. With 850 mb winds greater than or equal to 25 kts, the highest precipitation rates occur during W winds. 2) Multiplying the hourly precipitation rate by the number of hours the wind blows from each direction indicates that most precipitation falls during S,SW, and W winds at the surface and 850 mb. 3) Although the magnitude of the precipitation rate varies tremendously with wind direction, as does the location of maximum precipitation, the general regions receiving the heaviest precipitation are fairly consistent for all surface and 850 mb wind directions. These regions include: the Olympic Mountains, most notably near Quinalt and Camp Grisdale; Mt Baker; Silverton and Verlot extending south to Stampede Pass; Mt Rainier; and the area south of Mt

St. Helens. A greater density of precipitation gauges would better detail shifts in the position of maximum precipitation, or additional areas of maximum precipitation. 4) The regions that generally record precipitation minima include Puget Sound, the eastern extension of the Strait of Juan de Fuca, the area surrounding Longview, and the plateau east of the Cascade Mountains. In the Washington Cascades, a relative precipitation minimum exists on most of the precipitation pattern maps between the Snoqualmie Pass/Stampede Pass area to the north and Mt Rainier to the south. 5) The magnitude of precipitation for surface wind speeds greater than or equal to 15 knots or 850 mb winds greater than or equal to 25 kts was generally 1.5-3 times higher than precipitation rates for all wind speeds. 6) As the wind direction shifts, the precipitation minimum in the lee of the Olympic Mountains also shifts. The rotation of the rain shadow in the lee of the Olympics will be explored in detail in Chapter 1.5.A. 7) During W and NW winds, the precipitation rates on the precipitation pattern maps from surface and 850 mb level winds are similar because the winds at these two levels are often coincident for these wind directions. However, for all other wind directions, the hourly precipitation rates tend to be 2-3 times higher on the surface wind direction

precipitation pattern maps than on the 850 mb maps. This is a function of the number distribution of hours within each wind direction category (see Table 1.2). For example, a greater percentage of 850 mb winds blow from the S or SW than do surface winds. Therefore, the total precipitation from 850 mb S and SW winds is greater than the total precipitation from surface S and SW winds even though the mean hourly precipitation rates are less.

TABLE 1.2 Precentage of hours during the study period that the wind blew from each direction category for Hoquiam surface winds and Quillayute 850 mb winds.

HOQUIAM SURFACE WINDS

DIRECTION	%
NE	9
E	15
SE	15
S	9
SW	13
W	16
NW	9
N	13

QUILLAYUTE 850 MB WINDS

DIRECTION	%
NE	3
E	4
SE	4
S	37
SW	18
W	19
NW	8
N	7

1.5. AREA ANALYSES

In order to derive more specific information from the precipitation pattern maps, several of the areas that produce maximum precipitation will be analyzed in greater detail. These areas include : the Olympic Peninsula, Mt Rainier, Mt Baker, Snoqualmie Pass and Stevens Pass.

A. OLYMPIC PENINSULA

The Olympic Peninsula (Fig. 1.7) is effectively an orographic island with some peaks to nearly 8000 feet. From Figures 1.3 and 1.4 it is evident that the most intense precipitation in the Olympic Mountains occurs during surface S and SW winds, when the south side of the mountains averages .08 to .09 inches of rain per hour. Note that the precipitation rates during W and NW wind directions may appear less than during S and SW winds as a result of the location of the precipitation gauges. Camp Grisdale and Quinalt, the two sites measuring maximum precipitation in the Olympics, are both located on the S side of the mountains. No high elevation stations exist on the north or west sides. Precipitation associated with 850 mb level winds is most intense during

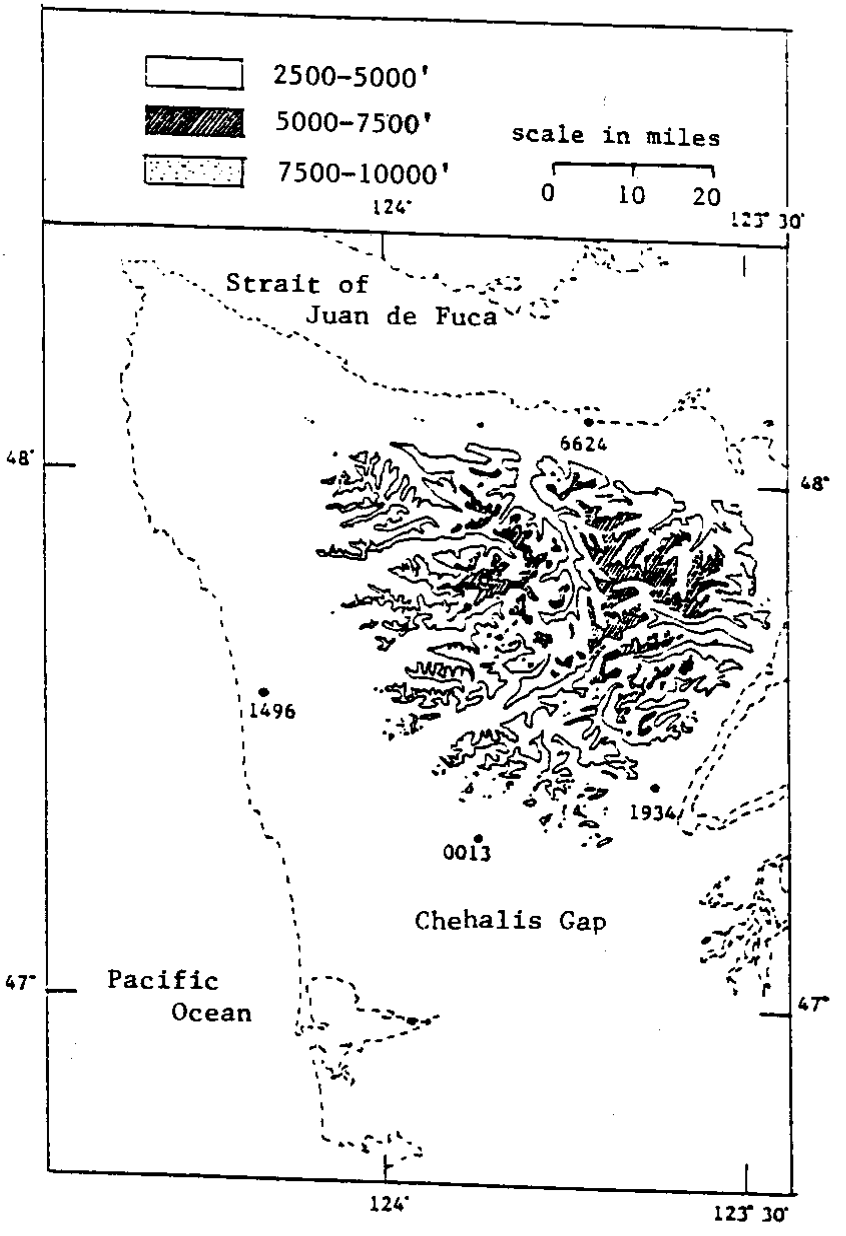

Figure 1.7 Topographic map for the Olympic Peninsula with Clearwater (1496), Cushman Dam (1934), Port Angeles (6624) and Aberdeen (0013) identified by station number.

S,SW, and W winds, with the heaviest precipitation falling on the S and W side of the Olympic Mountains.

Figure 1.8 shows mean hourly precipitation rates as a function of wind direction for Clearwater (1496) (shaded bars) and Cushman Dam (1934) (plain bars), two sites on opposite sides of the Olympic Mountains. As would be expected, the maximum precipitation rates at both sites generally occur during S to W wind directions; however, the wind direction with heaviest precipitation shifts from S at the surface to SW at 850 mb. Surface S winds and 850 mb SW winds are often coincident because the wind direction often veers with height. The shift of the rain shadow in the lee of the Olympic Mountains with wind direction is demonstrated when the ratios between the hourly precipitation rates of Clearwater/Cushman Dam are compared for each of the eight Hoquiam surface wind directions (Fig. 1.9a). Cushman Dam receives heavier precipitation than Clearwater during NE and E winds, as would be expected with Cushman Dam on the windward side of the Olympic Mountains. During N and NW winds, when Cushman Dam is very effectively rain shadowed by the Olympic Mountains, Clearwater receives the heavier precipitation.

The hourly precipitation rate ratios for the Quillayute 850 mb wind directions (Fig. 1.9b) for

a.

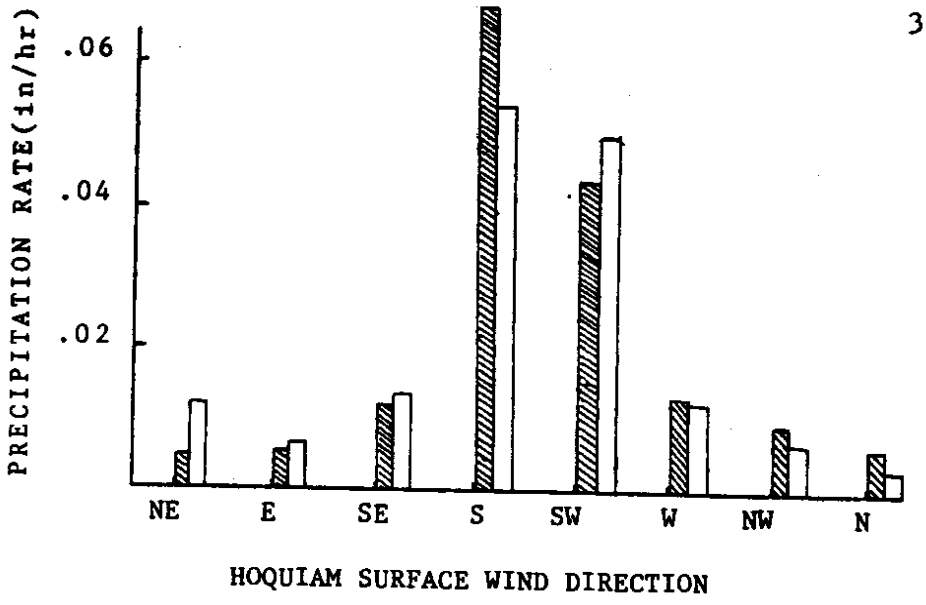

b.

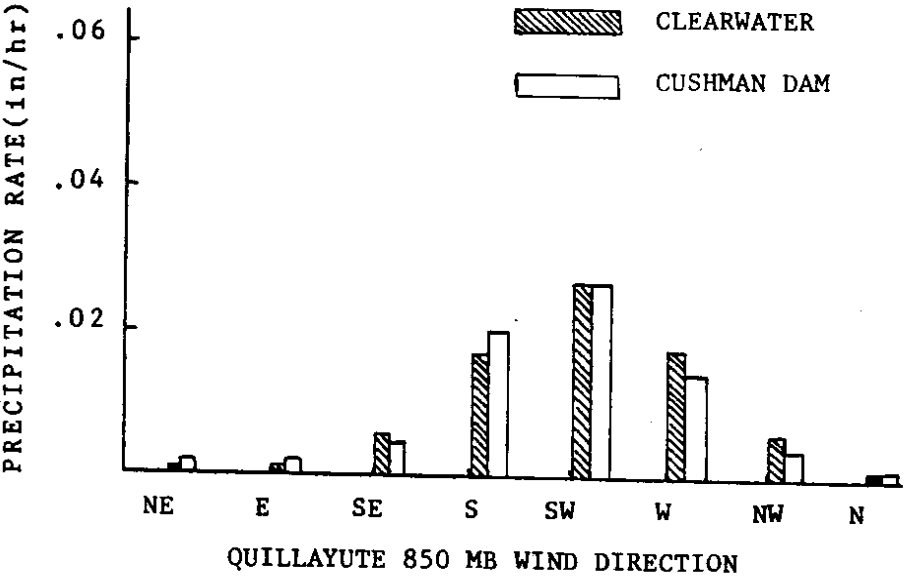

Figure 1.8 a,b Mean hourly precipitation rates as a function of (a) Hoquiam surface wind direction and (b) Quillayute 850 mb wind direction. Shaded bars give precipitation rates at Clearwater. Plain bars indicate precipitation rates at Cushman Dam.

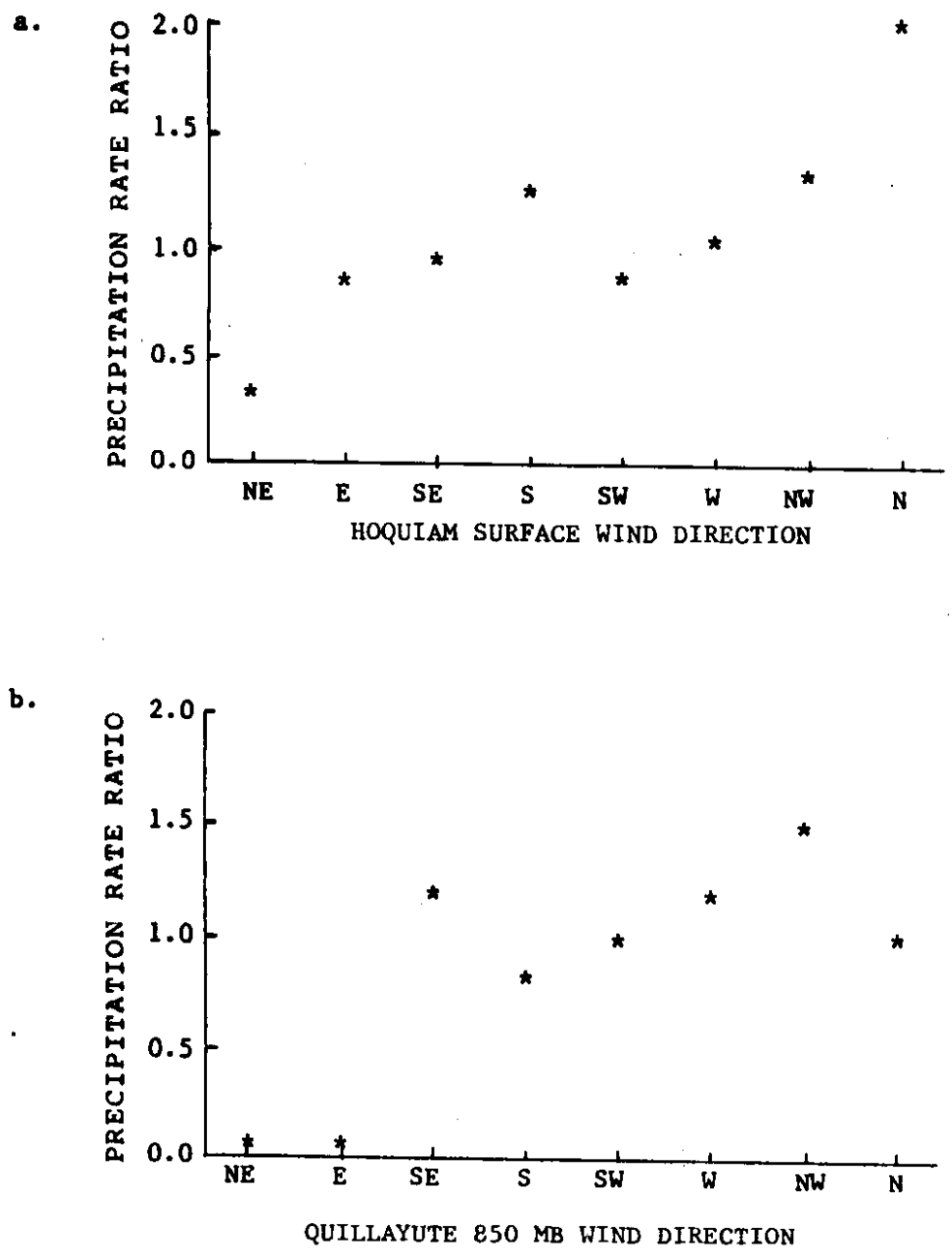

Figure 1.9a,b Clearwater/Cushman Dam precipitation rate ratio as a function of (a) surface wind direction at Hoquiam and (b) 850 mb level wind direction at Quillayute.

Clearwater/Cushman Dam are somewhat different than in Figure 1.9a. These variations can be explained by differences in the often ageostrophic surface winds and the relatively geostrophic upper level winds. For example, surface easterlies often occur ahead of a cold front when a moist southwesterly flow aloft produces similar precipitation rates at Clearwater and Cushman Dam. In contrast, 850 mb E winds generally occur when a positively tilted upper level ridge over British Columbia produces an offshore flow at all levels, which results in dry conditions at Clearwater in the lee of the Olympics.

A second example from the Olympic Peninsula illustrates the need to understand the overall synoptic situation to explain the precipitation ratios. Port Angeles (6624), on the Strait of Juan de Fuca, is compared to Aberdeen (0013), which is located south of the Olympic Mountains. The location of these two sites is shown in Figure 1.7. The precipitation rates in Figure 1.10 and the ratios in Figure 1.11 show the same general pattern as the Clearwater/Cushman Dam case, although Port Angeles always receives less precipitation than Aberdeen. During east winds at the surface, Port Angeles has surprisingly little precipitation compared to Aberdeen. East winds at Hoquiam generally occur when the surface low pressure associated with a weather disturbance is

a.

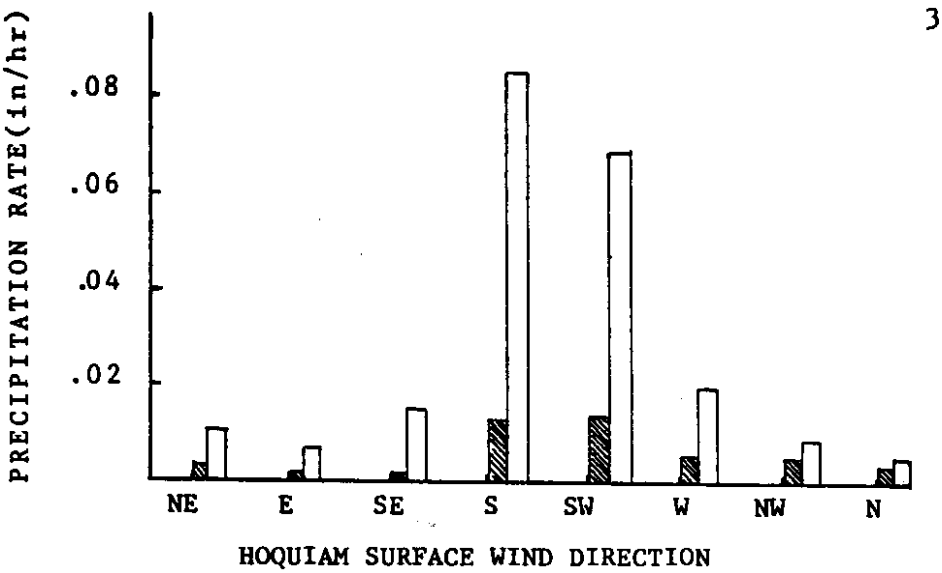

b.

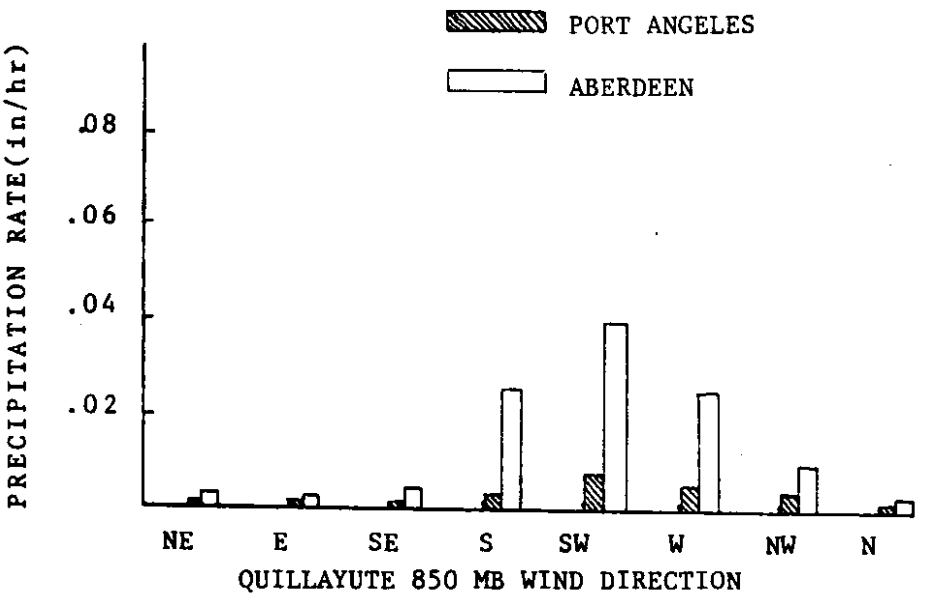

Figure 1.10 a,b Mean hourly precipitation rates as a function of (a) Hoquiam surface wind direction and (b) Quillayute 850 mb wind direction. Shaded bars give precipitation rates at Port Angeles. Plain bars indicate precipitation rates at Aberdeen.

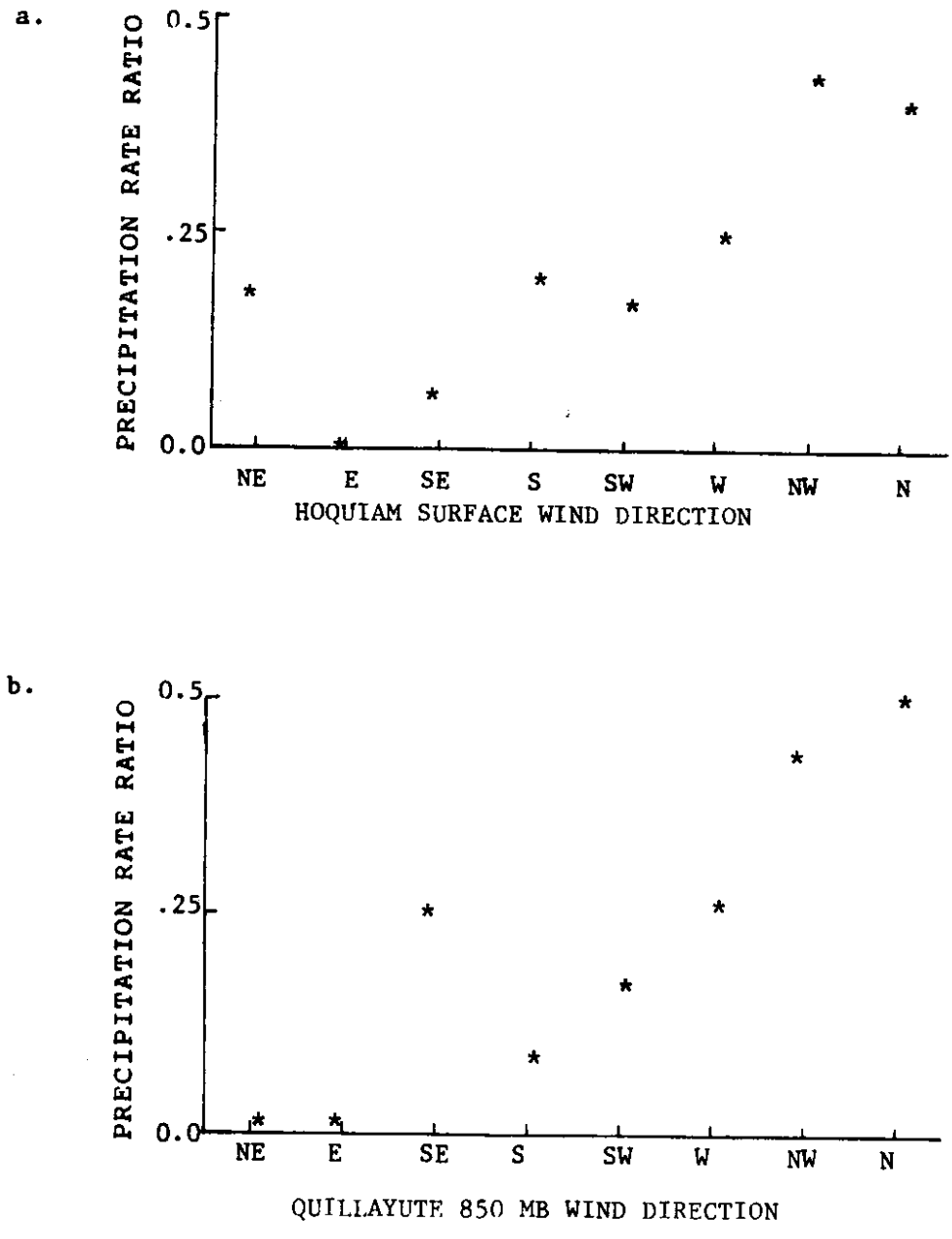

Figure 1.11 a,b Port Angeles/Aberdeen precipitation rate ratio as a function of (a) surface wind direction at Hoquiam and (b) 850 mb level wind direction at Quillayute.

offshore, with warm overrunning precipitation often moving into the region from the SW at higher elevations. In this situation, Port Angeles is shielded from the main source of moisture by the Olympic Mountains, while Aberdeen lies on the SW side of the mountains. Strong east winds flowing from the Fraser River out the Strait of Juan de Fuca should enhance upslope precipitation at Port Angeles, but surface wind observations indicate that while strong east winds are recorded on the Canadian side of the Strait of Juan de Fuca, Port Angeles generally reports light winds. Schoenberg's (1983) thesis supports this observation. With light winds, Port Angeles does not benefit from upslope precipitation enhancement. The precipitation ratios increase significantly for NW and N winds, when Aberdeen, in the lee of the Olympic Mountains, receives relatively less precipitation.

The 850 mb precipitation rate ratios for Port Angeles/Aberdeen (Fig. 1.11b) are qualitatively the same as the surface ratios.

B. MT RAINIER

From Figures 1.3 and 1.4, it is evident that for most wind directions at the surface and 850 mb level, Mt Rainier (Fig. 1.12) receives more precipitation than

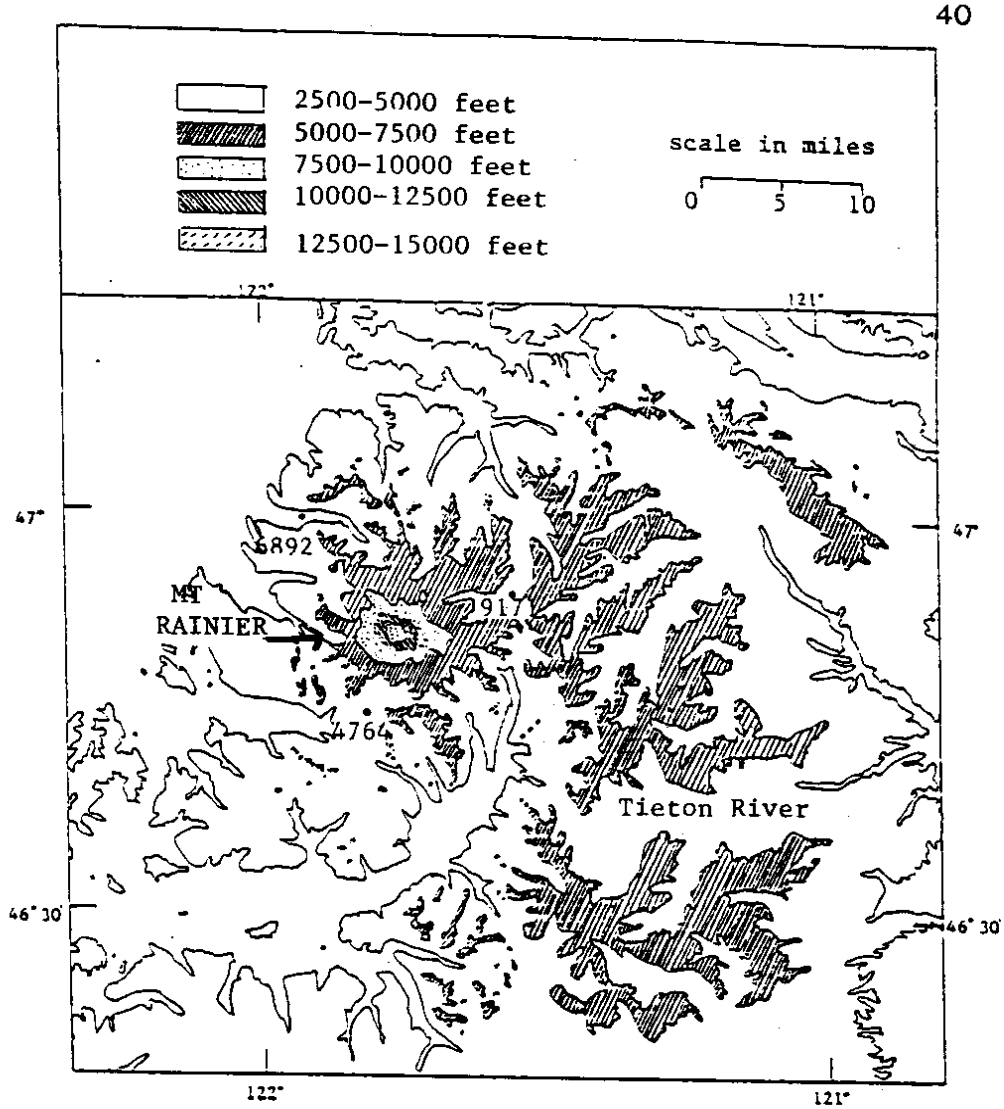

Figure 1.12 Topographic map for the Mt Rainier region with Carbon River Entrance (6892), Longmire (4764) and White River Ranger Station (9171) identified by station number.

surrounding areas. This increase in precipitation is most apparent when the mountain provides a barrier to moist SW and W winds moving inland south of the Olympic Mountains, and to NW winds flowing through the Strait of Juan de Fuca and south through Puget Sound. During S and SW winds, Mt Rainier receives 1/3 to 1/2 the precipitation of the Olympic Mountains because Mt Rainier lies downwind of high elevation terrain barriers in the Cascades that block the flow of moist air. In W and NW flow, Mt Rainier apparently receives more precipitation than the Olympics. However, this may be an illusion resulting from the lack of high elevation precipitation measurement sites on the W and NW sides of the Olympics.

Mt Rainier produces a rain shadow effect similar to the Olympic Mountains on the surrounding terrain. Precipitation data from three precipitation measuring sites located near Mt Rainier (Fig. 1.12), Carbon River Entrance (elevation,1735') to the northwest, Longmire (2762') to the south, and White River Ranger Station (3500') to the east, demonstrate this rain shadow. When analyzing the precipitation rate ratios for these stations, note that the winds are measured along the Pacific coast. The actual surface winds near Mt Rainier are greatly affected by local channeling and by deflection by the Olympics and Mt Rainier itself, and

often differ from values obtained at Hoquiam.

In Figure 1.13 the precipitation rates for Carbon River Entrance (6892) and White River Ranger Station (9171) are shown for various wind directions. At the surface and 850 mb level, the maximum precipitation rates occur for S through W and NW wind directions, with minimum precipitation rates for E and SE winds. The position of the maximum precipitation rate shifts from surface SW winds to 850 mb W winds. For SE surface winds, White River receives more precipitation than Carbon River Entrance, since the Carbon River gauge is in the lee of Mt Rainier. Carbon River receives more precipitation for surface W through N winds, ie, when the Carbon River Entrance gauge is windward from Mt Rainier. Funneling of NW surface winds up the White River valley explains the relative increase in precipitation at the White River Ranger Station compared to surface W and N winds.

The 850 mb precipitation rates (Fig. 1.13b) demonstrate a pattern similar to the corresponding surface rates. With Mt Rainier extending above 14000 feet, and several of the surrounding ridges rising above 5000 feet, the 850 mb winds would be expected to experience channeling effects similar to the surface winds, thus producing similar precipitation patterns.

Figures 1.14 and 1.15 show the hourly precipitation

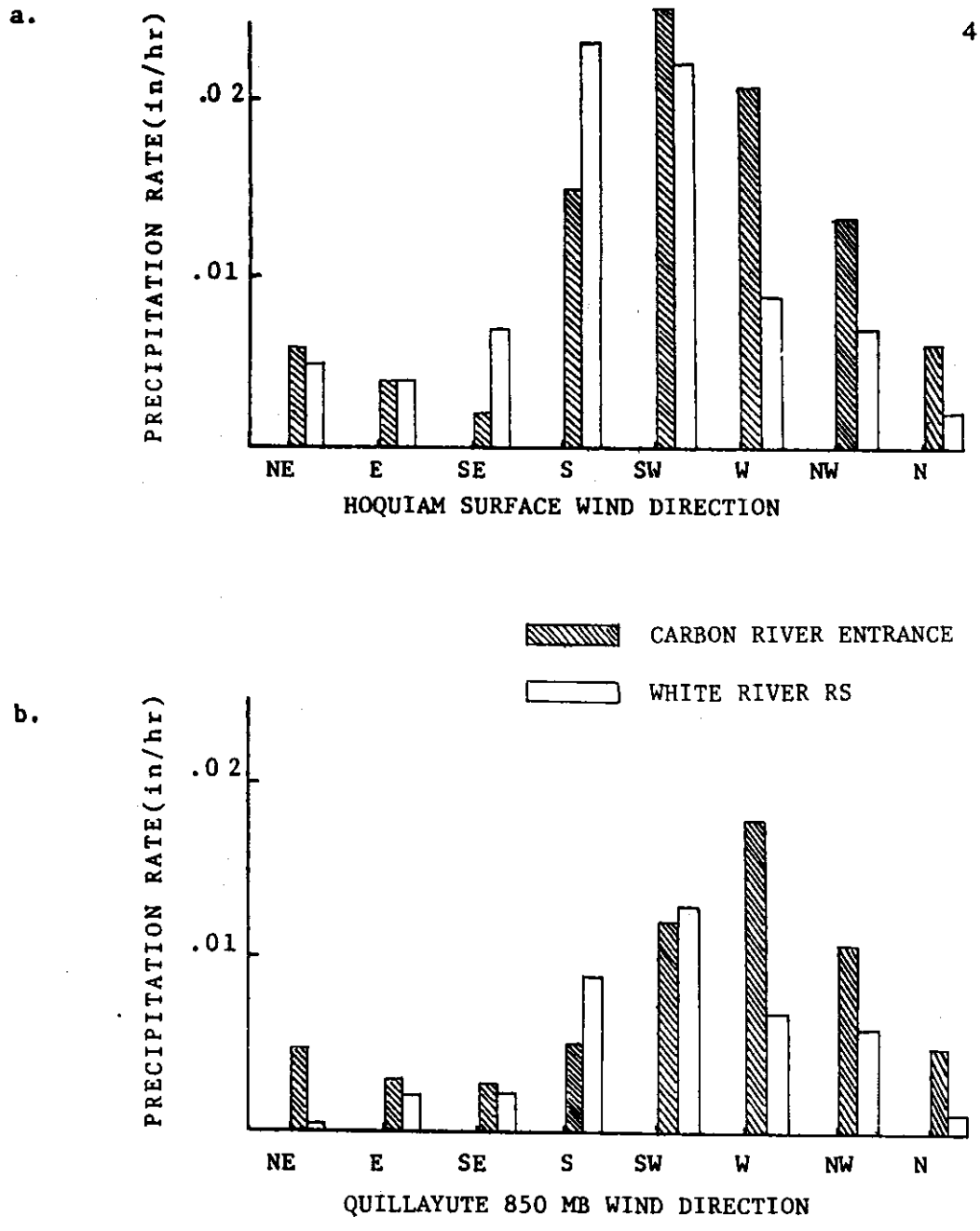

Figure 1.13 a,b Mean hourly precipitation rates as a function of (a) Hoquiam surface wind direction and (b) Quillayute 850 mb wind direction. Shaded bars give precipitation rates at Carbon River Entrance Station. Plain bars indicate precipitation rates at White River Ranger Station.

a.

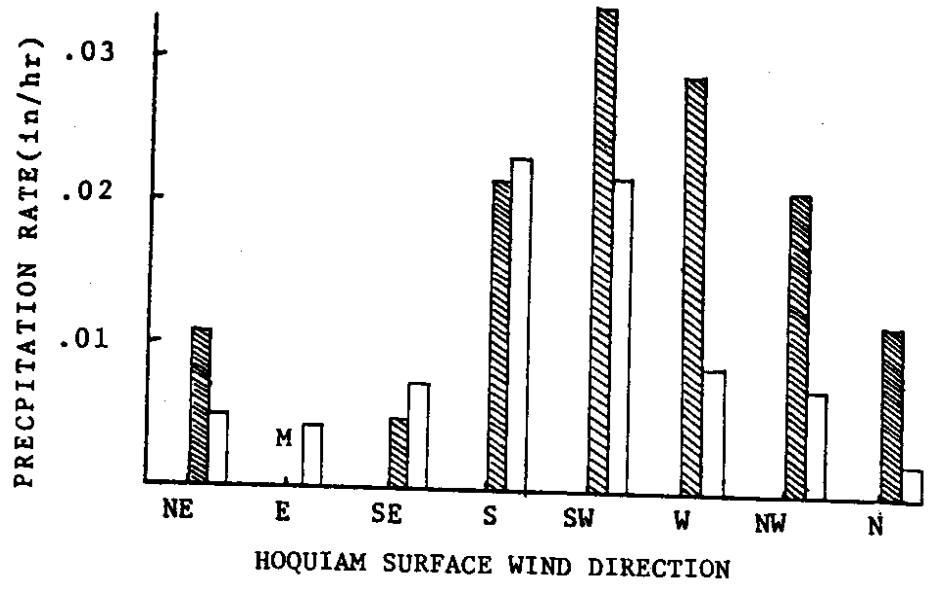

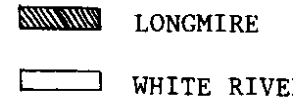

b.

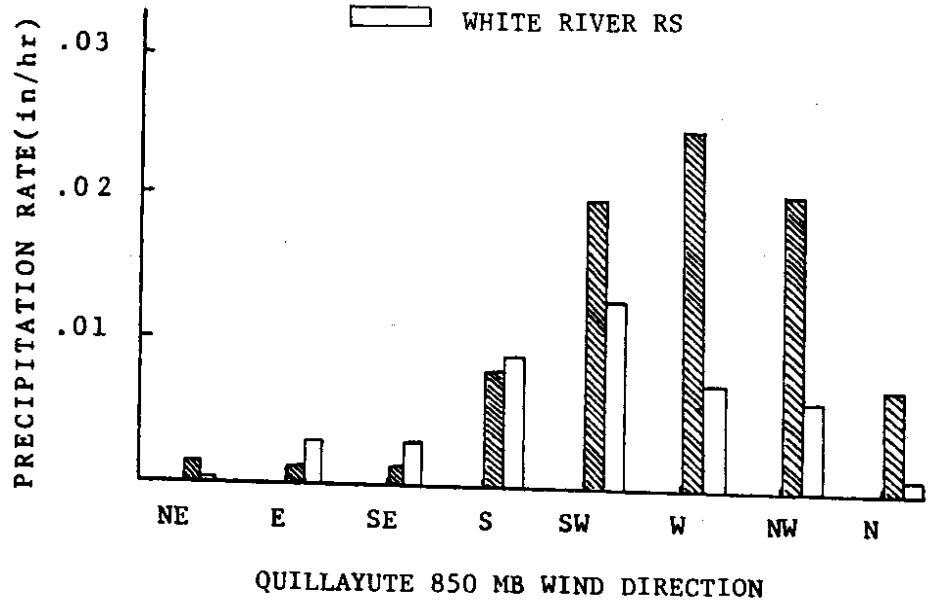

Figure 1.14 a,b Mean hourly precipitation rates as a function of (a) Hoquiam surface wind direction and (b) Quillayute 850 mb wind direction. Shaded bars give precipitation rates at Longmire. Plain bars indicate precipitation rates at White River Ranger Station.

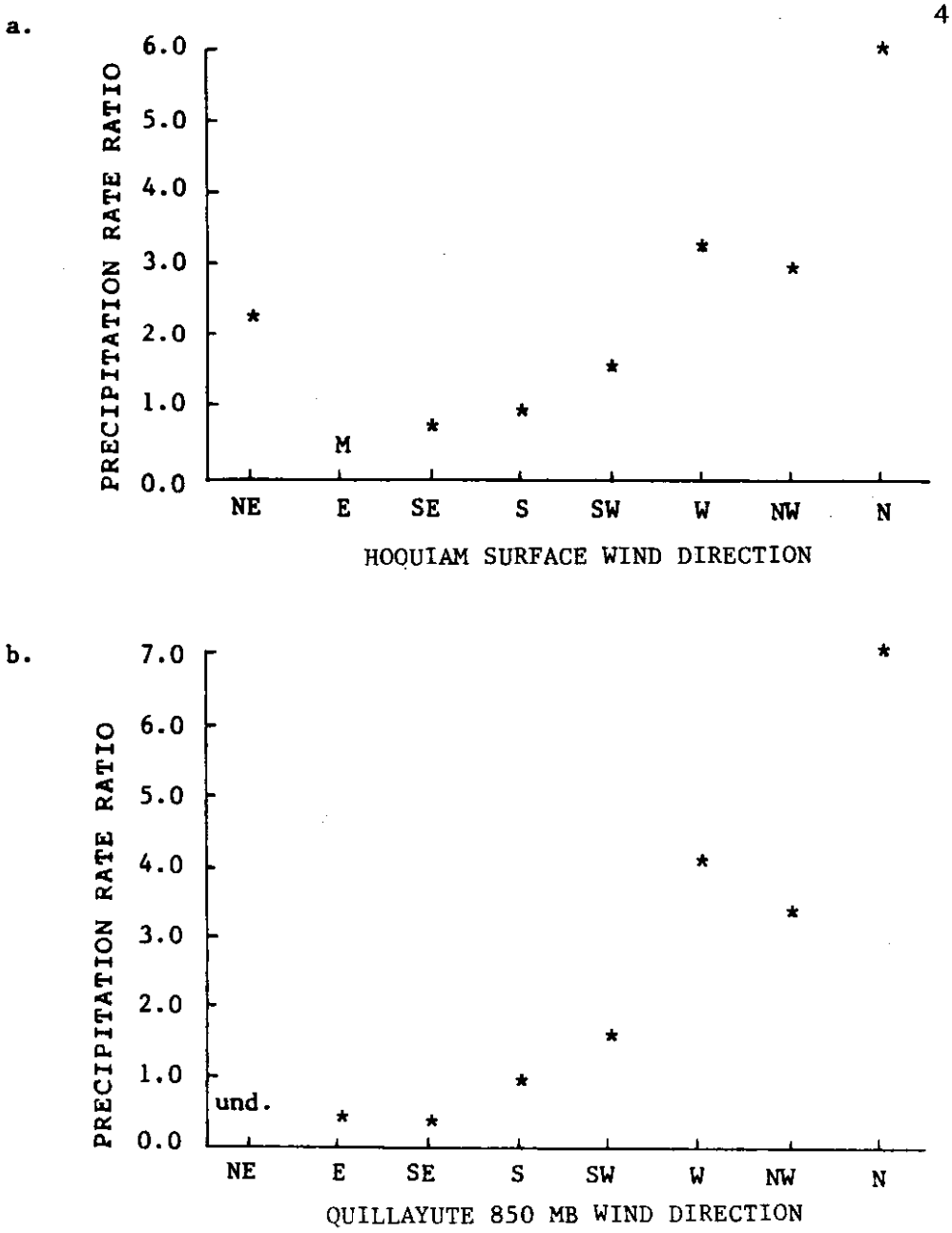

Figure 1.15 a,b Longmire/White River Ranger Station precipitation rate ratio as a function of (a) surface wind direction at Hoquiam and (b) 850 mb level wind direction at Quillayute. The ratio labeled und. refers to a case for which White River Ranger Station's mean hourly precipitation rate was 0. M refers to missing data.

rates and ratios, respectively, for Longmire and White River Ranger Station as a function of wind direction. Paradise, 4 miles north of Longmire, and Crystal Mountain, east of the White River Ranger Station, both receive daily quantitative precipitation forecasts during the winter. Although forecasters have observed that Crystal Mountain receives large quantities of precipitation relative to Paradise during SE winds, this had not been quantified. The SE wind ratio in Figure 1.15a illustrates this phenomenon. Presumably, SE winds are channeled toward White River Ranger Station and Crystal Mountain from the Tieton and Ohanepecosh River drainages, while Longmire is shadowed by the Goat Rocks region to its SE. During surface SW thru NW winds, Longmire receives more precipitation than White River Ranger Station, as would be expected with Longmire situated upwind of Mt Rainier. Longmire receives more precipitation than White River Ranger Station during N and NE winds when White River Ranger Station is very effectively rain shadowed by surrounding high elevation terrain.

The 850 mb precipitation rate ratios (Fig. 1.15b) for Longmire and White River Ranger Station are nearly the same as the surface ratios because the 850 mb and low level flow are similar in the high elevation terrain

surrounding Mt Rainier.

C. MT BAKER

Mt Baker, a volcanic peak rising above 10000 feet (Fig. 1.16), lies 30 miles east of Bellingham. The precipitation pattern maps (Figs. 1.3 and 1.4) show that a precipitation maxima exists near Mt Baker and that this region generally receives more precipitation than Mt Rainier. The Mt Baker region receives its heaviest precipitation relative to other sites in the Washington Cascades during southerly surface winds and southwesterly 850 mb winds when Mt Baker, which extends westward of the main axis of the Cascades, intersects the moist flow. Three National Weather Service precipitation sites form a triangle around Mt Baker: Glacier Ranger Station (3160), Mt Baker Lodge (5663), and Upper Baker Dam (8715). The locations of these three stations are shown in Figure 1.16. On most of the precipitation pattern maps Mt Baker Lodge, elevation 4150', receives heavier precipitation than Glacier Ranger Station (935') and Upper Baker Dam (690'). This may be accounted for by orographic precipitation enhancement associated with the higher elevation at Mt Baker Lodge.

The hourly precipitation rates and ratios for

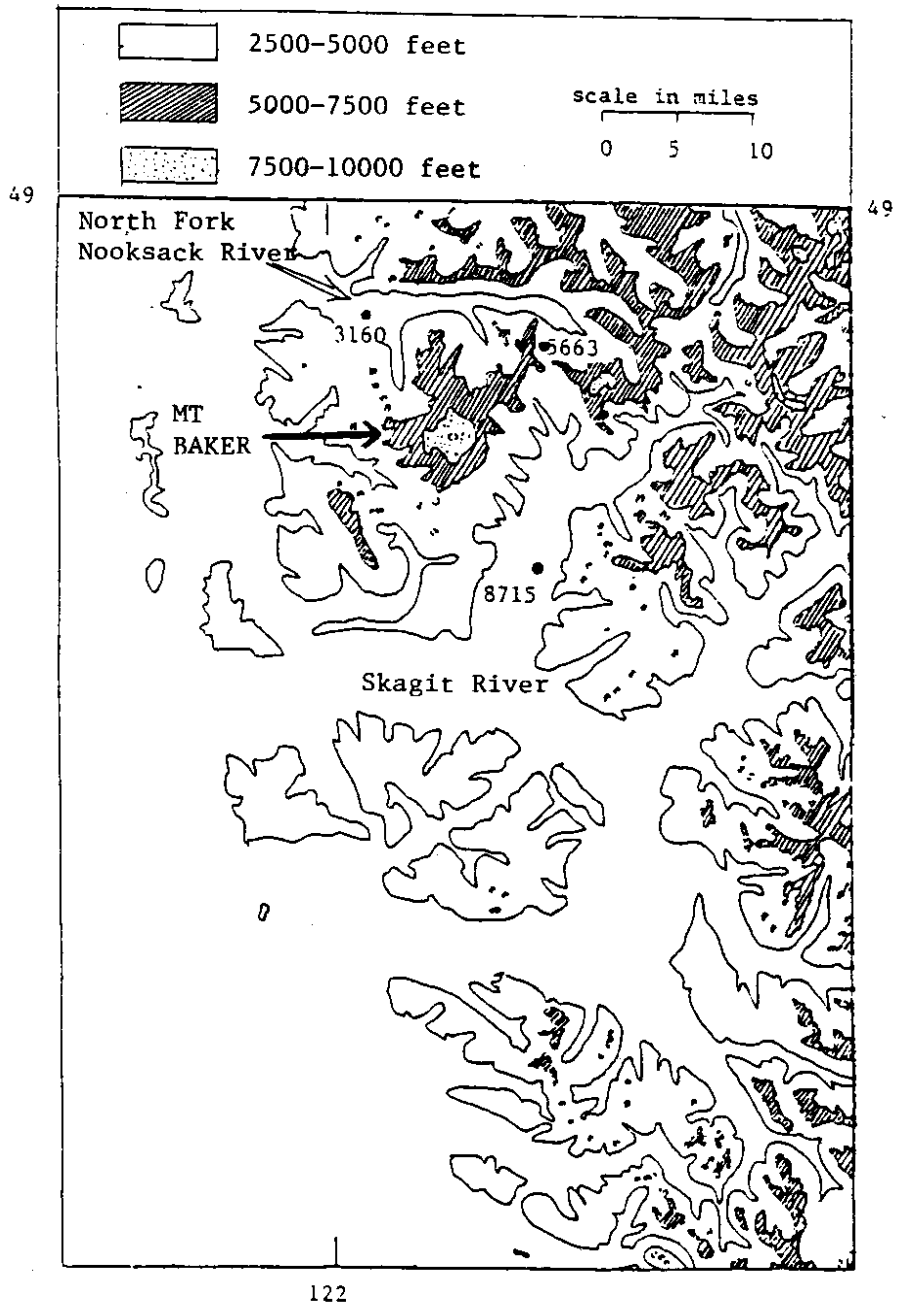

Figure 1.16 Topographic map for the Mt Baker region with Glacier Ranger station (3160), Mt Baker Lodge (5663) and Upper Baker Dam (8715) identified by station number.

Glacier Ranger Station, north of Mt Baker, and Upper Baker Dam, SE of Mt Baker in the Baker River Drainage, are given in Figure 1.17 and 1.18. Upper Baker Dam receives more precipitation than Glacier Ranger Station in all but NW surface winds. Upper Baker Dam would be expected to receive more precipitation than Glacier Ranger Station during SE,S, and SW winds, when Glacier is rainshadowed by Mt Baker, and during W winds, when air moving in through the Strait of Juan de Fuca, and channeled up the Skagit River drainage, produces enhanced precipitation on the south slopes of Mt Baker. In contrast, NW winds, coming down the Strait of Georgia, enhance precipitation on the NW slopes of Mt Baker and at Glacier Ranger Station.

The hourly precipitation rate ratios based on Quillayute 850 mb winds in Figure 1.18b for Glacier Ranger Station and Upper Baker Dam have a higher amplitude than the surface ratios. The greatest contrast occurs during NW winds when precipitation upwind of Mt Baker at Glacier Ranger Station is enhanced, and during E and NE winds when Upper Baker Dam, situated in a N-S oriented valley downwind of high elevation terrain, is very effectively rain shadowed.

D. SNOQUALMIE PASS AREA

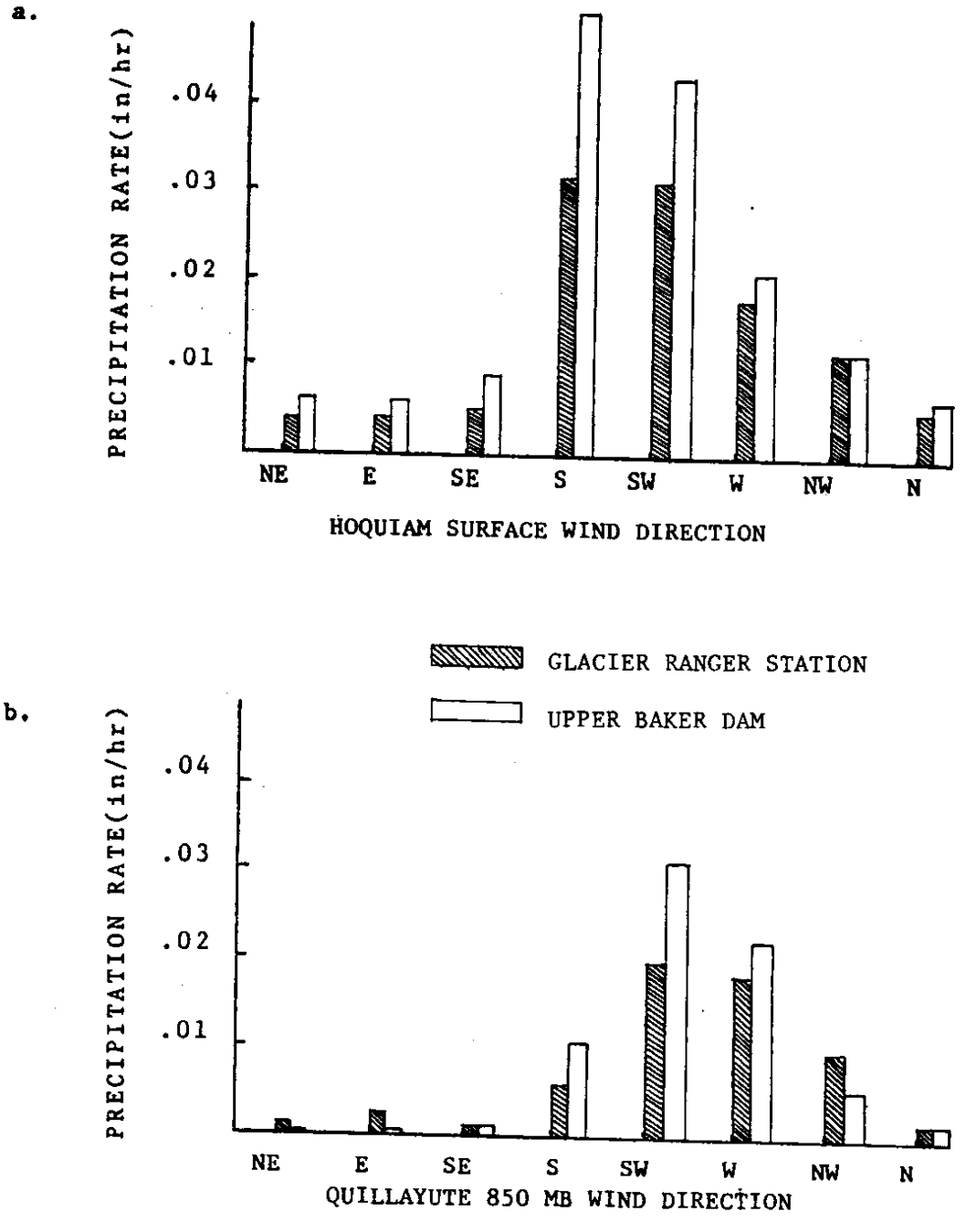

Figure 1.17 a,b Mean hourly precipitation rates as a function of (a) Hoquiam surface wind direction and (b) Quillayute 850 mb wind direction. Shaded bars give precipitation rates at Glacier Ranger Station. Plain bars indicate precipitation rates at Upper Baker Dam.

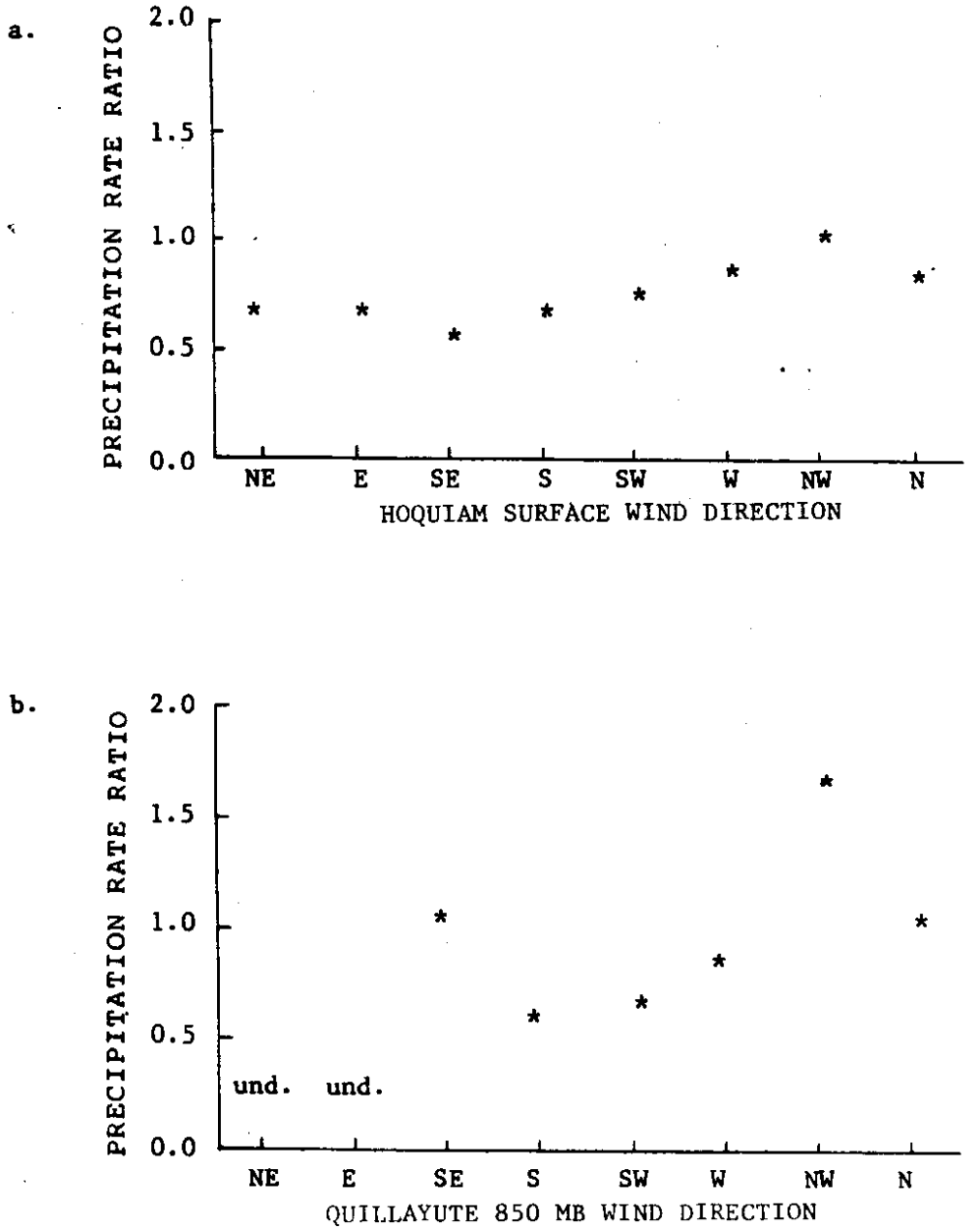

Figure 1.18 a,b Glacier Ranger Station/Upper Baker Dam precipitation rate ratio as a function of (a) surface wind direction at Hoquiam and (b) 850 mb level wind direction at Quillayute. The ratio labeled und. refers to cases for which Upper Baker Dam's mean hourly precipitation rate was 0.

Snoqualmie Pass, at 3000 feet elevation, provides the lowest heavily traveled pass through the Washington Cascades (Fig. 1.19). Several sites measuring precipitation are located near Snoqualmie Pass (3020'): Snoqualmie Falls (440'), a site west of the Cascade Crest and just west of the significant rise of the Cascade mountains; Cedar Lake (1560'), 15 miles west of Snoqualmie Pass; Stampede Pass (3958'), 12 miles south of Snoqualmie Pass; and Easton (2170'), 8 miles east of the Cascade Crest. On most of the precipitation pattern maps, Snoqualmie Pass and Stampede Pass receive heavier precipitation than sites to their E and W. The notable exception occurs for NW surface and 850 mb winds, when Cedar Lake receives more precipitation than Snoqualmie Pass.

The hourly precipitation rates as a function of wind direction for Snoqualmie and Stampede Passes are shown in Figure 1.20. Snoqualmie and Stampede Passes receive their heaviest precipitation from surface winds from the S through W. In contrast, the precipitation from 850 mb winds is generally greatest during W and NW winds. These wind directions, S through W at the surface and W to NW at 850 mb, occur after the passage of a cold front, which suggests that the heaviest precipitation is post-frontal.

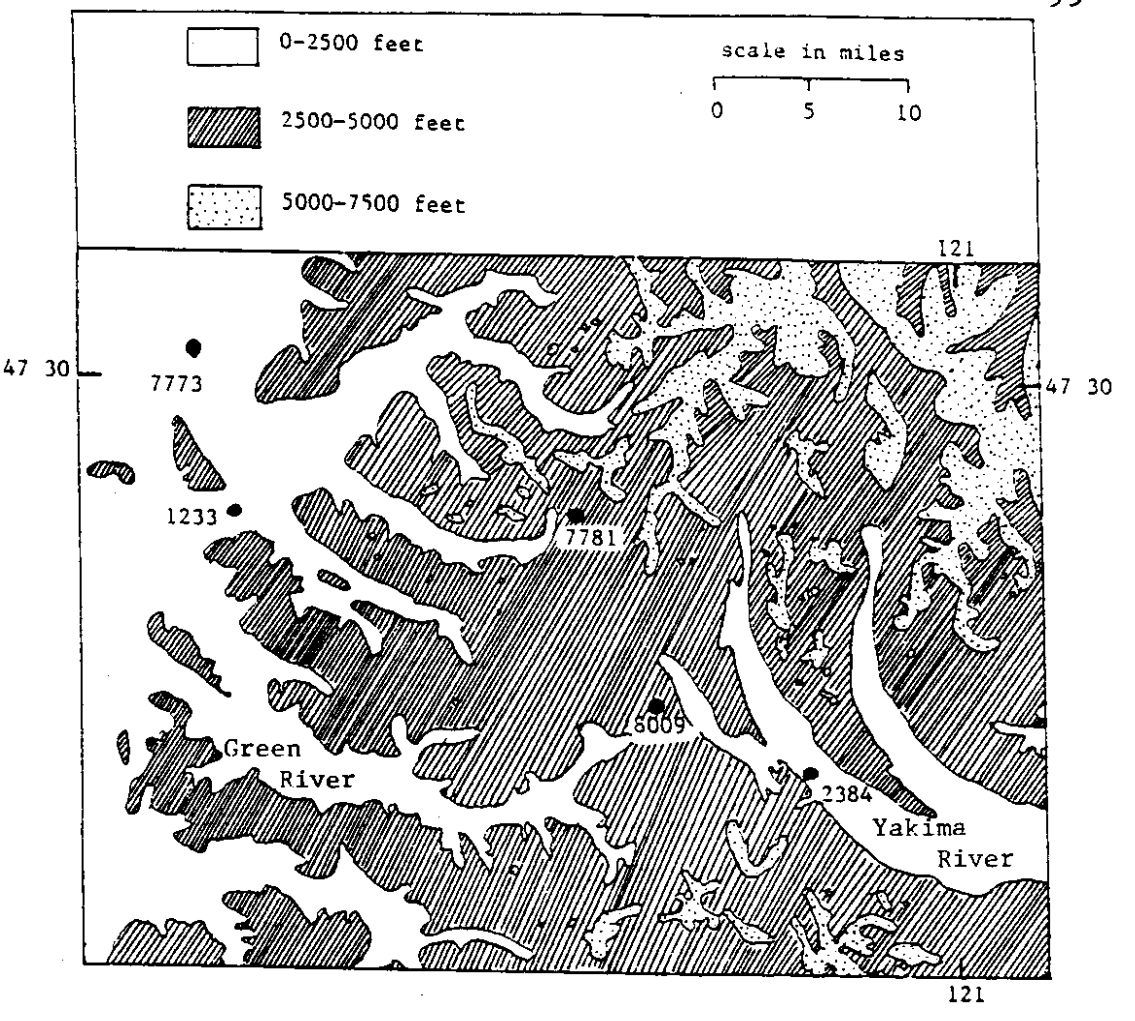

Figure 1.19 Topographic map for the Snoqualmie Pass area with Snoqualmie Falls (7773), Cedar Lake (1233), Snoqualmie Pass (7781), Stampede Pass (8009) and Easton (2384) identified by station number.

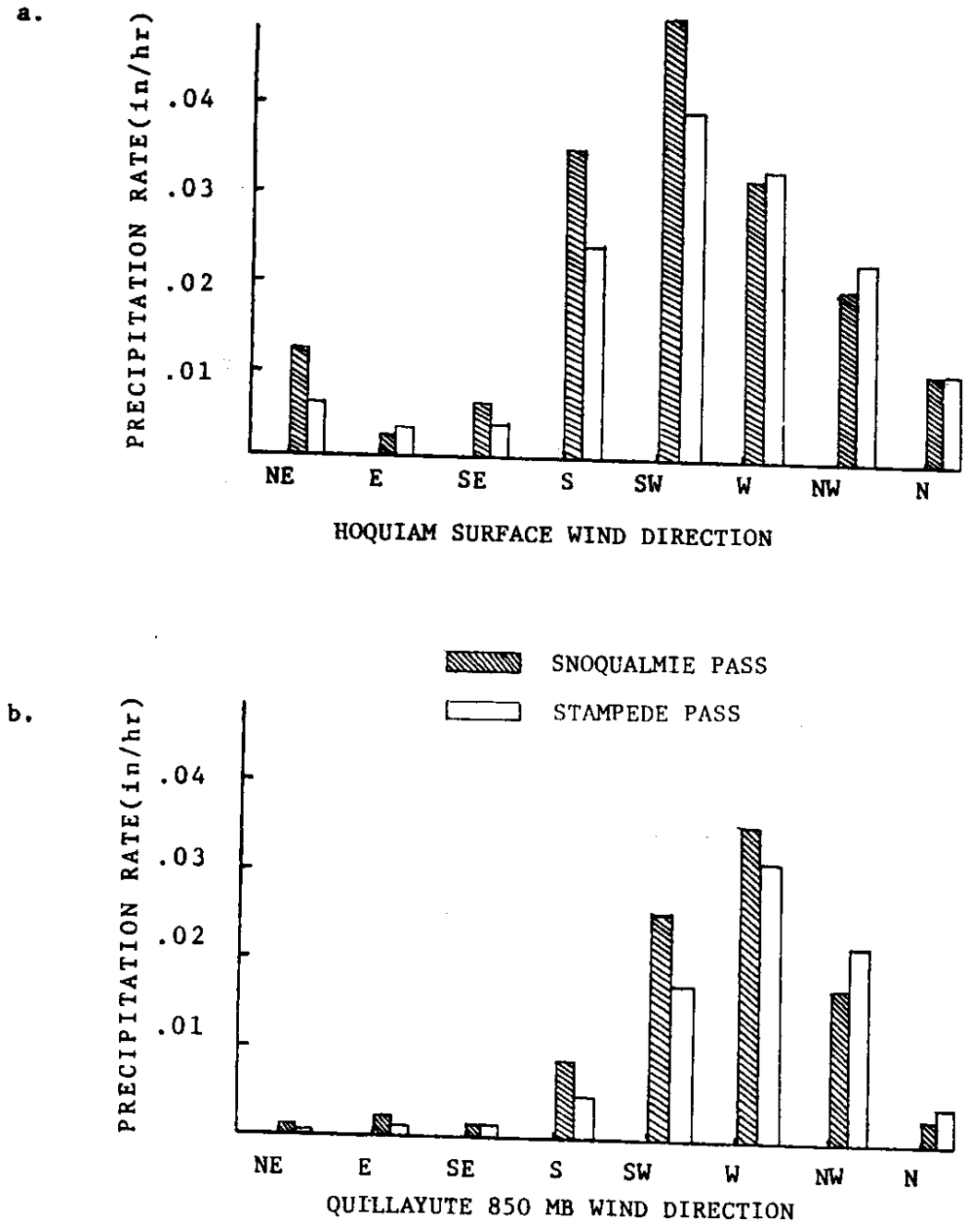

Figure 1.20 a,b Mean hourly precipitation rates as a function of (a) Hoquiam surface wind direction and (b) Quillayute 850 mb wind direction. Shaded bars give precipitation rates at Snoqualmie Pass. Plain bars indicate precipitation rates at Stampede Pass.

This contrasts the findings of Browning, Hill and Pardoe (1974) in south Wales, where the heaviest precipitation occured in the warm sector ahead of the cold front. Stampede Pass receives more precipitation than Snoqualmie Pass for NW winds when Snoqualmie Pass is in the lee of the 5-6000 foot high Preacher Mountain-Denny Mountain region. Snoqualmie Pass receives heavier precipitation than Stampede Pass for S and SW wind directions and similar precipitation for the remaining wind directions.

The relative precipitation rates for Snoqualmie and Stampede Passes derived from Quillayute 850 mb winds (Fig. 1.20b) are similar to the surface wind rates.

E. STEVENS PASS

Stevens Pass, at 4070 feet elevation, is a major pass through the Cascades north of Snoqualmie Pass (Fig. 1.21). Although Stevens Pass lies along the Cascade Crest, reference to Figures 1.3 and 1.4 indicates that Stevens Pass receives less precipitation than lower elevation stations to the west during S thru NW winds at both the surface and 850 mb level. In these cases, Stevens Pass generally lies 10-20 miles east of the area of maximum precipitation. Correlating precipitation rates with the low elevations of precipitation measuring sites

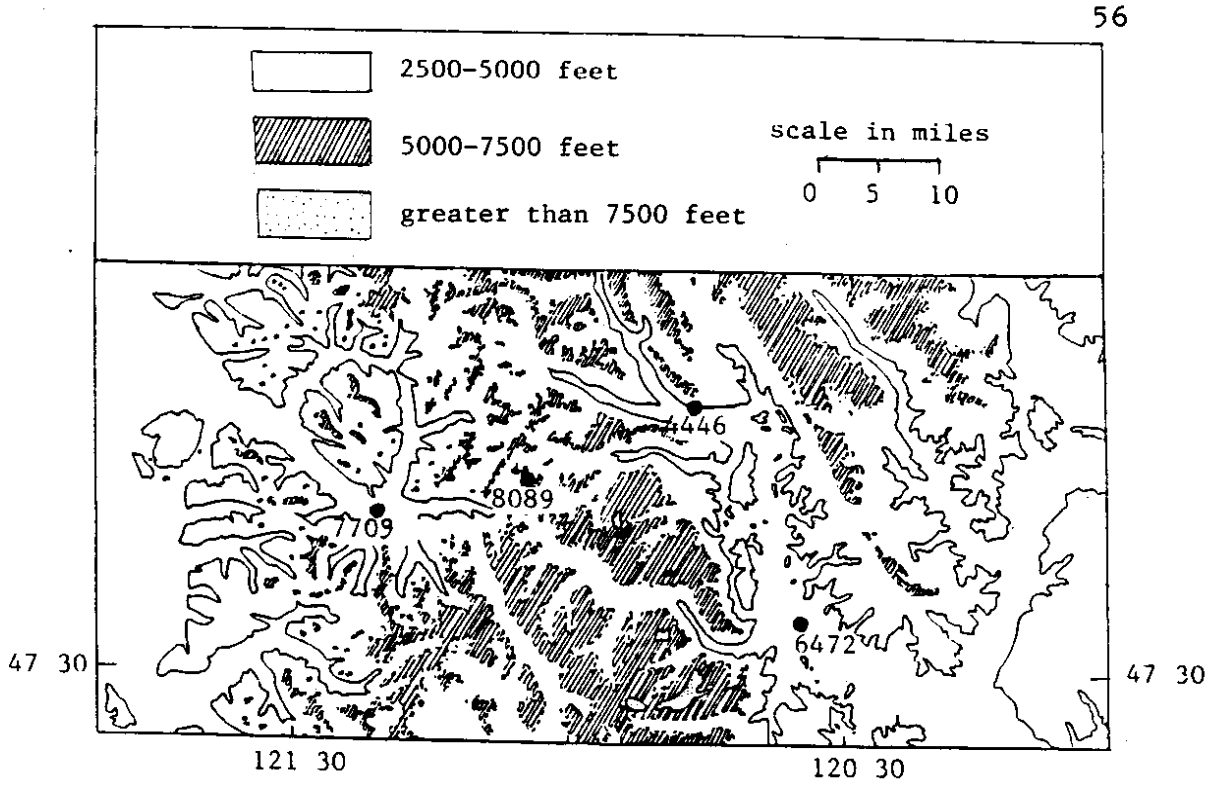

Figure 1.21 Topographic map for the Stevens Pass area with Skykomish (7709), Stevens Pass (8089), Lake Wenatchee (4446) and Peshastin (6472) identified by station number.

west of Stevens Pass may be misleading. The effective elevation of the measurement sites, ie, the elevation of an area surrounding the site (within a five mile radius, for example), may be equivalent or higher than the effective elevation near Stevens Pass. For example, Skykomish, elevation 1030', is situated adjacent to 5000' peaks. The initial orographic lift provided by the terrain near Skykomish may result in the heaviest precipitation in that area. Alternativly, inefficient catchment of snow at Stevens Pass during strong winds may produce a bias in the records. Most of the sites upwind of Stevens Pass are at elevations sufficiently low to primarily receive rain or wet heavy snow, and thus avoid the problem of snow catchment.

Four National Weather Service precipitation gauges are located adjacent to Route 2, which crosses Stevens Pass in an E-W direction. The four gauge sites are: Skykomish (1030'), twelve miles west of Stevens Pass; Stevens Pass (4070'), at the Cascade crest; Lake Wenatchee (2005'), fifteen miles east of the pass, and Peshastin (1050'), a site in the foothills east of the mountains. Precipitation amounts as a function of wind direction for the four stations are presented in Figure 1.22. From Figure 1.22, it is evident that the sites east of the Cascade crest receive considerably less

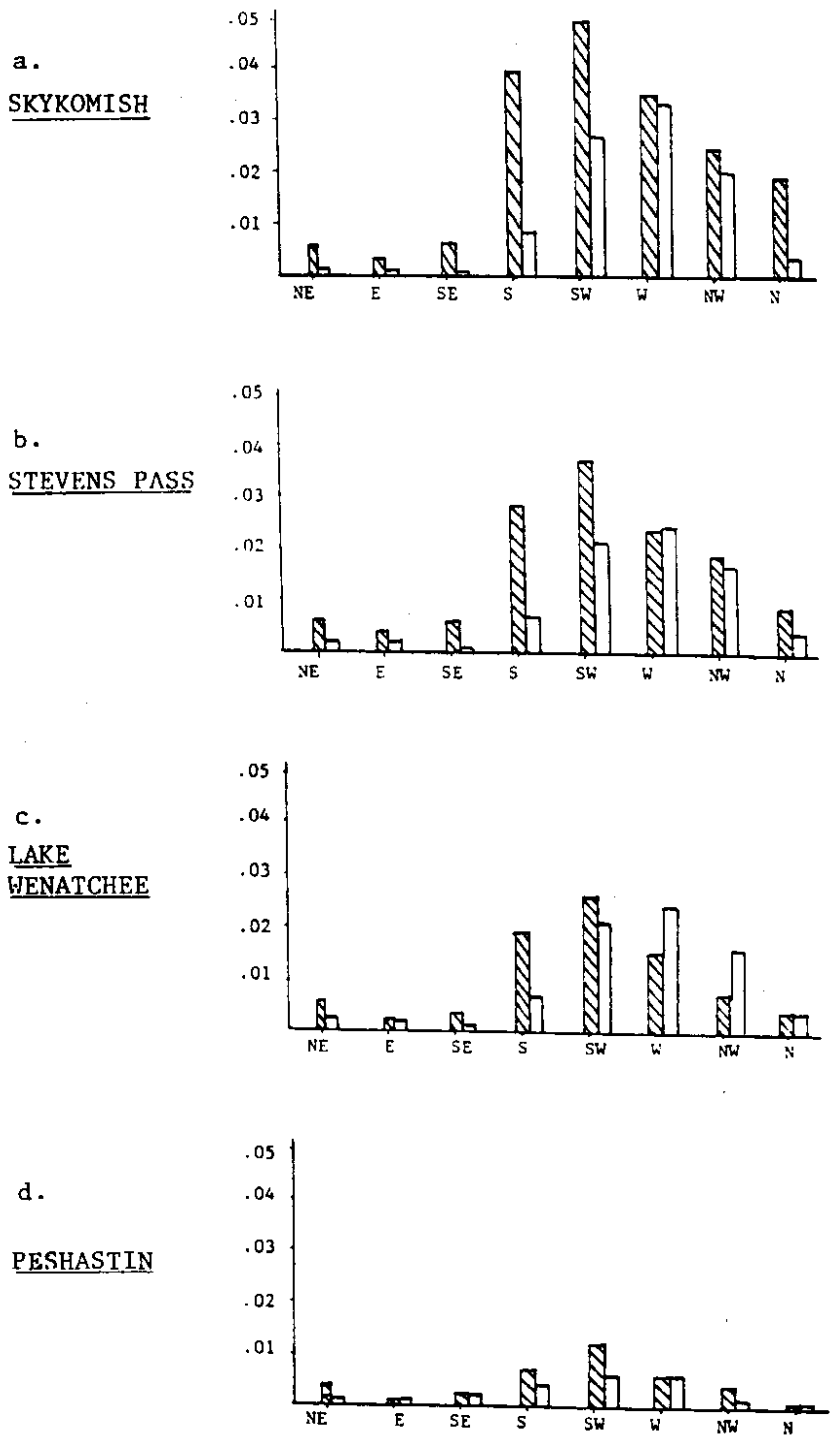

Figure 1.22 a-d Hourly precipitation rates as a function of wind direction for (a) Skykomish, (b) Stevens Pass, (c) Lake Wenatchee and (d) Peshastin. Shaded bars depict precipitation rates as a function of surface wind direction at Hoquiam. Plain bars indicate precipitation rates as a function of 850 mb level wind direction at Quillayute.

precipitation during all wind directions than Skykomish and Stevens Pass, and will therefore not be included in the following discussion.

The Skykomish/Stevens Pass hourly precipitation rate ratios associated with Hoquiam surface winds, presented in Figure 1.23 a, indicate that the two stations receive equal precipitation from N, NE, and SE winds. Stevens Pass receives more precipitation from E winds, while Skykomish receives more from the remaining S thru NW wind directions. During E winds, Stevens Pass, at the Cascade Crest, benefits from orographic lifting of air from the east slopes, while Skykomish is on the downwind side of the mountains. During the winter, strong inversions east of the Cascade Crest often trap cold moist air in which low clouds and fog develop. As this moist air is forced up the east slopes of the Cascades and thru the Cascade Passes, these areas receive orographically enhanced precipitation. This example contrasts previously discussed surface E wind ratios, in which warm overrunning clouds and moisture produced more precipitation at the site furthest west. Skykomish receives more precipitation during S through W and N directions. As previously discussed, Skykomish, which is closer to the moisture source in S through NW winds may benefit from initial orographic lifting of the airmass.

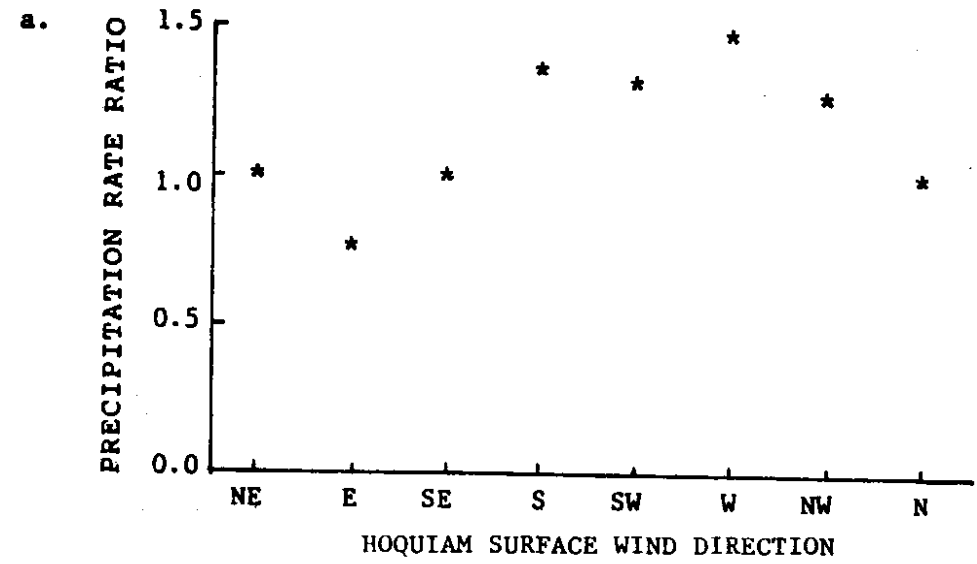

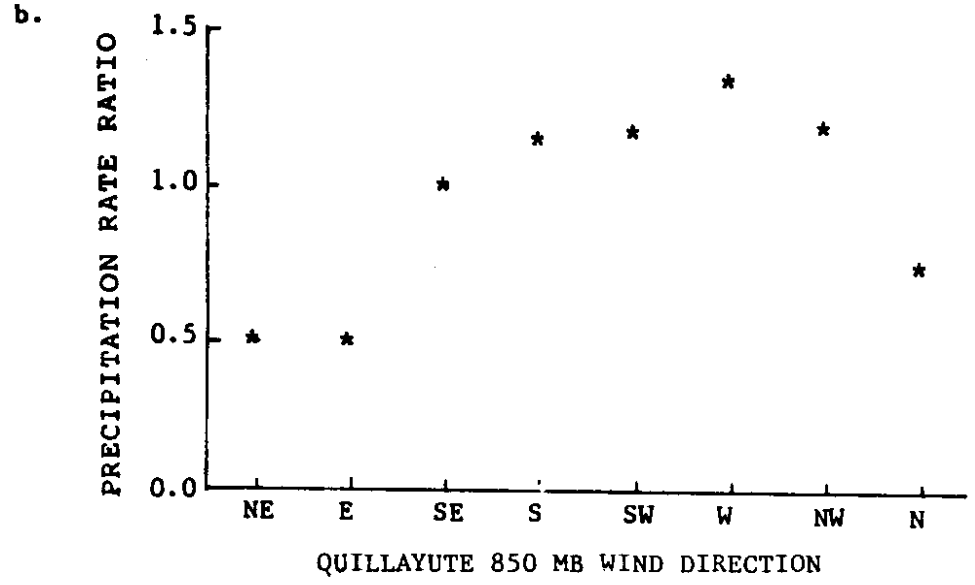

Figure 1.23 a,b Skykomish/Stevens Pass precipitation rate ratio as a function of (a) surface wind direction at Hoquiam and (b) 850 mb level wind direction at Quillayute.

The precipitation rate ratios from the Quillayute 850 mb winds for Skykomish/Stevens Pass shown in Figure 1.23 b demonstrate a pattern very similar to the surface wind ratios.

1.6. PUGET SOUND CONVERGENCE ZONE

Under certain atmospheric conditions, air flowing around the Olympic Mountains converges in Puget Sound (Fig. 1.24). This phenomena, known as the Puget Sound Convergence Zone (PSCZ), has been analyzed by Mass (1981). During convergence zone events, enhanced cloudiness and precipitation associated with the line of convergence is situated in an E-W band across Puget Sound, with generally cloud-free regions to the north and south of the convergence clouds. Forecasters have observed that convergence zones extend eastward to the Washington Cascades; however, the effect of the convergence cloudiness on precipitation quantities in the Cascades has not been quantified. In the following discussion, a precipitation pattern map produced from PSCZ criteria for Hoquiam surface winds will be presented, and two case studies analyzed.

Mass (1981) concluded that wind speed and direction on the Washington coast were key parameters in determining the formation of a PSCZ. For 10 cases studied, most convergence zone events occured when the Hoquiam surface wind direction was between 250 and 320, with the wind speed from 6-15 kts for several hours. Most

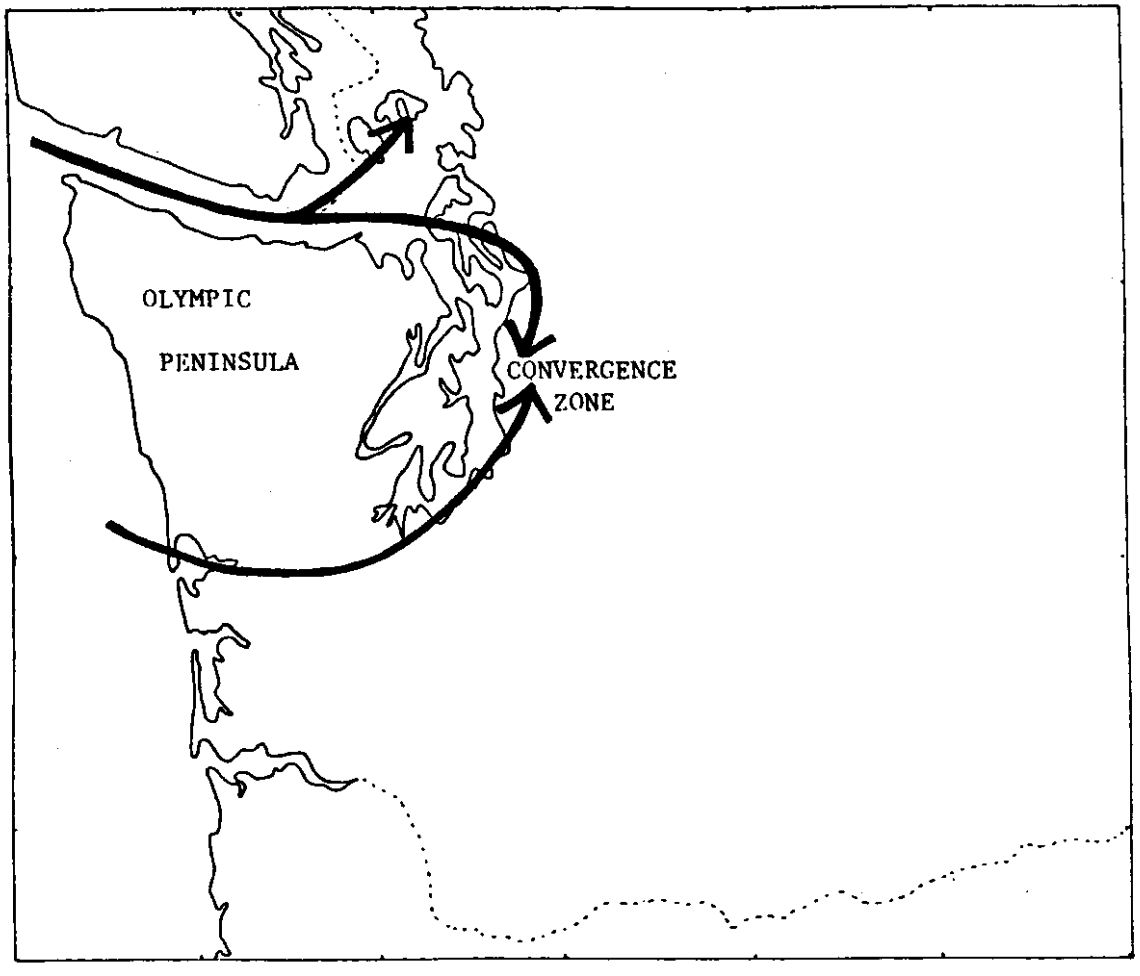

Figure 1.24 Surface windflow pattern for a typical Puget Sound Convergence Zone.

PSCZs occur after a cold- or occluded-frontal passage, because as the wind shifts from south to west or northwest, it falls into the critical direction category. However, it is possible for a PSCZ to occur without an associated frontal passage.

Mass tested the following coastal surface wind criteria for 23 convergence zone cases during January, February, April, and May 1978: Hoquiam wind direction, 260-320; Hoquiam wind speed, 5-15 kts; and duration, 4 hours. He found that the criteria predicted all but one of the cases, however, the criteria forecast 7 cases that did not occur. Mass states that most of these 7 cases only marginally fit the criteria (short duration or weak winds).

Using coastal surface wind criteria similar to Mass, a composite precipitation pattern map was produced from hourly records during the months December, January, February, and March from 1977 through 1981. The map in Figure 1.25 is based on Hoquiam surface wind directions from 270-330, wind speeds greater than or equal to 8 kts, and durations greater than or equal to 3 hours. Precipitation quantities are given in inches per hour. Central Puget Sound experiences a precipitation maximum relative to the drier regions north and south. A precipitation maximum near Stampede and Snoqualmie Passes

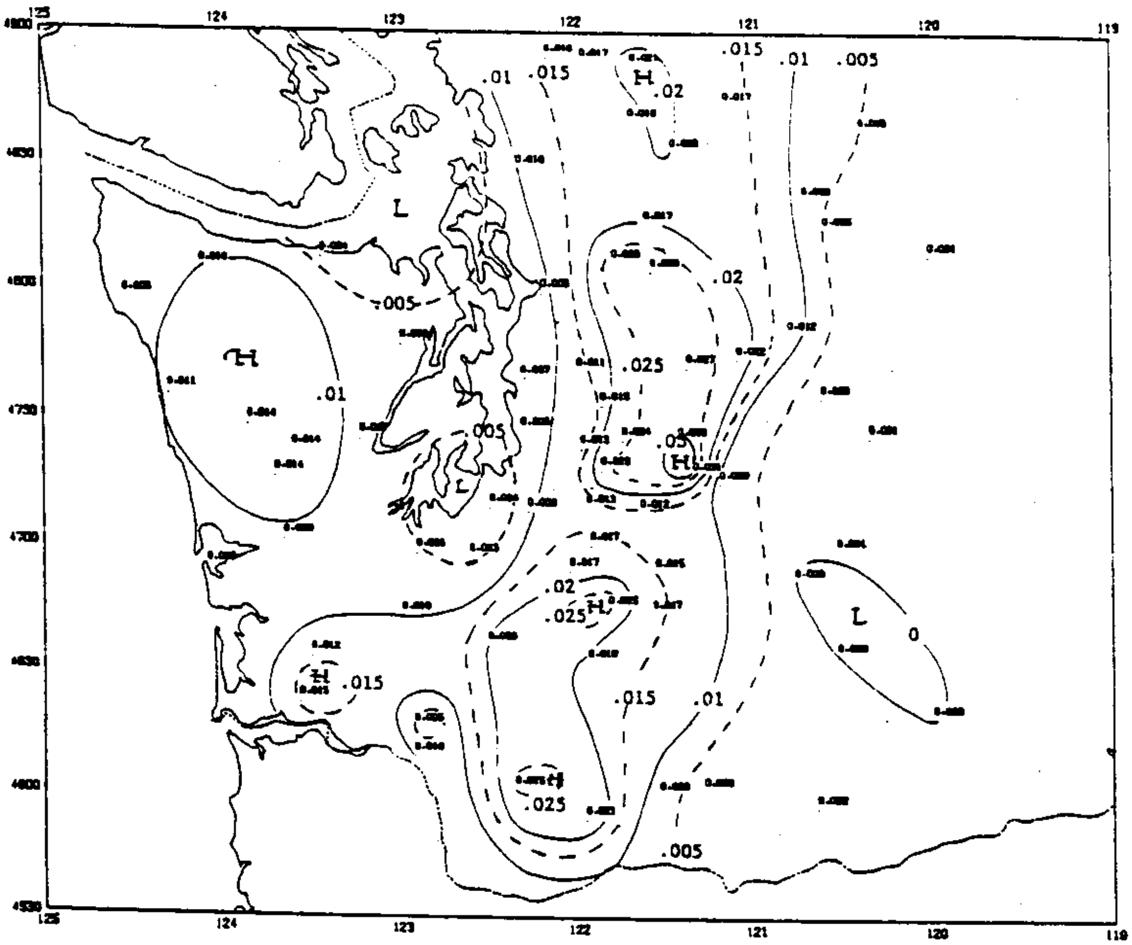

Figure 1.25 Mean hourly precipitation pattern map for <u>Puget Sound convergence Zone</u> events that fit the following criteria: Hoquiam surface wind direction from 270-300, wind speeds greater than or equal to 8 kts and duration greater than or equal to 3 hours.

indicates that the convergence extends to the Cascades.

A PSCZ case from 13 November 1984 is presented in Figure 1.26. Precipitation quantities are given in hundredths of an inch for the 24 hour period ending at 16 GMT 14 November. There is a very pronounced precipitation maximum extending from northern Elliott Bay in Seattle, east thru Lake Sammamish to Skykomish and Stevens Pass.

The synoptic weather conditions associated with this well defined PSCZ fit typical convergence criteria. Hoquiam surface winds remained between 260 and 310 at 8-14 kts from 20 GMT Nov. 13 to 3 GMT Nov. 14. Figure 1.27 shows the surface wind pattern for 0 GMT Nov. 14. W to NW winds existed along the entire Washington coast, with Hoquiam reporting NW winds of 10 kts. The well developed convergence line over Seattle is illustrated by the surface winds. The satellite photo for 0 GMT the 14th shows enhanced cloudiness associated with the line of convergence extending eastward across Puget Sound to the Cascades.

The precipitation pattern map for a PSCZ case from 24 February 1985 is presented in Figure 1.28. A cold front moving onto the Washington Coast at 12Z on the 24th produced a marked windshift at Hoquiam from SW to WNW, with sustained WNW winds from 11-25 kts for the next 12 hours. From Auburn radar data at 1225 GMT the 24th

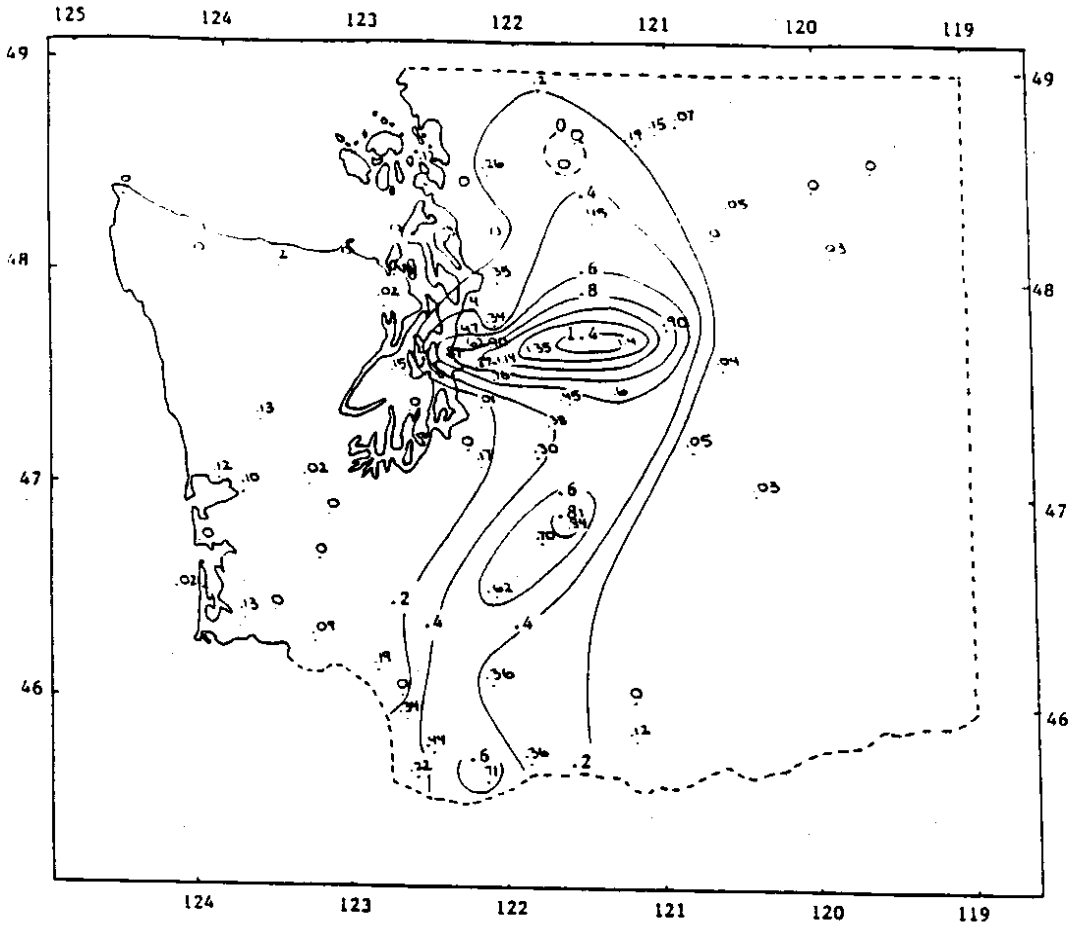

Figure 1.26 Precipitation map for the 13 November 1984 Puget Sound Convergence Zone event. Precipitation quantities are in inches of water equivalent for the 24 hour period ending at 0800 PST 14 November. The solid line contour interval is .2 inches of water equivalent.

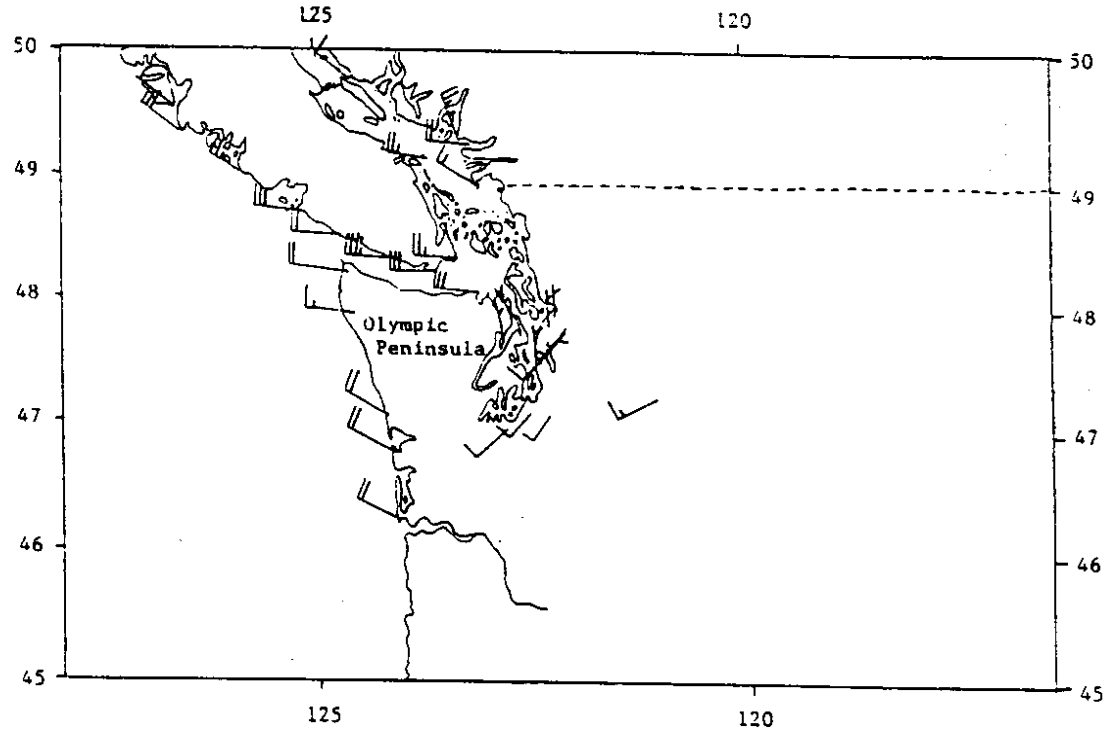

Figure 1.27 Surface wind observations for 0 GMT 14 November 1984.

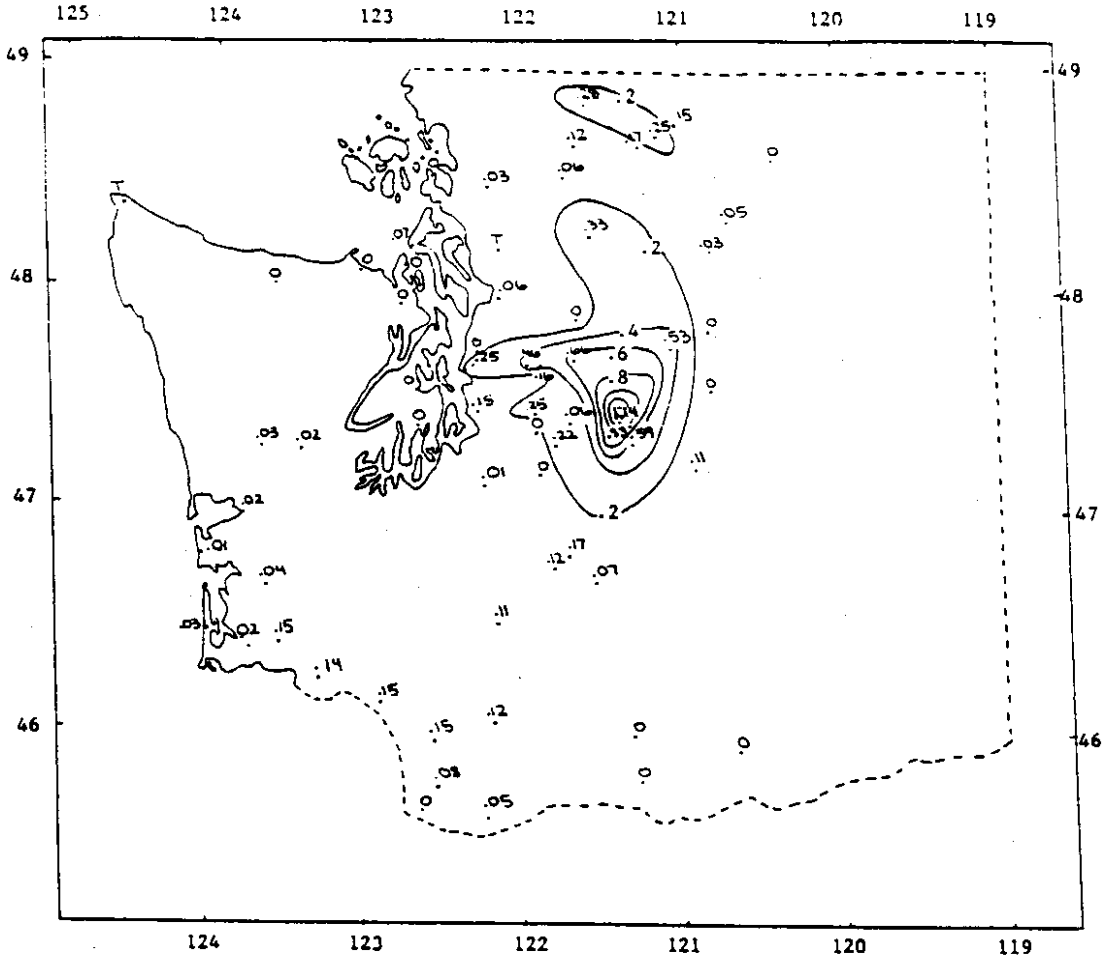

Figure 1.28 Precipitation map for the 24 February 1985 Puget Sound Convergence Zone event. Precipitation quantities are in inches of water equivalent for the 24 hour period ending at 0800 PST 25 February. The solid line contour interval is .2 inches of water equivalent.

(Figure 1.29a), an extensive precipitation area is evident throughout western Puget Sound and along the Cascades from the Canadian border south to Seattle. The precipitation area shrank the next several hours as a convergence zone developed, until by 1625 GMT radar echoes stretched from Puget Sound to the Cascades (Fig. 1.29b). The convergence pattern continued into the night, with the primary precipitation area extending from Seattle toward Snoqualmie Pass, shown best in the radar echo from 2025 GMT 24 February (Fig. 1.29c).

It is evident from the 13 November and 24 February PSCZ events that convergence zones can significantly enhance precipitation at Snoqualmie and Stevens Passes. During the November 13th PSCZ event the Skykomish Valley and Stevens Pass received significantly more precipitation than did Snoqualmie Pass, however, the opposite was true during the Feb. 24th event. To produce accurate quantitative precipitation forecasts for the Cascade passes during convergence events, it is necessary to determine which pass will receive most convergence precipitation. The direction of the 850 mb flow might influence the position of the line of convergence relative to the two passes. On Feb. 24th, the Quillayute 850 mb winds shifted from 265 at 12 GMT to 305 by 0 GMT the 25th. During the morning, when the 850 mb winds were

a.

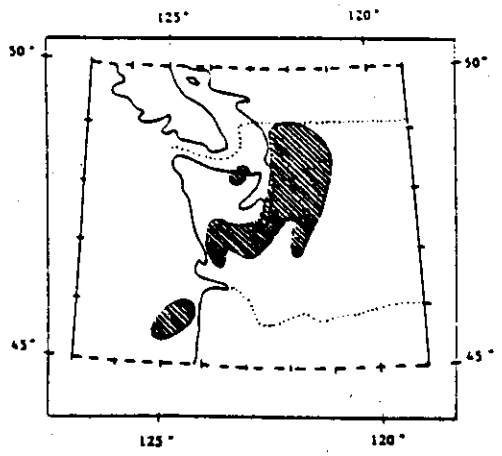

b.

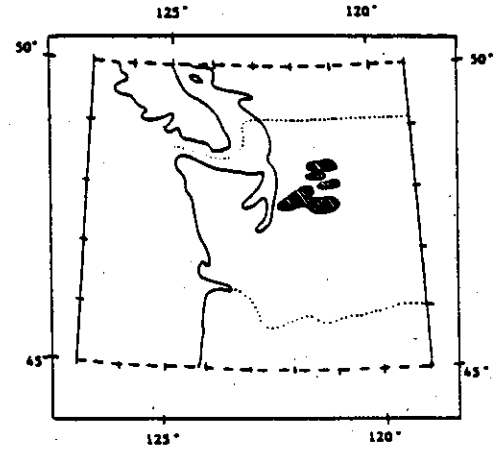

c.

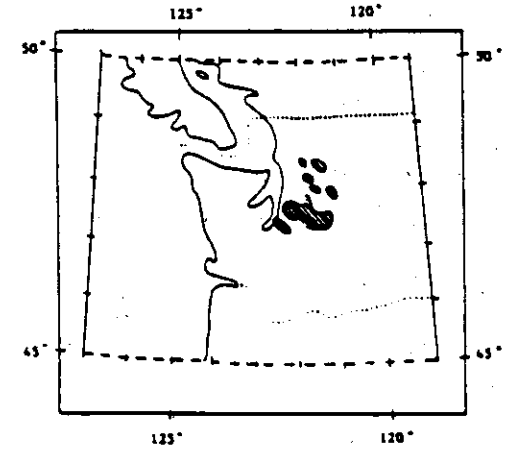

Figure 1.29 a-c Auburn radar data for 24 February 1985 at (a) 1225 GMT, (b) 1625 GMT and (c) 2025 GMT. The radar series depicts the development of a Puget Sound Convergence Zone.

westerly, Snoqualamie and Stevens Pass both received moderate precipitation. During the afternoon and evening, when the 850 mb winds were northwesterly, precipitation at Stevens Pass decreased, then stopped completely by 6 pm (PST), while at Snoqualmie Pass precipitation remained heavier and continued until 11 pm (PST). For the Nov. 13th convergence event this hypothesis fails. On Nov. 13th, the line of convergence extended E-W across Puget Sound when the Quillayute 850 mb winds were from the NW. Orographic precipitation from more PSCZ events needs to be analyzed before a correspondence between the 850 mb flow direction (or other parameters) and the location of convergence precipitation at the Cascade Passes can be verified.

Chapter 2. OROGRAPHIC PRECIPITATION MODEL

2.1. LITERATURE REVIEW

To predict or diagnose mesoscale variations in precipitation, a detailed mesoscale windfield is necessary. Such a mesoscale windfield can greatly deviate from the synoptic scale flow. For example, the surface drag changes markedly as the air flows from the ocean on to land, with friction causing the air to decelerate and turn. Topographic features produce airflow deflection around obstacles, blocking by barriers, and channeling through gaps or valleys. Thermal effects further influence the mesoscale windfield. Differential heating and cooling produce land-sea breezes and slope winds, while heating or lifting of potentially unstable air at low levels creates convective activity. The interaction of the mesoscale windfield with topography determines a vertical velocity field, which in turn, is a factor in precipitation.

Several types of models have been developed to account for terrain effects. Three dimensional primitive equation models (Pielke,1974; Mahrer and Pielke,1976; Nickerson and Magaziner,1976; Anthes and Warner,1978) produce realistic flow in complex terrain if the boundary

conditions and model initialization are sufficiently detailed. Although these models should give considerably better results than two-dimensional models, complex initialization problems at the model boundaries combined with the expense of running them makes their use on an operational basis unrealistic. For these reasons, a two-dimensional model is used in this work.

Two-dimensional models are either x-z or x-y models. The x-z models consider flow over a barrier of infinite length with no variation along the y-axis, which runs parallel to the barrier. The x-y models, which allow the use of realistic terrain, assume a specified vertical variation of meteorological parameters.

Sarker (1966,1967) and Elliott and Shaffer (1962) developed x-z models with parameterized precipitation, whereas, Fraser et al (1972) and Hobbs et al (1973) included microphysical processes in their x-z model for the Washington Cascades. Rhea(1978) developed a steady-state multi-layer x-z model for Colorado which considers realistic topography, but does not allow any variation in the wind direction. The model uses the observed 700 mb level wind direction to pick one of 36 terrain maps that correspond to each 10 of azimuth. Precipitation resulting from forced orographic lifting is calculated by following an airmass across the topography.

In the model, a constant precipitation efficiency is assumed, with the remaining condensate carried to the next grid point downstream. Evaporation of precipitation falling into unsaturated layers is included. Armstrong and Williams (1981) tested Rhea's model on 21 mountain sites in Colorado for the winter of 1979-80. The mean error (forecast-measured precipitation) for the entire winter was 5.6 mm with a standard deviation of 5.8 mm. However, Rhea (1978) found significant errors in individual cases, especially during March and April when convective activity increases.

The accuracy of precipitation forecasts from x-z models is limited because it is unrealistic to assume that the wind direction does not vary through complex terrain. Therefore, x-y models, which use realistic terrain, provide the simplest method for forecasting mesoscale winds and precipitation.

Several x-y two-dimensional models have been developed. Lavoie's (1972,1974) steady-state diagnostic primitive equation x-y model divides the atmosphere into three layers: the surface layer, characterized by a superadiabatic lapse rate; a thouroughly mixed planetary boundary layer topped by a distinct inversion or discontinuity; and an upper layer with a constant and stable lapse rate. The primitive equations are solved for

the planetary boundary layer (PBL) using vertically averaged variables. Lavoie's model incorporates the effects of the forced ascent of an airmass over topography, frictional convergence as air flows from water over land, and heat and moisture fluxes. For input, the model requires large scale geostrophic winds, a free atmosphere lapse rate, the change in temperature across the inversion on top of the PBL and the height of the PBL along the inflow boundary. Overland et al. (1979) base their Puget Sound wind model on Lavoie's model. Although the model duplicates the observed winds in several case studies, the PBL intersects the topography across much of the Olympics and Cascades, resulting in no calculated winds for these regions. Additionally, the model requires cases with well-mixed PBL's, and is very sensitive to the initialization heights of the PBL along the inflow boundary.

Danard(1971,1976a,1976b,1977) developed a single level diagnostic x-y model which is based on a simplified set of primitive equations (the continuity equation is not included) in sigma coordinates. Danard included the effects of orography, frictional convergence and heating on the surface wind in his 1976 version of the model. As input data, the model requires only a single radiosonde sounding and an inland surface temperature unaffected by

the land-water discontinuity. Mass(1981) described a modified version of the Danard model that includes diabatic heating and improved boundary conditions and numerics. Mass and Dempsey (1985) and Dempsey (1985) further refined the Danard and Mass models. The Mass and Dempsey windflow model, which provides the surface wind field for the orographic precipitation model presented in this thesis, is described in detail in the following section.

2.2. MASS AND DEMPSEY (1985) AND DEMPSEY (1985) WIND MODEL

The Mass and Dempsey wind model calculates surface wind and temperature by integrating the horizontal momentum equation and surface temperature tendency equation in sigma coordinates using a second-order Adam's Bashforth scheme. The horizontal momentum equation includes terms for advection, Coriolis acceleration, the pressure gradient force, frictional drag and horizontal diffusion. Changes in surface temperature occur by temperature advection, adiabatic heating and cooling in response to changes in surface pressure, diabatic heating and cooling and horizontal diffusion. Surface pressure, an unknown in both equations, is calculated by integrating the hydrostatic equation between the surface and a reference pressure level. Model initialization requires the geopotential height and temperature at a reference level (usually 850 mb), taken from the National Meteorological Center (NMC) analysis for the model domain, and the free atmosphere lapse rate between 850 and 700 mb taken from a sounding near the inflow boundary. The model equations are integrated to steady state using a time step of 180 seconds, requiring approximately 160 time steps. The model is run on a 75x74

point grid with a 7.5 km resolution. Although a higher resolution would be preferable for the precipitation model, the hydrostatic balance assumed for the wind model by Mass and Dempsey limits the possible grid length reduction. Model initialization, integration and graphics requires approximately 30 seconds on the CRAY1 at NCAR if a 75x74 point grid is used and the average tendencies of the wind components are required to fall below 10^{-5} ms^{-1} .

2.3. PRECIPITATION MODEL DESCRIPTION

The orographic precipitation model addition to the Mass-Dempsey wind model assumes that precipitation is proportional to vertical velocity. In this section, the methods used to calculate the vertical velocity field are outlined, followed by a discussion of the precipitation parameterization.

A. VERTICAL VELOCITY CALCULATION

The model vertical velocity can be decomposed into three individual vertical velocity components: the slope induced vertical velocity, which is the vertical component of the wind vectors from the Mass-Dempsey wind model; convergence vertical velocity, again from the wind model; and an imposed wind field vertical velocity, which is the vertical component of a separate geostrophic windfield imposed on the model terrain.

The Mass-Dempsey sigma coordinate model produces a slope parallel surface wind field. The vertical component of the wind vectors are calculated at each grid point in the domain using a method similar to Danard's (1976). h_1, h_2, h_3 and h_4 are the average heights of the terrain grid points surrounding the wind vector (U) and dx and dy are

the distances between adjacent grid points in the x and y direction, respectively (Fig. 2.1a). The slopes dh/dx and dh/dy are calculated such that:

$$\frac{dh}{dx} = \frac{h_2 + h_4}{2} - \frac{h_1 + h_3}{2} \qquad (1)$$

$$\frac{dh}{dy} = \frac{h_1 + h_2}{2} - \frac{h_3 + h_4}{2} \qquad (2)$$

From dh/dx and dx, the hypotenuse of the right triangle shown in Figure 2.1b is calculated:

$$hypx = \sqrt{\left(\frac{dh}{dx}\right)^2 + (dx)^2} \qquad (3)$$

It follows that:

$$\frac{u}{hypx} = \frac{wsx}{\frac{dh}{dx}} \qquad (4)$$

Rearranging terms gives:

$$wsx = u \frac{dh}{dx} / hypx \qquad (5)$$

wsy is calculated using a similar logic:

$$wsy = v \frac{dh}{dy} \Big/ \sqrt{\left(\frac{dh}{dy}\right)^2 + (dy)^2} \qquad (6)$$

a.

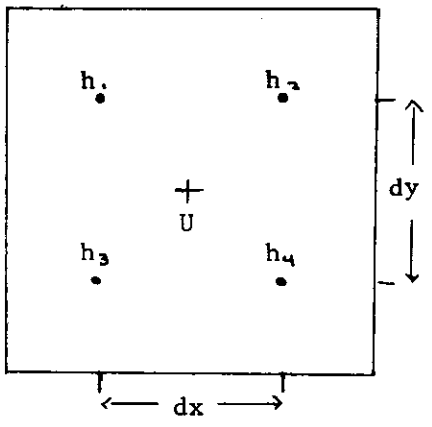

b.

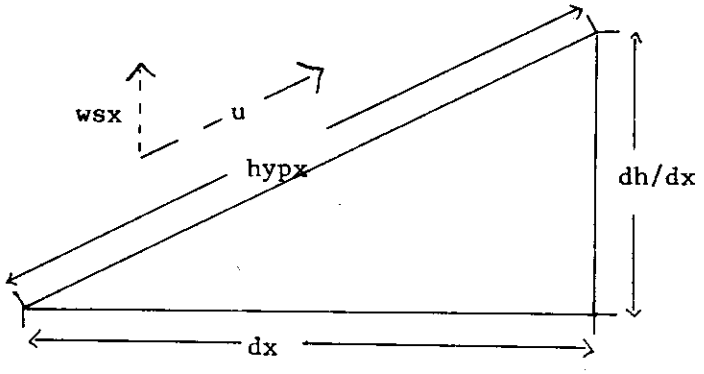

Figure 2.1 a. Grid height configuration for vertical velocity calculation
b. Wind vector (u) and vertical velocity (w_{sx}) relation to terrain parameters dx and dh/dx

ws, the slope induced surface wind vertical velocity, is the sum of the vertical components wsx and wsy.

$$ws = wsx + wsy \tag{7}$$

The vertical velocity from convergence is calculated using the velocity divergence form of the continuity equation.

$$\frac{1}{\rho}\frac{d\rho}{dt} + \nabla \cdot U = 0 \tag{8}$$

Expanding $\nabla \cdot U$ and assuming incompressibility gives

$$\frac{\partial w}{\partial z} = -\left(\frac{\partial u}{\partial x} + \frac{\partial v}{\partial y}\right) \tag{9}$$

where $\partial w / \partial z$ is the vertical velocity at the surface from convergence. $\partial u/\partial x + \partial v/\partial y$ are calculated from the u and v wind components generated by the Mass-Dempsey model. Surface wind convergence is assumed to decrease linearly with height (H), becoming zero when H=2000m. This figure was chosen because it is consistent with the 2000m topographic influence assumption in the Mass-Dempsey wind model. The component of the vertical velocity from convergence is found by integrating $\partial w / \partial z$ from the

surface to 2000 m.

The winds produced by the Mass-Dempsey model result from the interaction of the surface flow with complex terrain. In high elevation terrain, momentum from higher levels in the atmosphere is also felt; therefore, a separate wind field representing the large scale flow is imposed on the model terrain. The large scale wind field has a constant wind direction with height, taken as the 850 mb level wind direction from the Quillayute radiosonde ascent for the time corresponding to the model run. The variation of wind speed with height, which changes from case to case, fits the vertical wind profile measured by the radiosonde ascent. In order to eliminate the effect of the surface flow from the large scale windfield, the surface wind speed taken from the sounding is subtracted at all levels from the vertical wind speed profile. At each grid point, a wind speed that depends on grid point elevation is assigned. The vertical components of the wind vector (w_{LSx} and w_{LSy}) are then calculated.

$$w_{LSx} = u_{LS}\frac{dh}{dx} \qquad (10)$$

$$w_{LSy} = v_{LS}\frac{dh}{dy} \qquad (11)$$

u_{LS} and v_{LS} are the u and v components of the large scale

wind field. w_{LS}, the vertical velocity resulting from the large scale wind field, is the sum of the vertical components w_{LSx} and w_{LSy}:

$$w_{LS} = w_{LSx} + w_{LSy} \qquad (12)$$

The w_{LS} calculation was tested with 7.5x7.5 and 15x15 km terrain grids. The positioning of the 15x15 km terrain grids relative to the wind vector was varied in several test runs. Three positions tested (Fig. 2.2) placed the wind vector: 1) in the center of the terrain grid, 2) 3.75 km in from the upwind border of the terrain grid and 3) 3.75 km inside the downwind grid boundary. A comparison of these different methods is found in Chapter 2.4.

In very stable air masses, air parcels forced over a barrier will sink symmetrically on the barrier's leeward side. In these cases, the total vertical velocity at each grid point is the sum of ws, w_{LS} and wc. In a neutral or slightly stable atmosphere, a lifted air parcel will remain near the level it is lifted to with only slight downward motion on the lee side. Therefore, negative components of ws, w_{LS} and wc are divided by 2 before the total vertical velocity at each grid point is summed. This assumption is an attempt to compensate for the lack

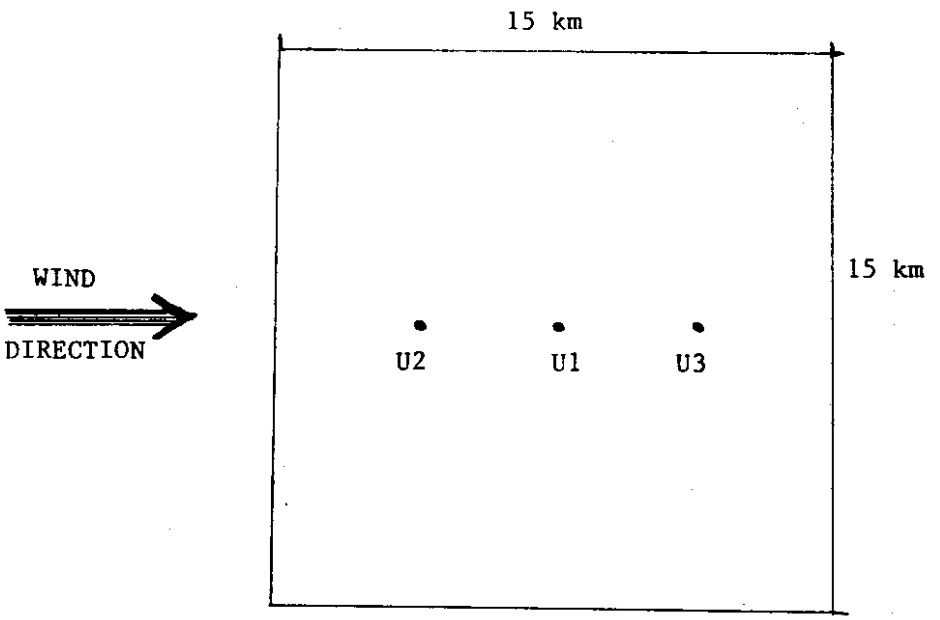

Figure 2.2 Three wind vector positions (U1, U2, and U3) relative to a 15 by 15 km terrain grid that were tested in the large scale wind field vertical velocity calculation.

of three-dimensionality in the model. Although a rigorous investigation of this assumption might result in a more precise factor value, division by 2 markedly improves the model results.

B. PRECIPITATION PARAMETERIZATION

In the model, precipitation is assumed to be directly proportional to vertical velocity. A very simple precipitation parameterization scheme is employed.

Condensation is given by:

$$C = w_{Total} \cdot \frac{dq_s}{dz} \cdot D \cdot t \qquad (13)$$

where D (1500m) is the depth of the lifted airmass and t is the length of time that the airmass is lifted. t varies from case to case depending on the duration of precipitation. dq_s/dz, the change in the saturated mixing ratio with height, can be taken directly from the pseudo-adiabatic chart or can be calculated using

$$\frac{dq_s}{dz} = \left(\Gamma_m - \Gamma_a\right) \frac{c_p}{L} \qquad (14)$$

where c_p is the specific heat of dry air at constant pressure, L is the latent heat of vaporization, and Γ_m

and Γ_d are the moist and dry lapse rates, respectively.

If all the precipitation that forms falls in the same grid where it is generated, precipitation (P_T) equals:

$$P_T = C \times E_1 + P_S \qquad (15)$$

assuming a constant condensation to precipitation efficiency (E_1). E_1 equals .5 in the two cases presented in Chapter 2.4. This value was chosen as an average of the mean condensation to precipitation efficiencies that Elliott and Shaffer (1962) calculated for the Santa Ynez (E=.35) and San Gabriel (E=.67) Mountains in California. P_S is the synoptic precipitation term, ie, the amount of precipitation that falls over the ocean or flat terrain.

Under strong wind conditions, or in winter when precipitation may fall as snow, it is unrealistic to assume that all precipitation falls vertically to the ground. Additionally, small cloud droplets and ice particles may get carried considerable distances downwind before they precipitate or evaporate. To account for particle fall trajectories and non-precipitating cloud droplets, a constant percentage of the condensation (R) in each grid is carried to the next grid downwind where it is combined with the condensation generated at that

grid point. R is calculated as follows:

$$R=(C-CxE_1)xE_2 \qquad (16)$$

E_2 is the condensation carrying efficiency, defined as the % of remaining condensate that is carried by the wind to the next grid downwind. E_2 is given a value of .75 for the two cases presented in Chapter 2.4; however, the total precipitation calculation is not very sensitive to the value of E_2. Taking account of R, precipitation equals

$$P_T=E_1(C+R)+P_S \qquad (17)$$

The precipitation calculation starts at the upwind border of the domain and progresses in the direction of the large scale flow.

Thus far, the precipitation calculation assumes that the amount of moisture available for condensation is constant across the domain. For several predominant wind directions, ie SW to NW, the Cascades act as an efficient moisture barrier, with the saturated mixing ratio decreasing as an airmass moves eastward. A comparison of Quillayute and Spokane soundings verifies this assumption. F, a moisture depletion factor, is included

in the precipitation calculation. For SW to NW wind directions, F is assigned such that condensation decreases by 30% from the Washington Coast to the eastern domain boundary.

$$P=E_{1}(CxF+R)+P_{s} \qquad (18)$$

2.4. MODEL SIMULATIONS

The model was run for an area of the Pacific Northwest from 45° to 50° N latitude and from 119-126.4° W longitude. The domain, which encompasses the Olympic and Cascade Mountains, is ideal for testing an orographic precipitation model because of the large variations in precipitation. The Olympics, on average, receive over 200 inches of rainfall annually, while the lowlands to the northeast only receive 20 inches. Mean annual precipitation in the Cascades varies from over 140 inches near Mts Rainier, Baker and St. Helens and over 170 inches near the crest in the north central Cascades to 10 inches east of the Cascade Mountains. Although this region has numerous low elevation precipitation measurement sites, the number of high elevation gauges is limited. Verification of a precipitation model in mountainous terrain is further complicated by the difficulty in getting accurate or representative precipitation measurements. Court (1960), measuring precipitation adjacent to a sharp ridge in the Santa Ynez region in California, found that two gauges approximately 10 feet apart gave seasonal totals that varied by one-third. Although this example is extreme, precipitation measuring sites within a few miles of each

other near Snoqualmie Pass regularly indicate different water equivalencies (Marriott and Moore,1984).

The model domain is divided into a 75 by 74 point grid, with each grid square measuring approximately 7.5 km on a side. Collier (1977), using a numerical model in which precipitation is proportional to vertical velocity, determined that a 1 km grid length gave accurate vertical velocity and precipitation estimates over North Wales. He found that longer grid lengths, which effectively smoothed the topography, resulted in decreasing model precipitation. In the Pacific Northwest, even with a 7.5 km grid, the model precipitation is considerably more detailed than the data available for verification. The average height of each grid square is calculated from 30 second terrain data available through NCAR (refer to Appendix C). The smoothed terrain is shown in Figure 2.3. A description of the area's geography is given in Chapter 1.1.

During the month of November 1984, a continuous series of weather systems moved through the Pacific Northwest and produced significant amounts of new snow in the mountains. On December 1st Mt Baker, Paradise on Mt Rainier and Snoqualmie Pass recorded over 230% of normal snow depth. The precipitation model results for two November 1984 cases are presented in this section. A

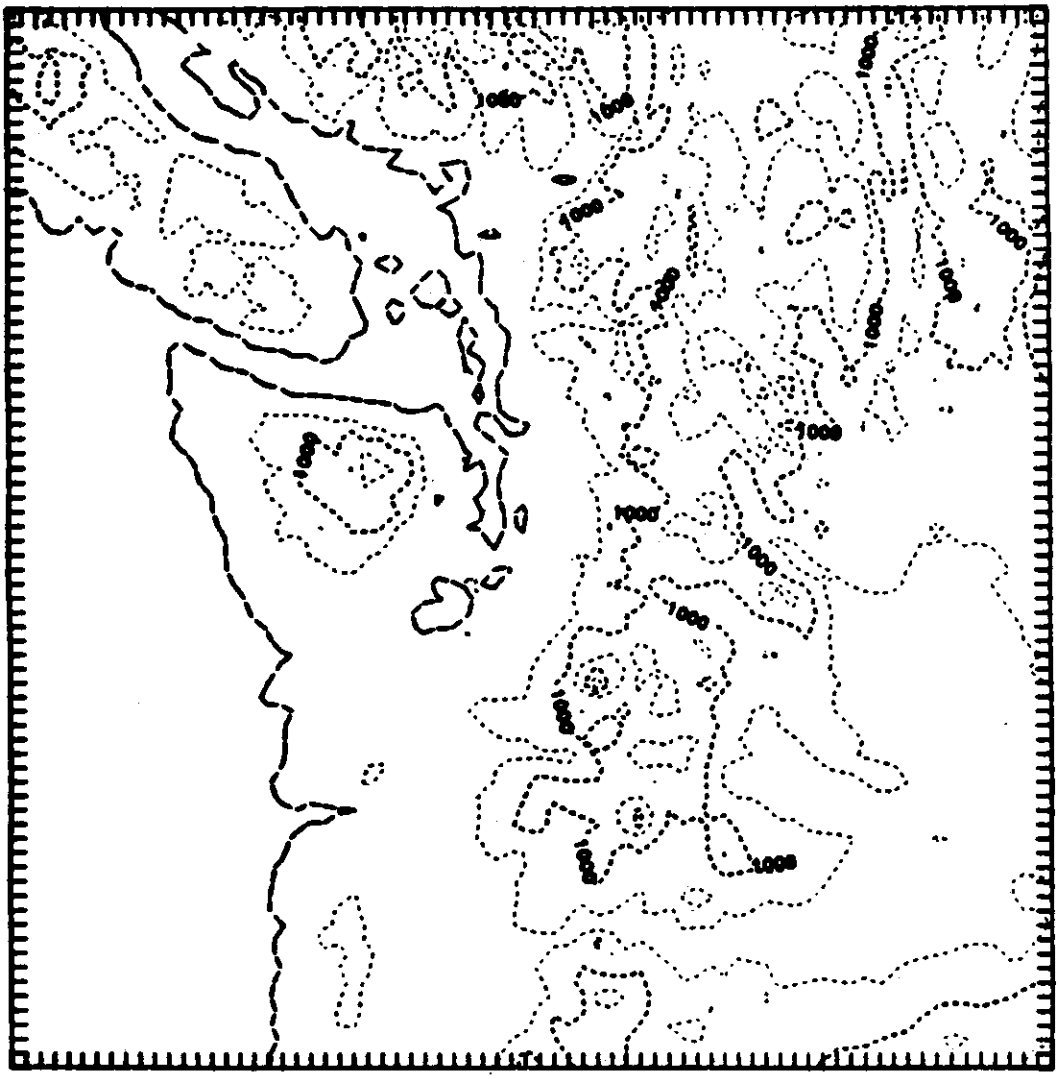

Figure 2.3 Smoothed topography used for precipitation model runs. Contour interval is 500 m.

moist southwesterly flow aloft characterizes the first case, while a more showery northwesterly flow aloft and well defined convergence zone in Puget Sound occured in the second case.

A. CASE 1: NOVEMBER 7, 1984 at 00 GMT SOUTHWESTERLY LARGE-SCALE FLOW

A cold front crossed western Washington around 14 GMT on November 6th. Winds at Hoquiam on the Washington coast shifted from E to SW at frontal passage, and remained SW until 05 GMT on November 7th, at which time coastal winds became more southerly. Surface pressures, lowest at 14 GMT on the 6th, continued to rise through 09 GMT November 7th. At the 500 mb level, a trough of low pressure extended from the Gulf of Alaska southward off the west coast from November 5th through the 8th. The model run was for 00 GMT November 7th. The corresponding 850 mb analysis is presented in Figure 2.4a. At 850 mb, a SW flow of 30-35 kts existed over the model domain with a trough of low pressure at 130° W longitude and a flat ridge of high pressure centered along 119° W longitude. The sounding for 00 GMT November 7th at Quillayute is shown in Figure 2.4b. A nearly saturated adiabatic lapse rate exists from the surface to 807 mb.

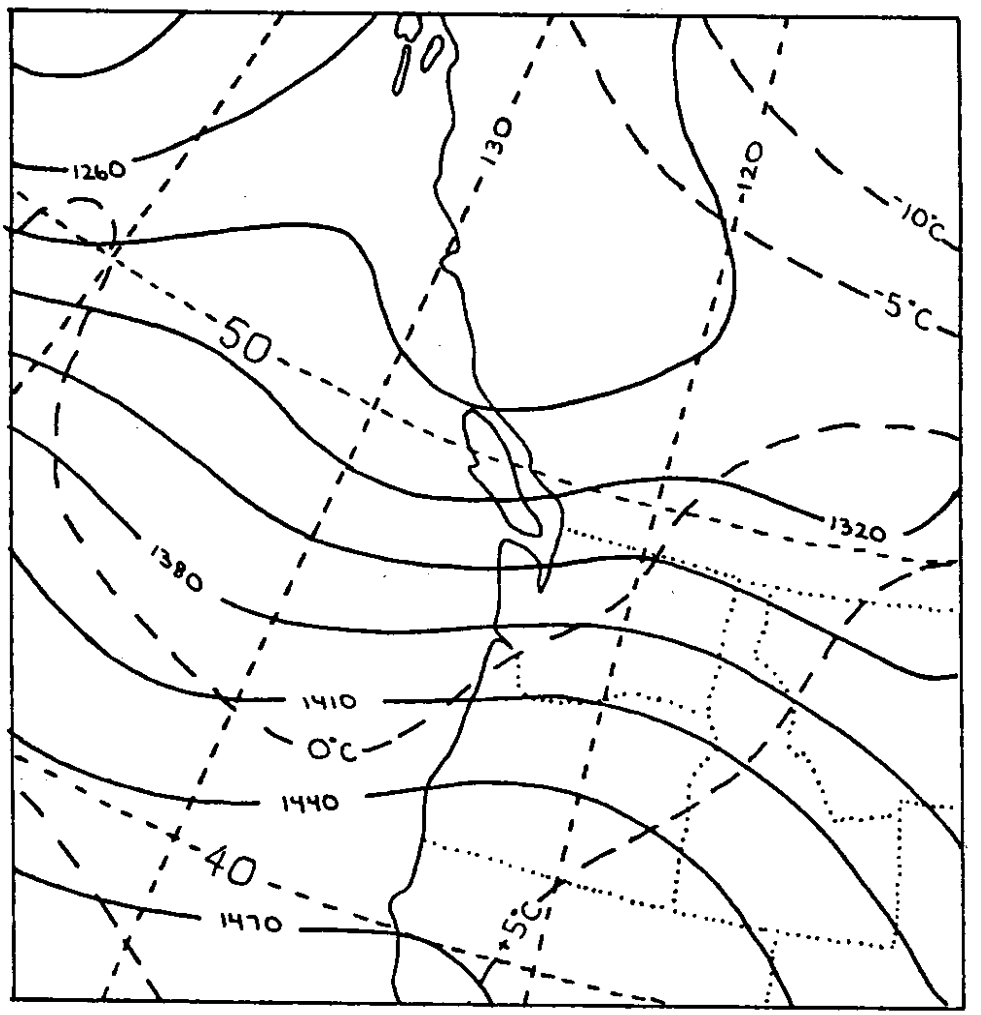

Figure 2.4.a NMC 850 mb height and temperature analysis for 00 GMT November 7, 1984. Height contours (solid lines) are in meters and temperature contours (heavy dashed lines) are in °C.

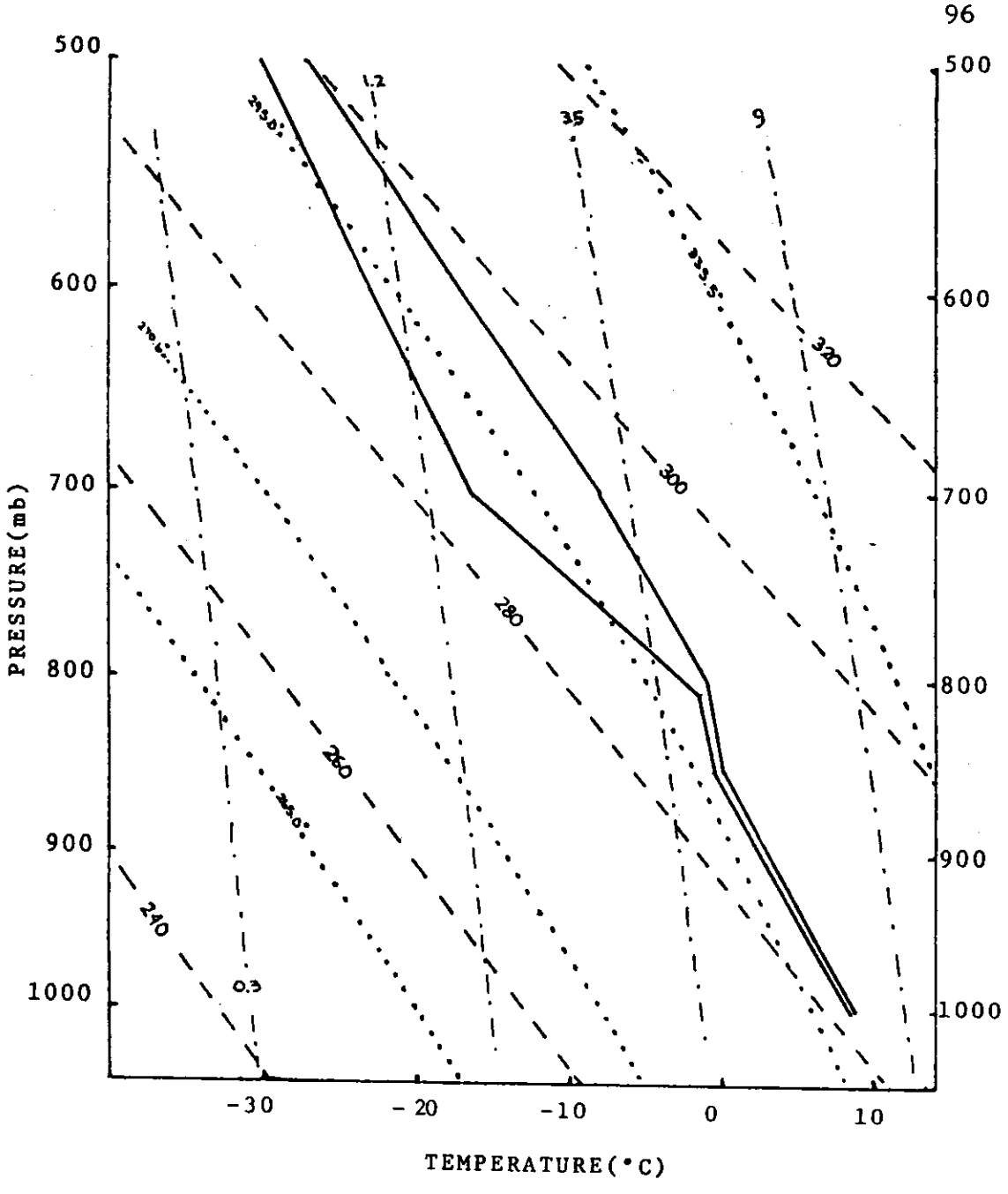

Figure 2.4.b Quillayute, Washington radiosonde sounding for 00 GMT November 7, 1984.

Figure 2.4c shows the observed surface winds. 10-25 kt winds prevailed along the coast and at Stampede Pass, while more southerly winds occured in Puget Sound and east of the Cascades. The winds in the Strait of Georgia were southeasterly. The Mass-Dempsey wind model run (Fig. 2.4d) duplicates the SW winds along the coast and the more southerly winds in Puget Sound and east of the Cascades; however, the model produces relatively strong SW winds down the leeward side of Vancouver Island and across the Strait of Georgia instead of reproducing the measured SE winds. Verification of the surface winds in the mountains is difficult because Stampede Pass is the only wind measurement available.

The vertical velocity fields from the surface wind field, convergence and the large scale wind field are presented in Figures 2.4 e-g. Figure 2.4h shows the total vertical velocity field. In Figures 2.4 e-h the contour interval is .2 m/sec. The surface wind and convergence vertical velocities were calculated with a 7.5 by 7.5 km grid; however, the large scale wind field vertical velocities were calculated with a 15 by 15 km grid with the wind vector 3.75 km inside the upwind terrain boundary. This method produced the best results; however, the large scale vertical velocity calculation was also run with a 7.5 by 7.5 km grid, and with 15 by 15 km grids

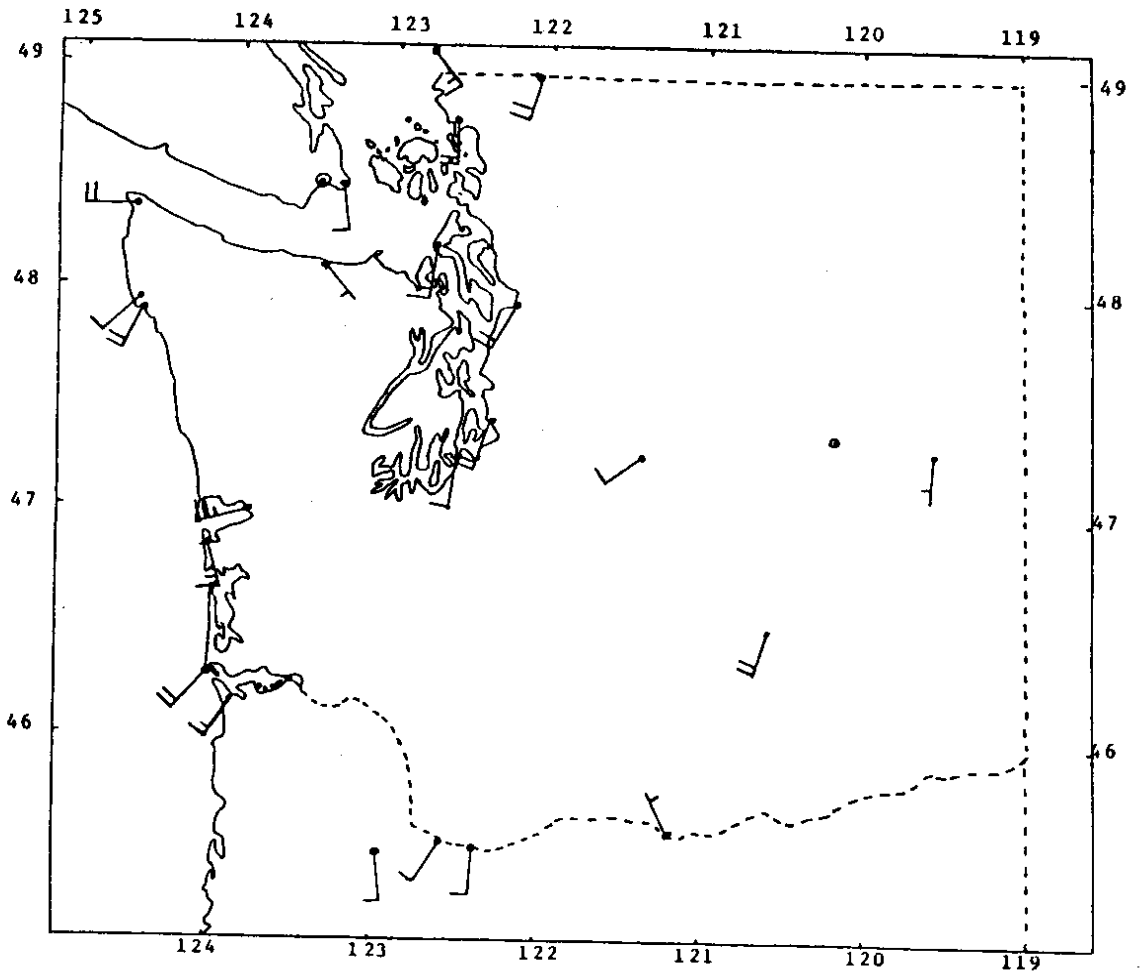

Figure 2.4.c Observed surface winds for 00 GMT November 7, 1984. On the wind flags, half barbs indicate 5 kts and full barbs equal 10 kts.

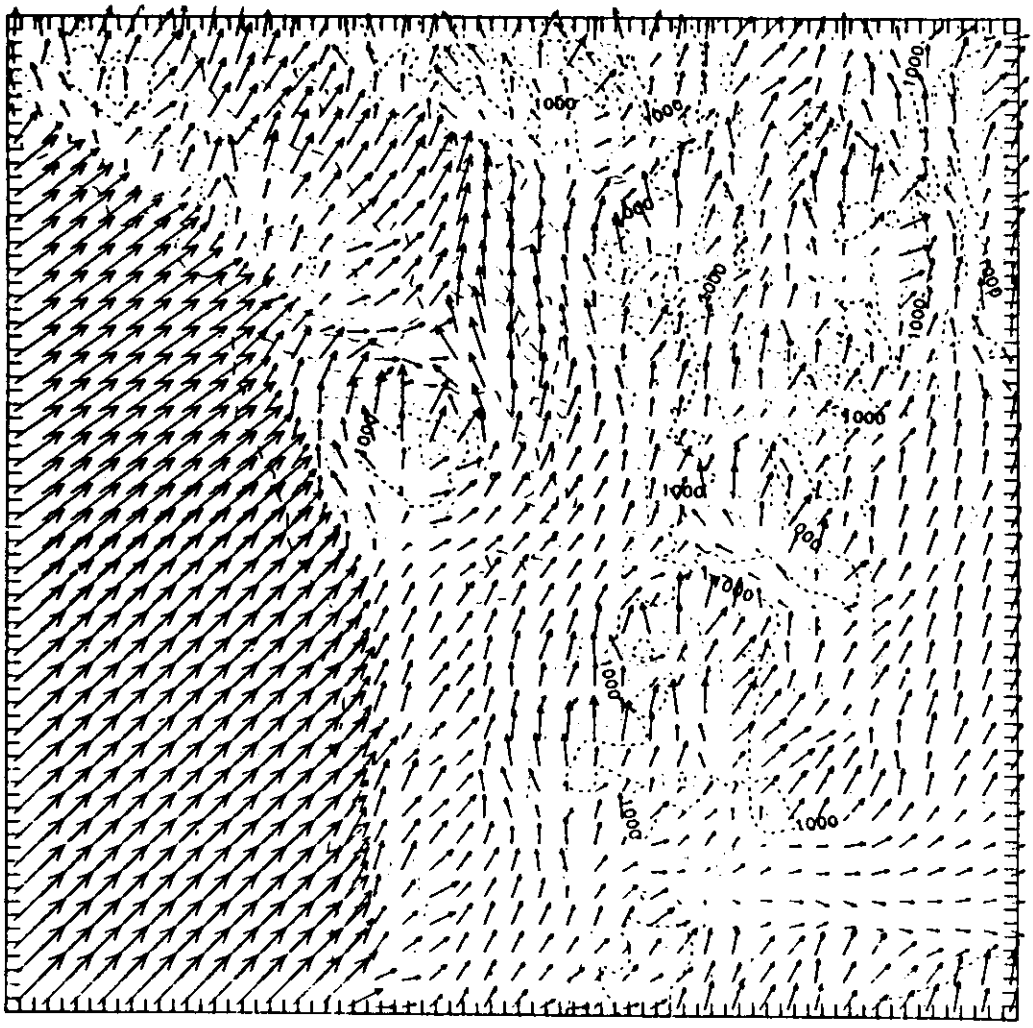

Figure 2.4.d Surface winds from Mass-Dempsey wind model run for 00 GMT November 7,1984.

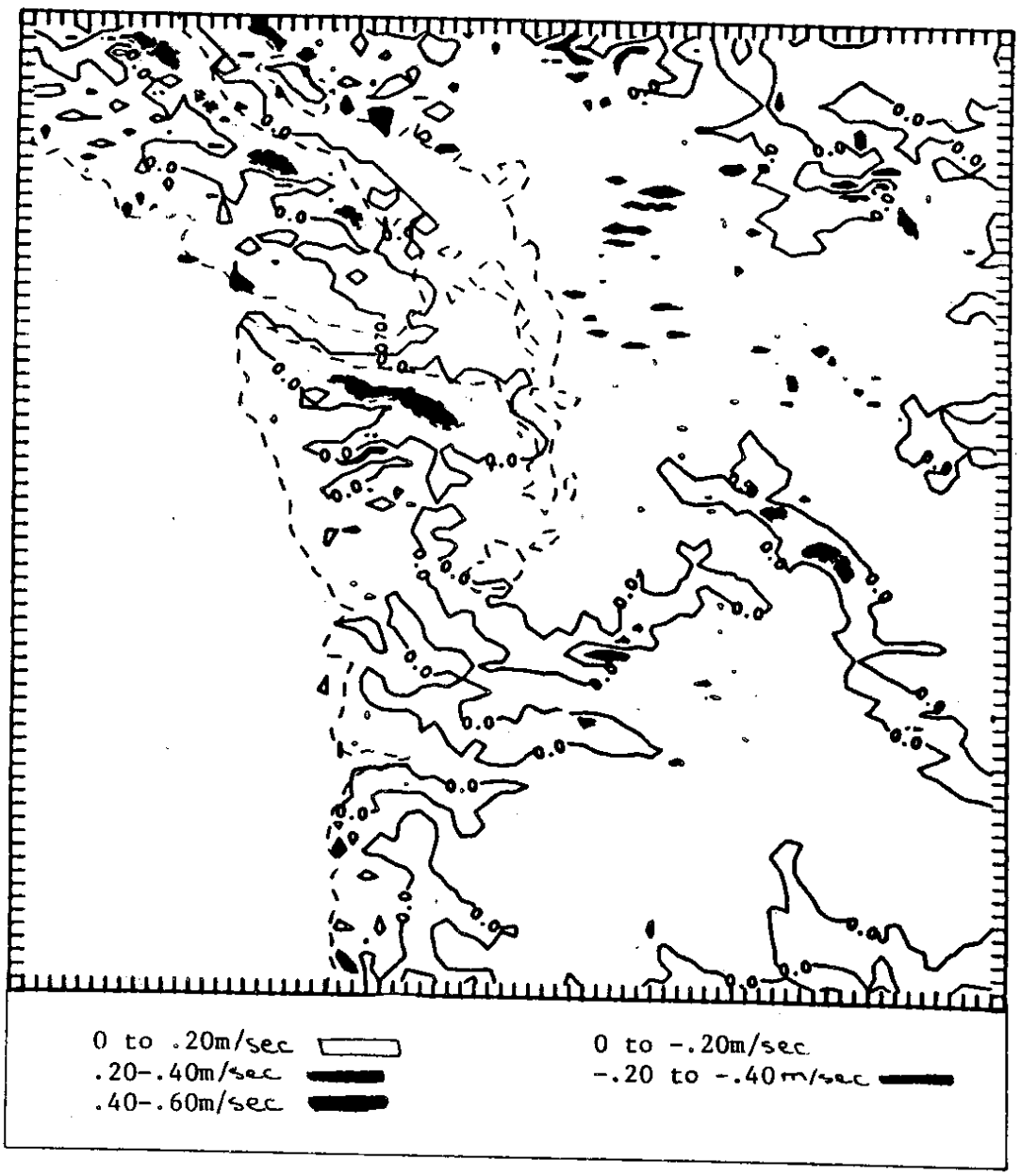

Figure 2.4.e Slope induced vertical velocities from Mass-Dempsey wind model surface winds. Contours are at .20 m/sec intervals.

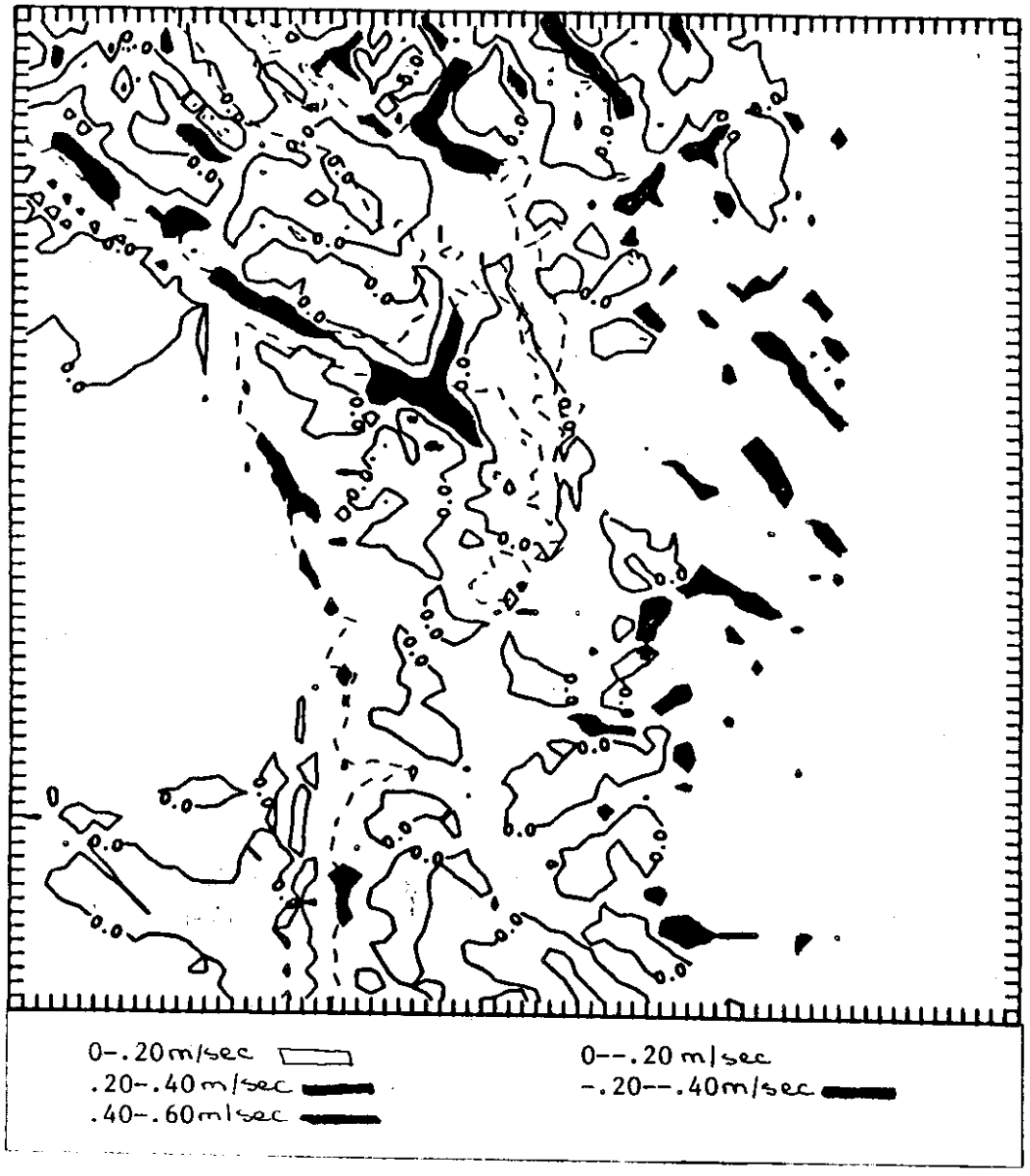

Figure 2.4.f Convergence vertical velocities from Mass-Dempsey wind model surface winds. Contours are at .20 m/sec intervals.

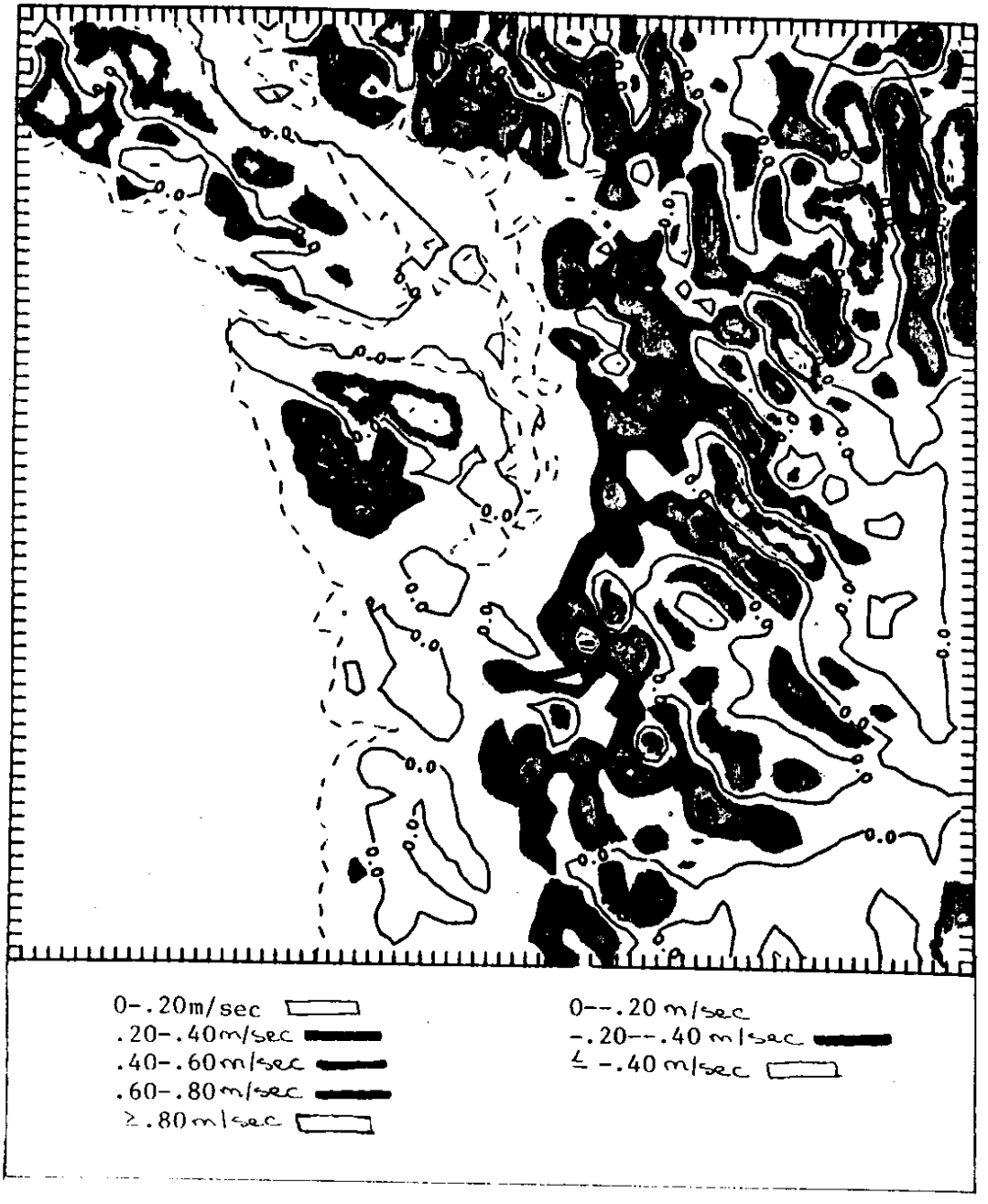

Figure 2.4.g Slope induced vertical velocities from large scale windfield. Contours are at .20 m/sec intervals.

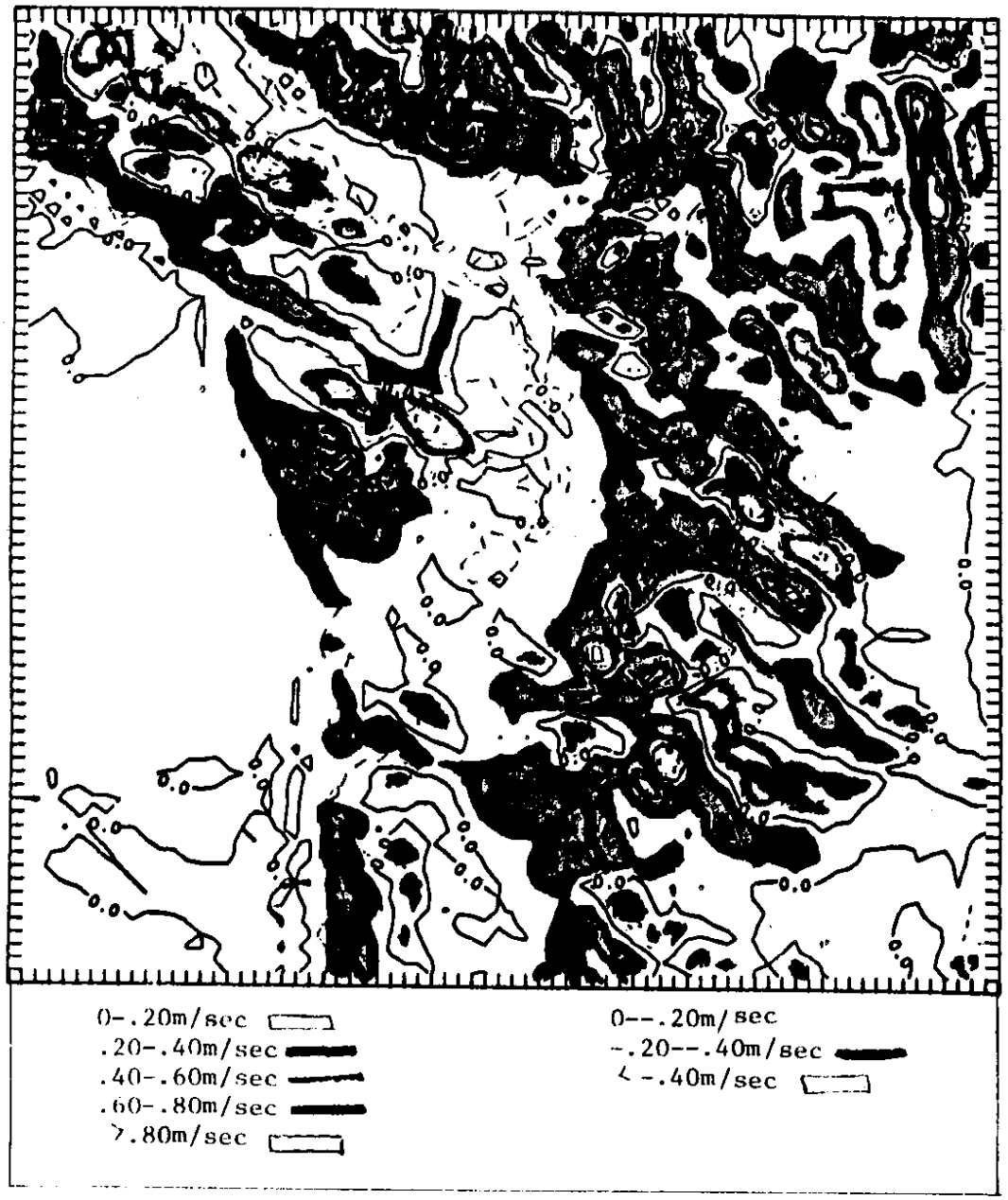

Figure 2.4.h Total vertical velocities from Mass-Dempsey wind model surface winds and large scale windfield. Contours are at .20 m/sec intervals.

with the wind vectors centered and 3.75 km inside the downwind border on separate runs. In Figure 2.4h the total vertical velocity field is dominated by the vertical velocities from the large scale wind field because the Quillayute sounding for 00 GMT had strong winds at relatively low levels (Fig. 2.4i).

The observed precipitation for a 24 hour period ending at 16 GMT November 7th is given in Figure 2.4j. The heaviest precipitation occured at Elwha Ranger Station on the north side of the Olympics and at Silverton in the north central Cascades. Relatively heavy precipitation areas covered the Olympic Mountains, the Cascades north-northeast from Mt Rainier and the Mt St. Helens area. Figure 2.4k shows the precipitation model run based on the equation 18 precipitation calculation. Many aspects of the model precipitation are qualitatively consistent with the observed precipitation. On the Olympic Peninsula the model realistically predicts relatively heavy precipitation on the SW side, with significantly less precipitation on the NE and E sides. The model did not produce the heavy precipitation measured at the Elwha Ranger Station. The model generally appears to duplicate the precipitation patterns over the Cascades. The Mt Rainier area, Mt St. Helens area, and the north central Cascades all experienced heavy

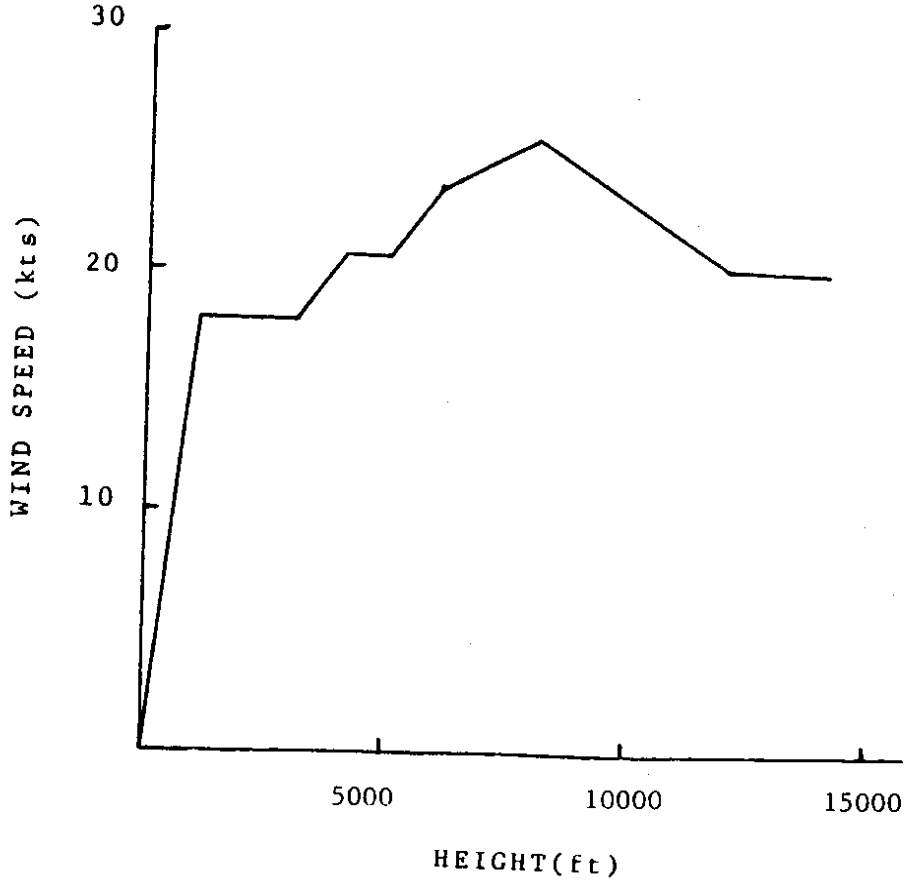

Figure 2.4.i Wind speed as a function of height for the Quillayute, WA radiosonde sounding for 00 GMT November 7, 1984.

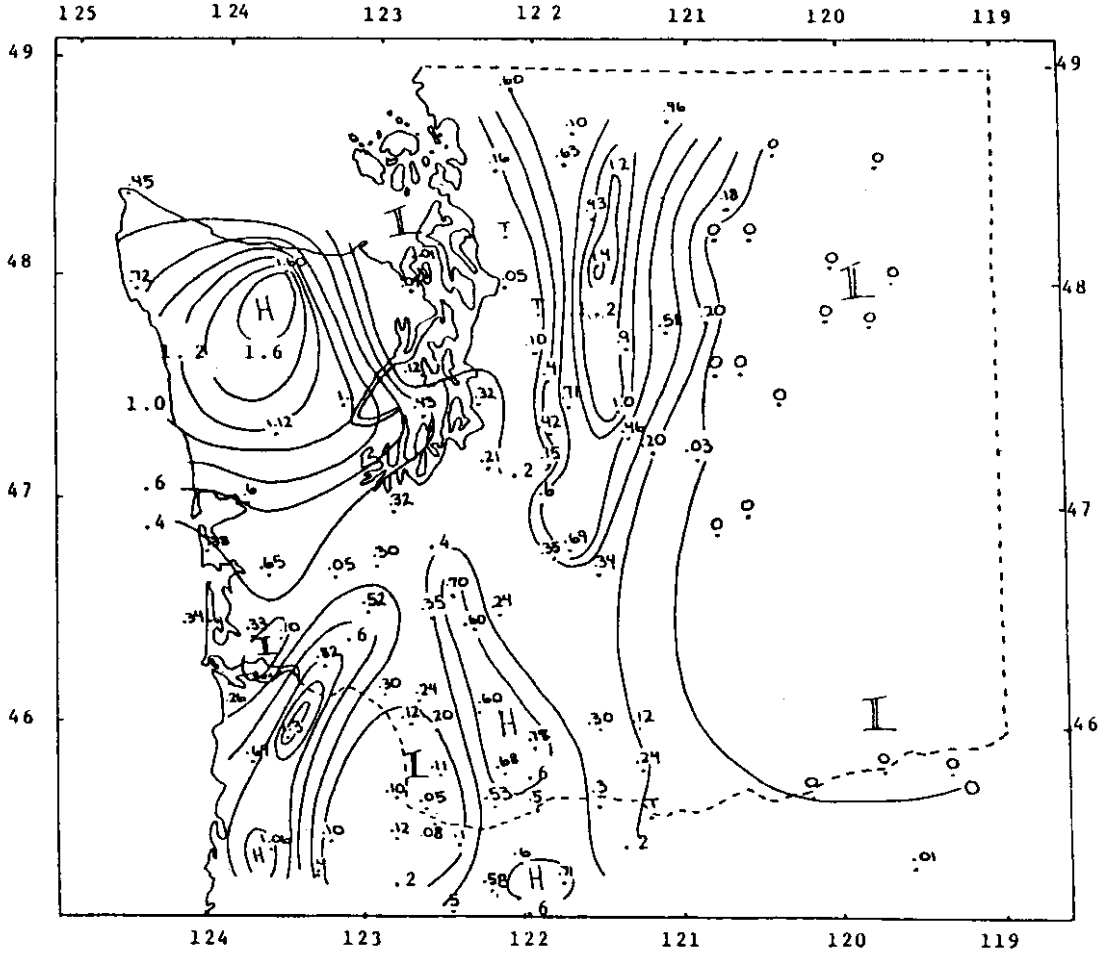

Figure 2.4.j Observed precipitation for 24 hour period ending at 1600 GMT November 7, 1984. Contour interval is .2 inches of water equivalent.

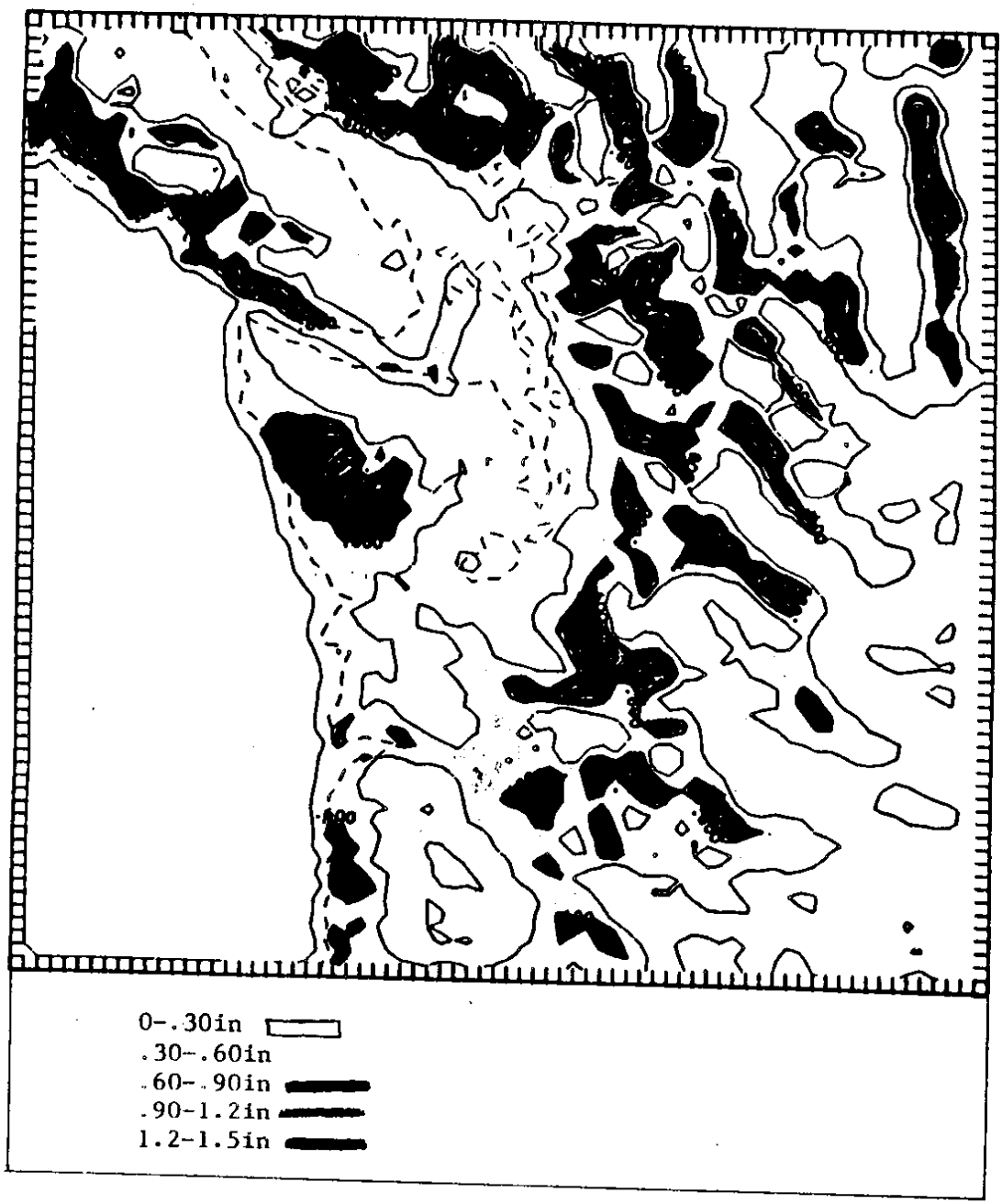

Figure 2.4.k Precipitation model run for 00 GMT November 7 1984. Contour interval is .3 inches of water equivalent.

precipitation, while several valley drainages received significantly less precipitation, most notably the Yakima and Wenatchee Rivers, and Lake Chelan east of the Cascade crest. Several of the precipitation gauge sites that recorded very light precipitation east of the mountains are in these drainages. The model predicts relatively heavy precipitation amounts over much of the higher terrain east of the Cascade crest. There are no precipitation gauge measurements to prove or disprove the predicted values; however, judging from mean annual rainfall maps and water resource predictions, the model is predicting too much precipitation for these areas. Table 2.1 gives observed and predicted precipitation for nine sites in Washington State. For six of the sites, the observed and predicted values are essentially the same. For Stevens Pass and Snoqualmie Falls the model precipitation was approximately 50% too high, while for Snoqualmie Pass it was 20% too low.

B. CASE 2: NOVEMBER 14, 1984 at 00 GMT NORTHWESTERLY LARGE-SCALE FLOW, PUGET SOUND CONVERGENCE ZONE

A cold front moved inland across the model domain on November 13th. Winds along the Washington coast shifted from E to WNW at 11 GMT November 13th, where they

TABLE 2.1 Observed and predicted precipitation for nine stations in western Washington for the 24 hour period ending at 1600 GMT November 7, 1984.

STATION NAME	OBSERVED PRECIPITATION	PREDICTED PRECIPITATION
Seattle	.32	.35
Skykomish	.9	.85
Snoqualmie Pass	1.0	.79
Stampede Pass	.46	.48
Stevens Pass	.51	.76
Snoqualmie Falls	.4	.57
Paradise/Longmire	.69/.35	.52
Lake Wenatchee	.20	.21
Quillayute	.72	.67

remained through 06 GMT the 14th. Southerly winds at 850 mb at 12 GMT November 13th were replaced by 20 kt NW winds by 00 GMT November 14th (Fig. 2.5a). The Quillayute sounding for 00 GMT November 14th is shown in Figure 2.5b. The air was weakly stable from the surface to an inversion at 850 mb. Above the inversion, the air was relatively stable.

Figure 2.5c shows the observed surface winds for 00 GMT November 14th. 15-30 kt NW winds prevailed along the Washington Coast, western Vancouver Island and Georgia Strait with W winds to 35 kts through the Strait of Juan de Fuca. Winds flowing around the Olympic Peninsula met in Puget Sound, with the formation of a well developed convergence zone. The Mass-Dempsey wind model run (Fig. 2.5d) duplicates the NW winds along the coast and down Georgia Strait as well as the W winds through the Strait of Juan de Fuca. The model produces strong convergence in Puget Sound; however, the position of the model's convergence is somewhat north of the observed convergence line, and the model does not duplicate any eastward component of the convergence surface winds. The model also produces a convergence zone in Georgia Strait. Although there are insufficient wind observations to verify the existence of this convergence zone, convergence zones in Georgia Strait have been observed

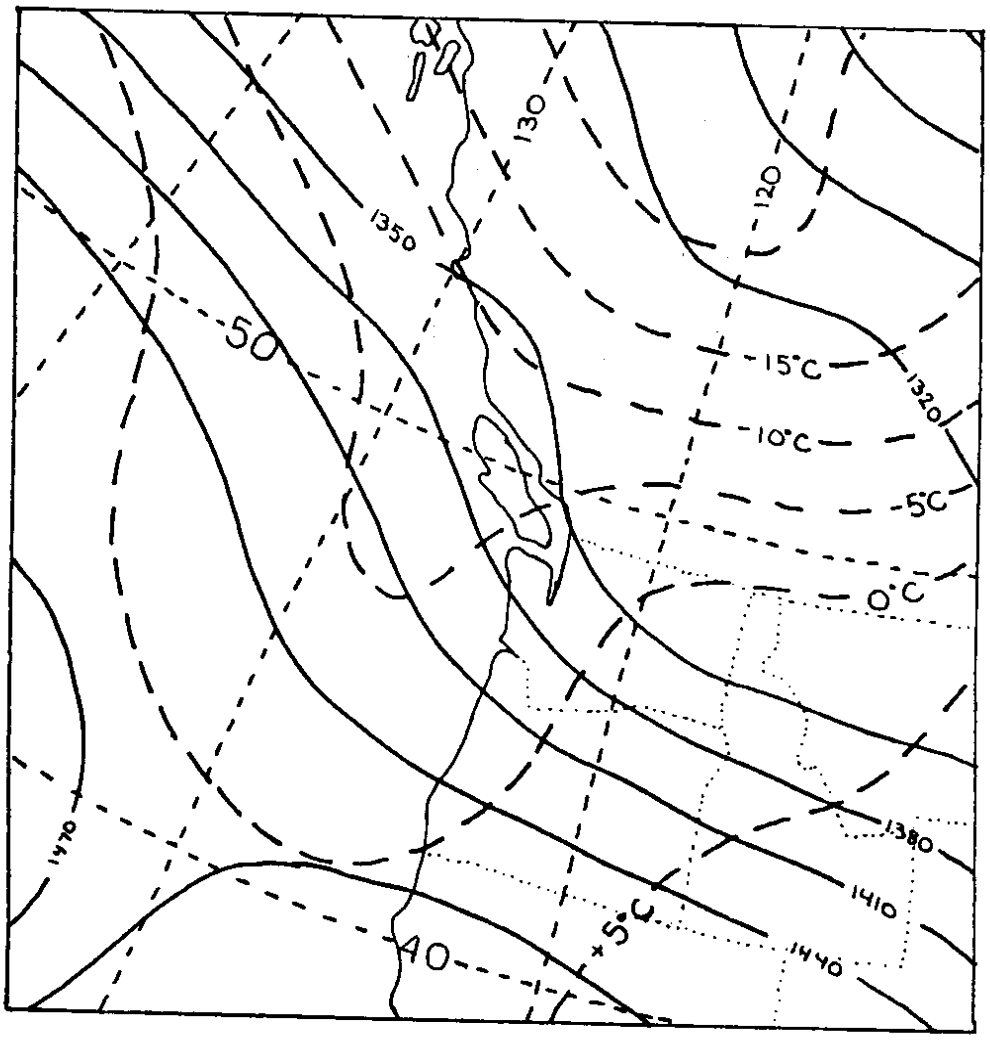

Figure 2.5.a NMC 850 mb height and temperature analysis for 00 GMT November 14, 1984. Height contours (solid lines) are in meters and temperature contours (heavy dashed lines) are in °C.

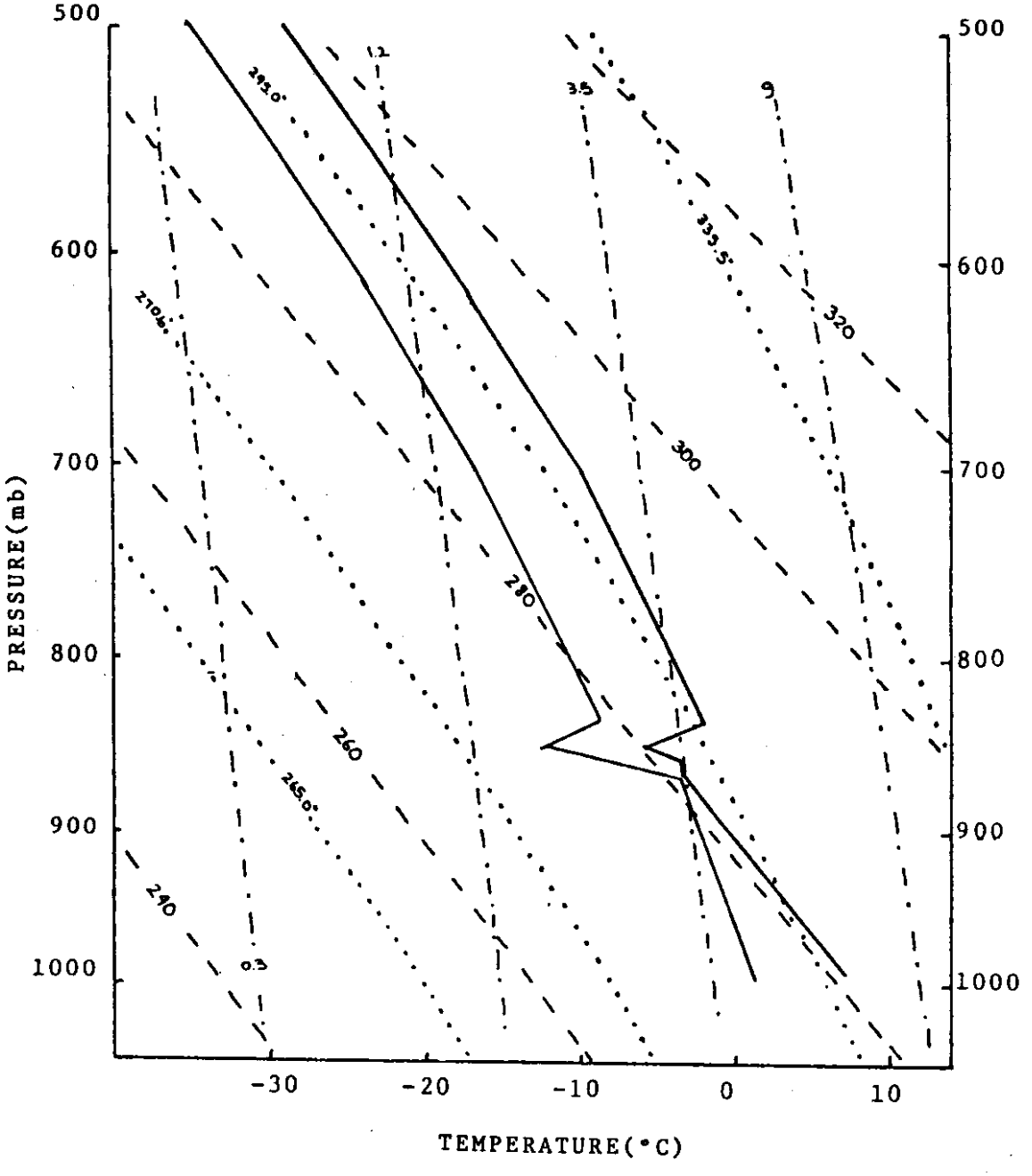

Figure 2.5.b Quillayute, Washington radiosonde sounding for 00 GMT November 14, 1984.

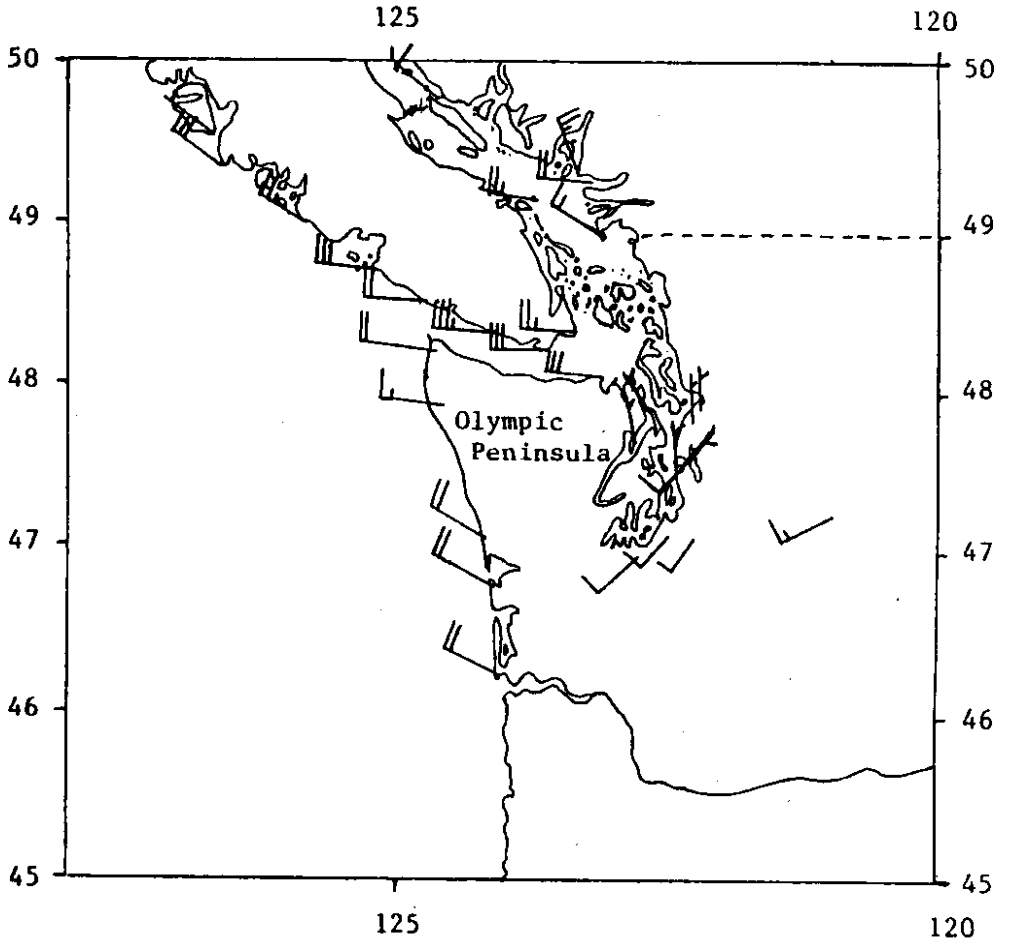

Figure 2.5.c Observed surface winds for 00 GMT November 14, 1984. On the wind flags, half barbs indicate 5 kts and full barbs equal 10 kts.

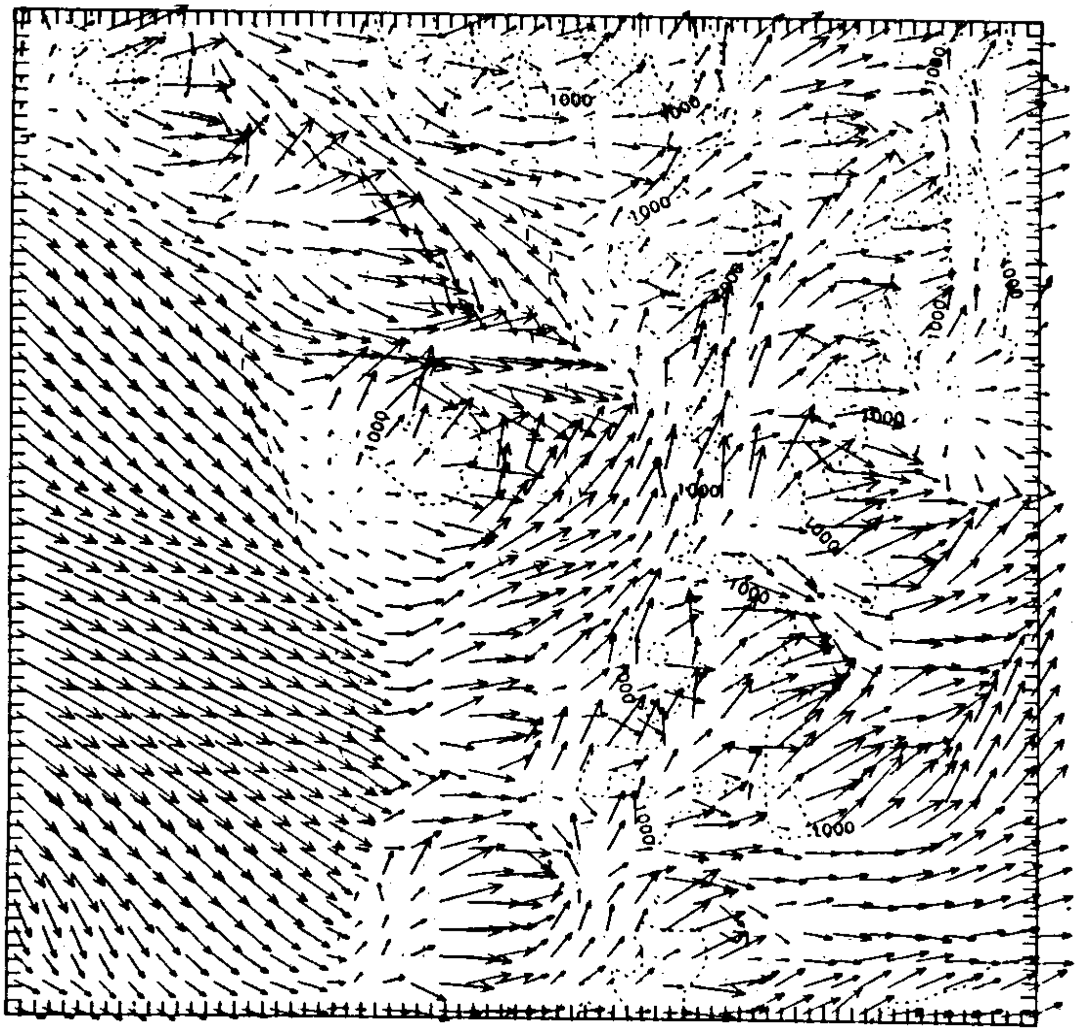

Figure 2.5.d Surface winds from Mass-Dempsey wind model run for 00 GMT November 14, 1984.

(Mass, personal communication). Although the model reproduces the SW winds at Stampede Pass it is impossible to make any general conclusions about the accuracy of the model winds in the Cascades.

Figures 2.5e-h show the vertical velocity components and the total vertical velocity field calculated from the Mass-Dempsey wind field and a large scale northwesterly flow. In Figures 2.5e-h the contour interval is .4m/sec. For this case, convergence dominates the total vertical velocities.

The observed precipitation for the 24 hour period ending at 1600 GMT November 14th is shown in Figure 2.5i. Heavy convergence zone precipitation extends from Puget Sound to the Cascades. Additional areas of heavy precipitation occured in the Mt Rainier area and from Mt St. Helens south to Mt Hood. Other areas in Washington received relatively little precipitation. Figure 2.5j shows the precipitation model run with a 15 by 15 km grid used with the large scale wind field. The model run qualitatively reproduces the convergence precipitation in Puget Sound with the precipitation extension to the Cascades, as well as the areas near Mt Rainier, Mt St. Helens and Mt Hood. The model produces many more areas with precipitation over the Cascades than are evident from the observations: however, the limited number of

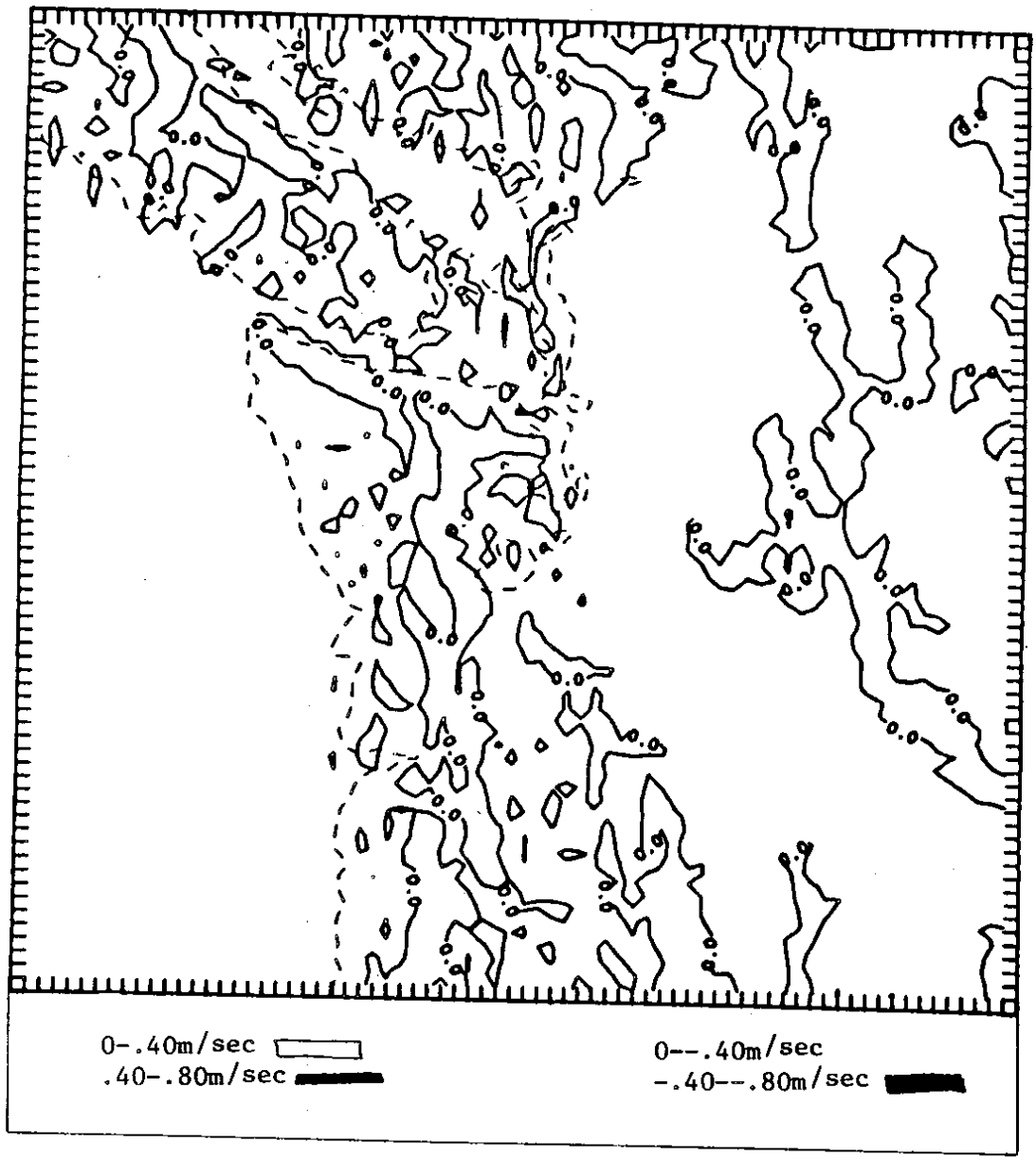

Figure 2.5.e Slope induced vertical velocities from Mass-Dempsey wind model surface winds. Contours are at .40 m/sec intervals.

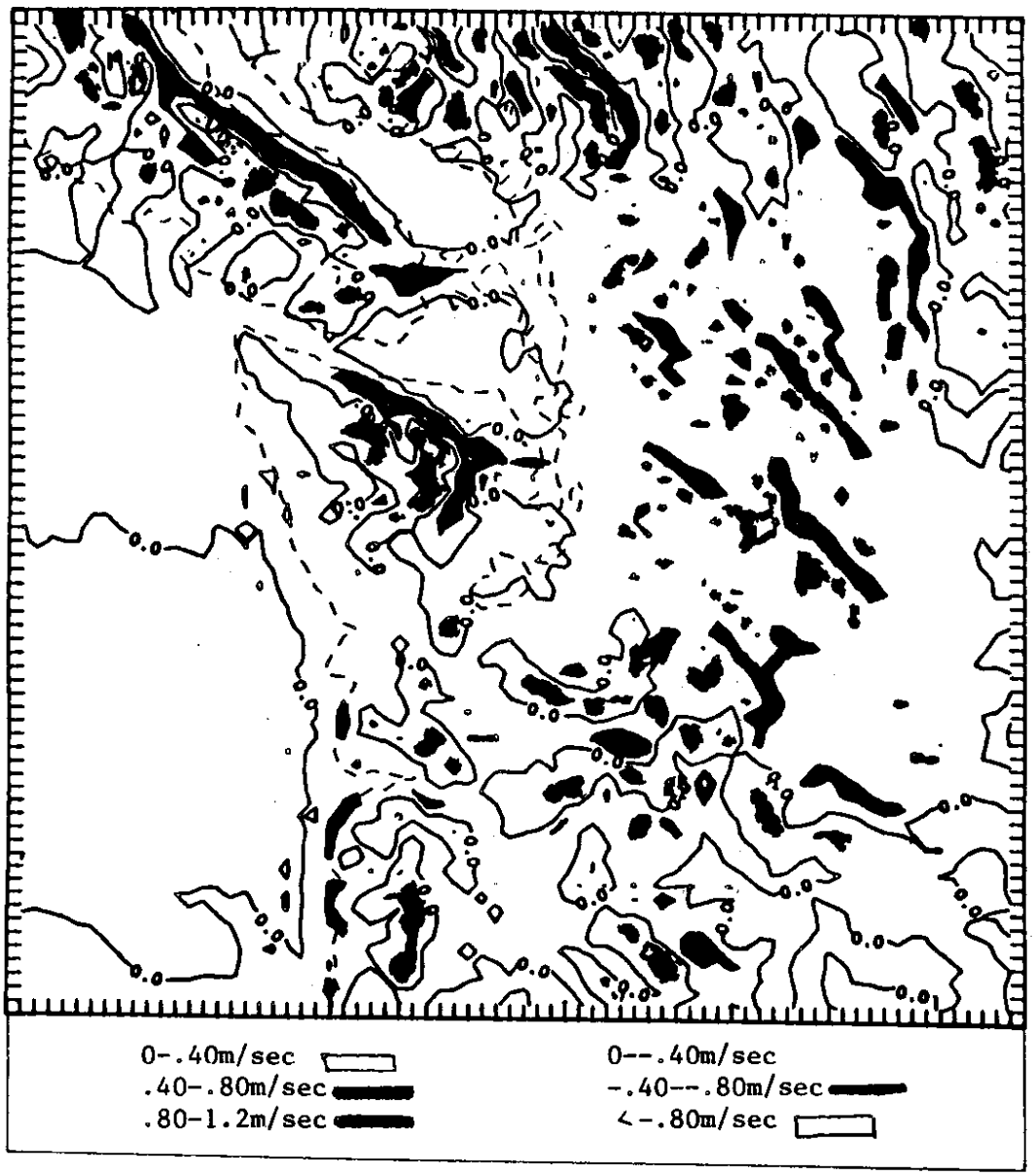

Figure 2.5.f Convergence vertical velocities from Mass-Dempsey wind model surface winds. Contours are at .40 m/sec intervals.

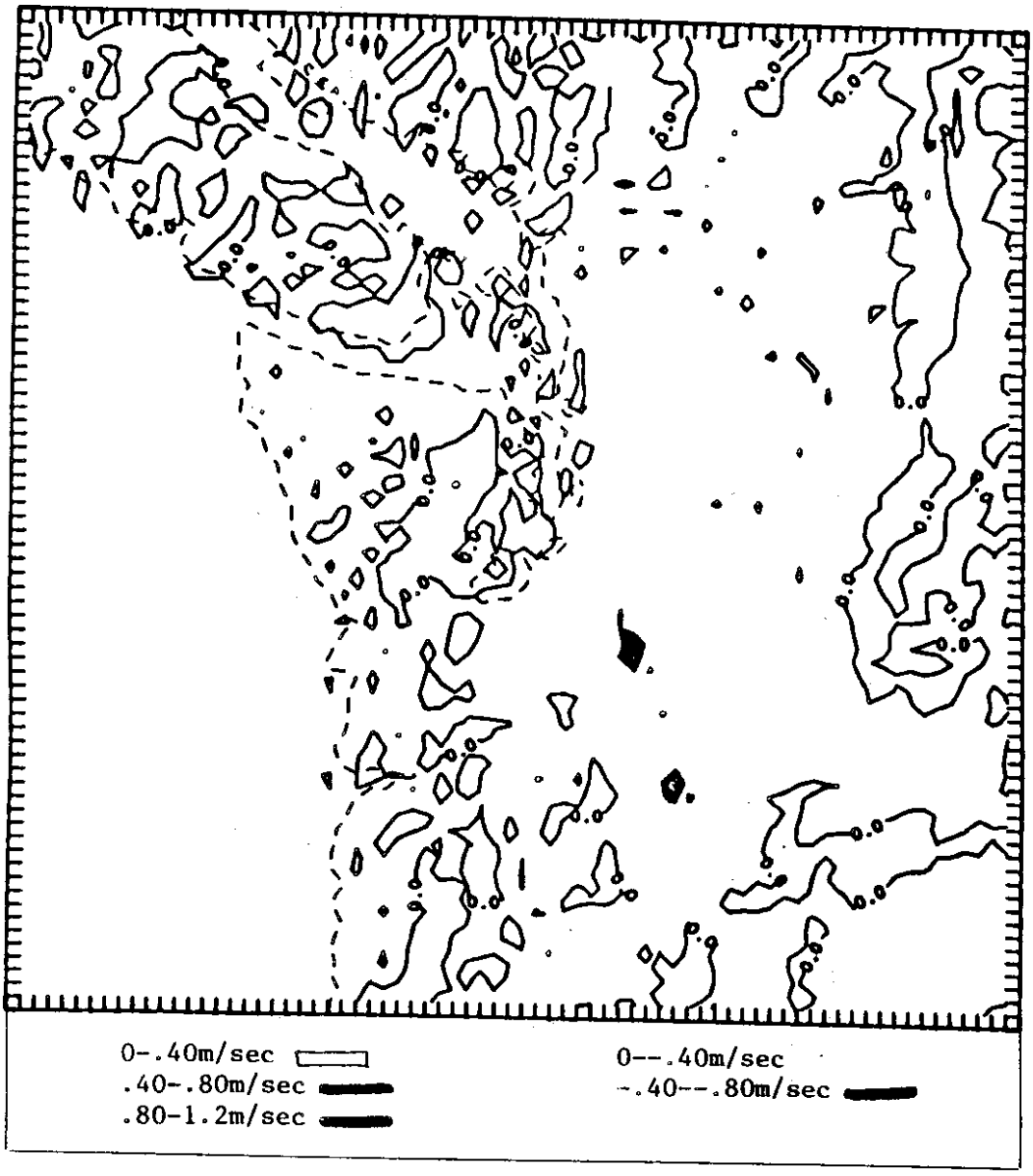

Figure 2.5.g Slope induced vertical velocities from large scale windfield. Contours are at .40 m/sec intervals.

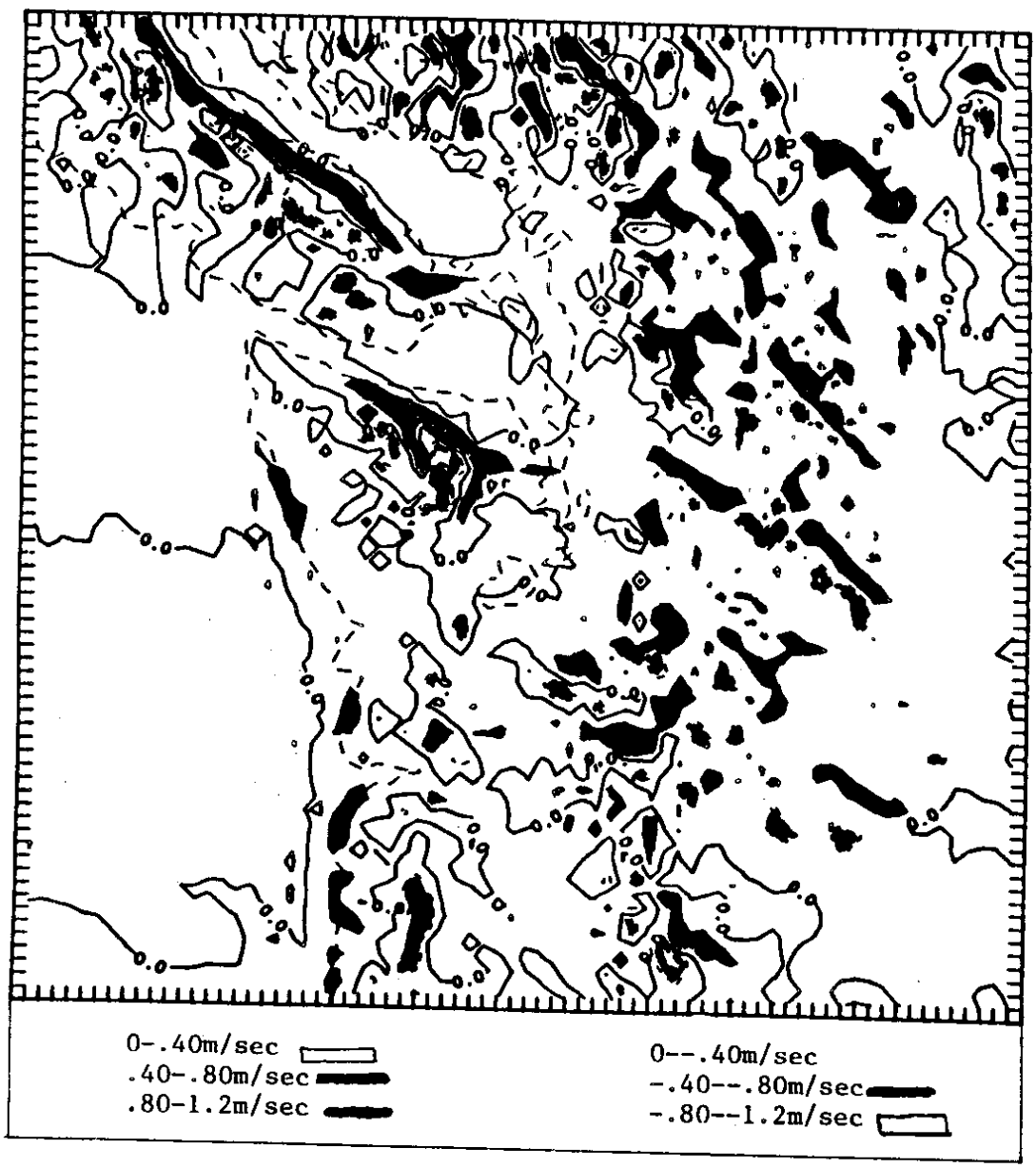

Figure 2.5.h Total vertical velocities from Mass-Dempsey wind model surface winds and large scale windfield. Contours are at .40 m/sec intervals.

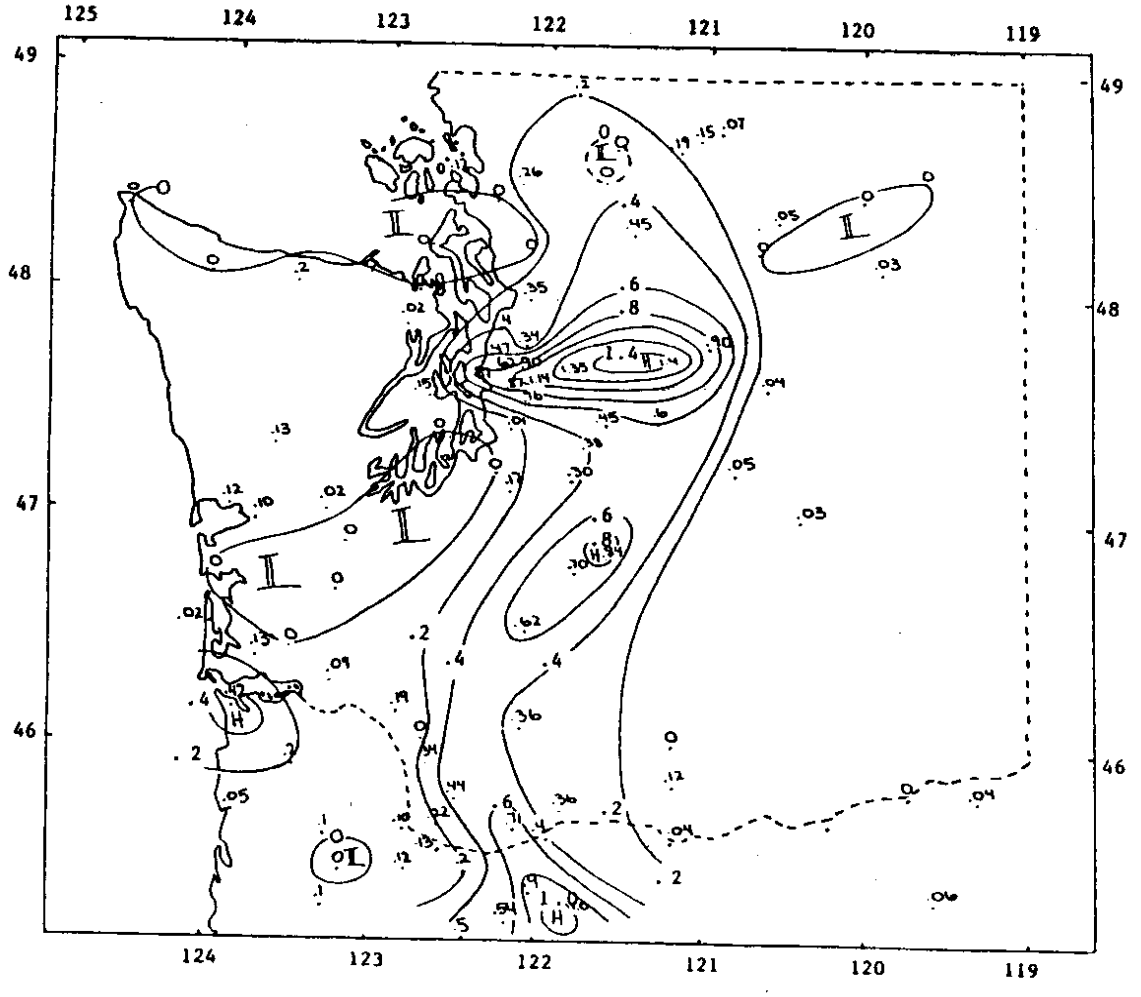

Figure 2.5.i Observed precipitation for 24 hour period ending at 1600 GMT November 14, 1984. Contour interval is .2 inches of water equivalent.

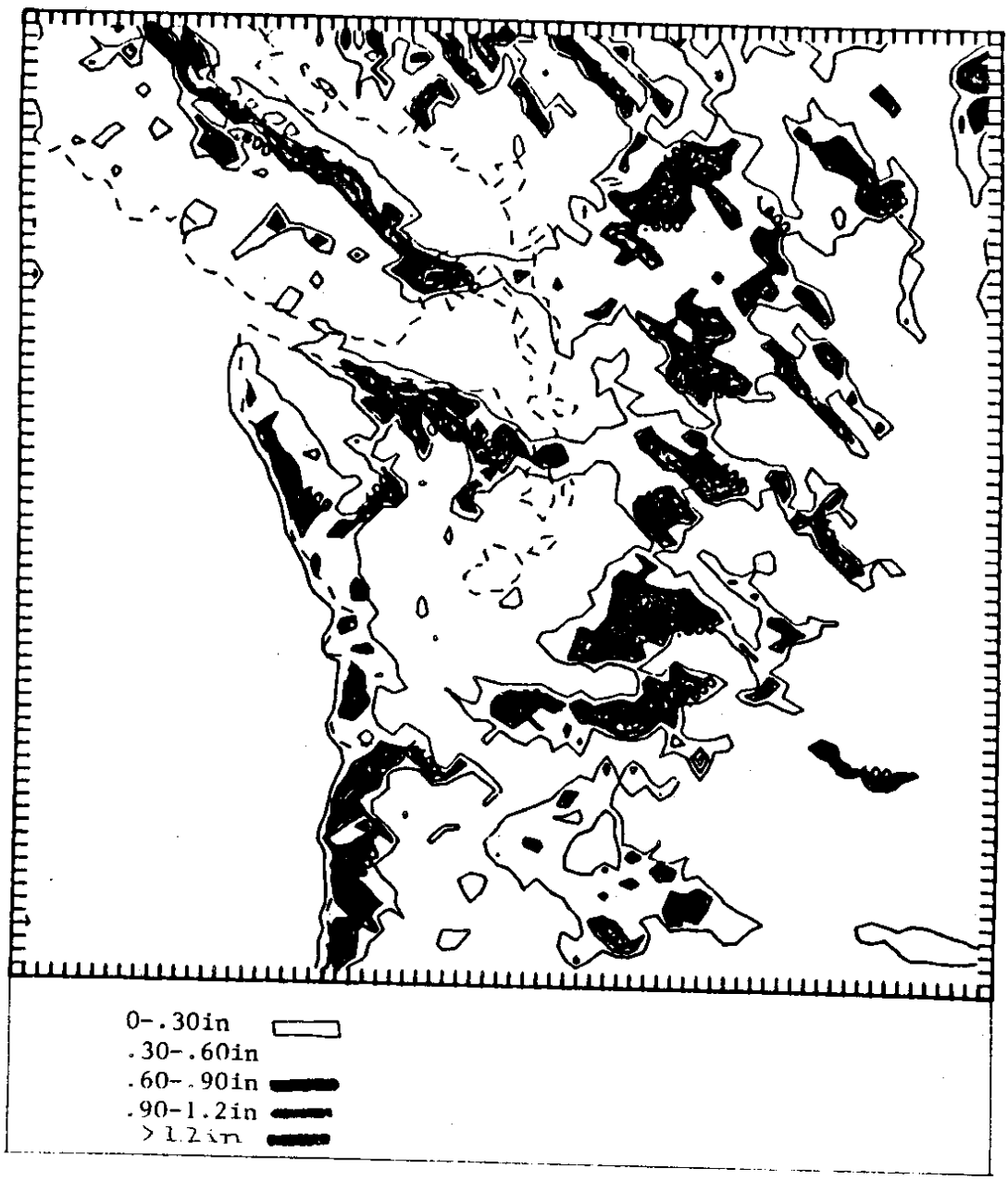

Figure 2.5.3 Precipitation model run for 00 GMT November 14, 1984. Contour interval is .3 inches of water equivalent.

precipitation gauges in the mountains makes it impossible to test the accuracy of the model in these areas. The model produces relatively heavy precipitation along the west coast of Washington and Oregon as a result of frictional convergence as the air flows from the ocean over land. The model also produces heavy precipitation on the east side of Vancouver Island, and along the northern Olympic Peninsula. The strong convergence in these areas results when the model produces strong downslope winds in the lee of high elevation terrain that converge with winds channeled through water passages. Although negative vertical velocities result in these areas from downslope surface winds and from downslope large scale wind field winds, these are not sufficient to compensate for the strong upward vertical velocities that result from convergence. Table 2.2 gives observed and model predicted precipitation for eight sites in Washington State. For four of the sites, the observed and predicted values are similar. For Skykomish and Stevens Pass, two sites that received heavy convergence precipitation, the model predicts significantly less precipitation than was observed. In contrast, the model overpredicts precipitation at Quillayute and Elwha Ranger Station.

The Mass-Dempsey wind model and precipitation model were run for a 'typical' northwesterly flow. Average 850

TABLE 2.2 Observed and predicted precipitation for nine stations in western Washington for the 24 hour period ending at 1600 GMT November 14, 1984.

STATION NAME	OBSERVED PRECIPITATION	PREDICTED PRECIPITATION
Quillayute	.01	.69
Elwha Ranger Station	.02	.50
Snoqualmie Pass	.4	.30
Stampede Pass	.44	.59
Paradise/Longmire	.84/.70	.73
Stevens Pass	.90	.23
Skykomish	1.4	0
Lake Wenatchee	.02	0

to 700 mb lapse rates and representative 850 mb height and temperature fields were chosen by averaging values for several specific cases with northwesterly flow during the winter of 1985-86. The surface wind field from the Mass-Dempsey wind model run is shown in Figure 2.6a, with the corresponding precipitation model run shown in Figure 2.6b. The general case is qualitatively similar to the November 14th case; however, the magnitude of convergence in Puget Sound and Georgia Strait is higher. The general case also produces more widespread light precipitation than occured on November 14th. The wind model again produces strong convergence in the lee of the Olympic Mountains and Vancouver Island, which results in an overprediction of precipitation in these areas.

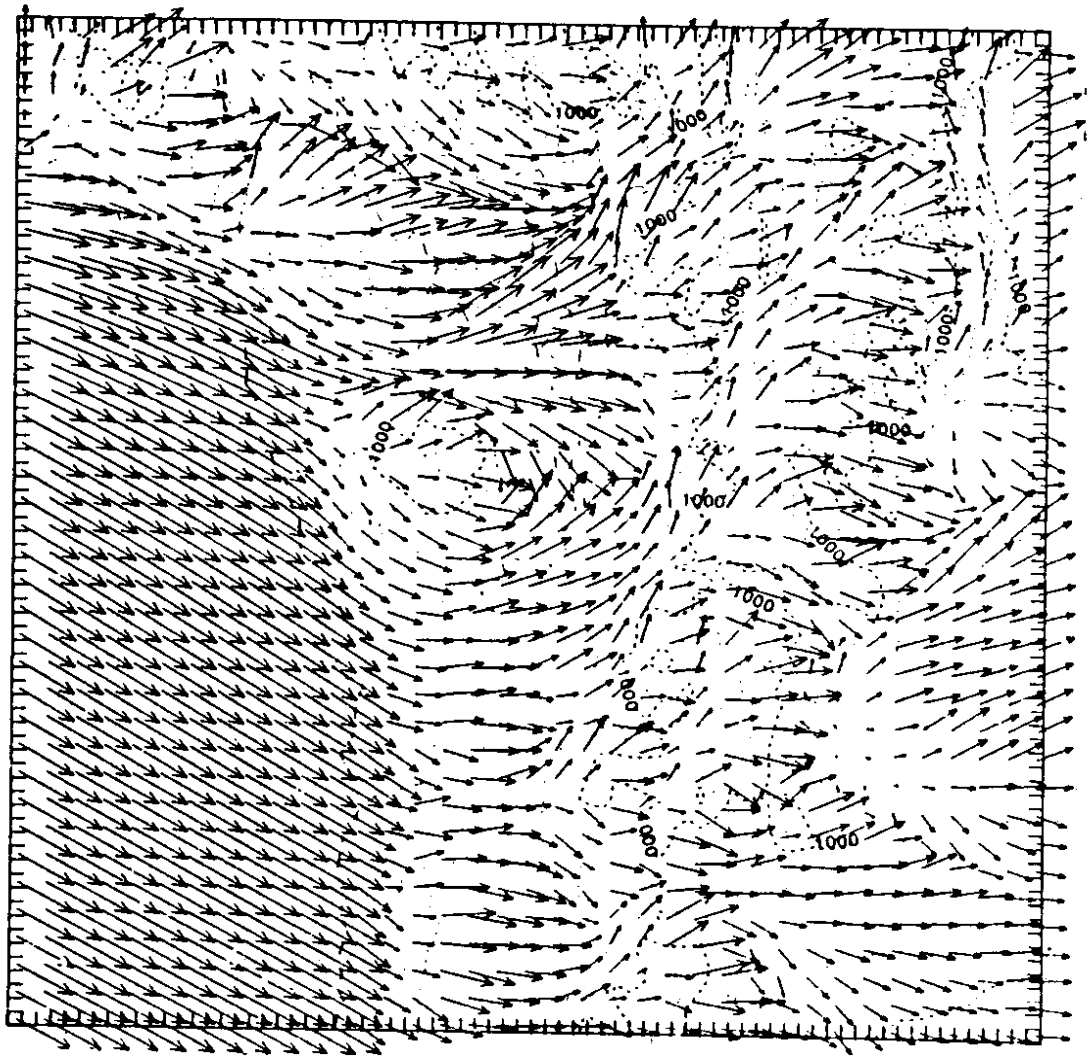

Figure 2.6.a Surface winds from Mass-Dempsey wind model run for a general northwesterly flow.

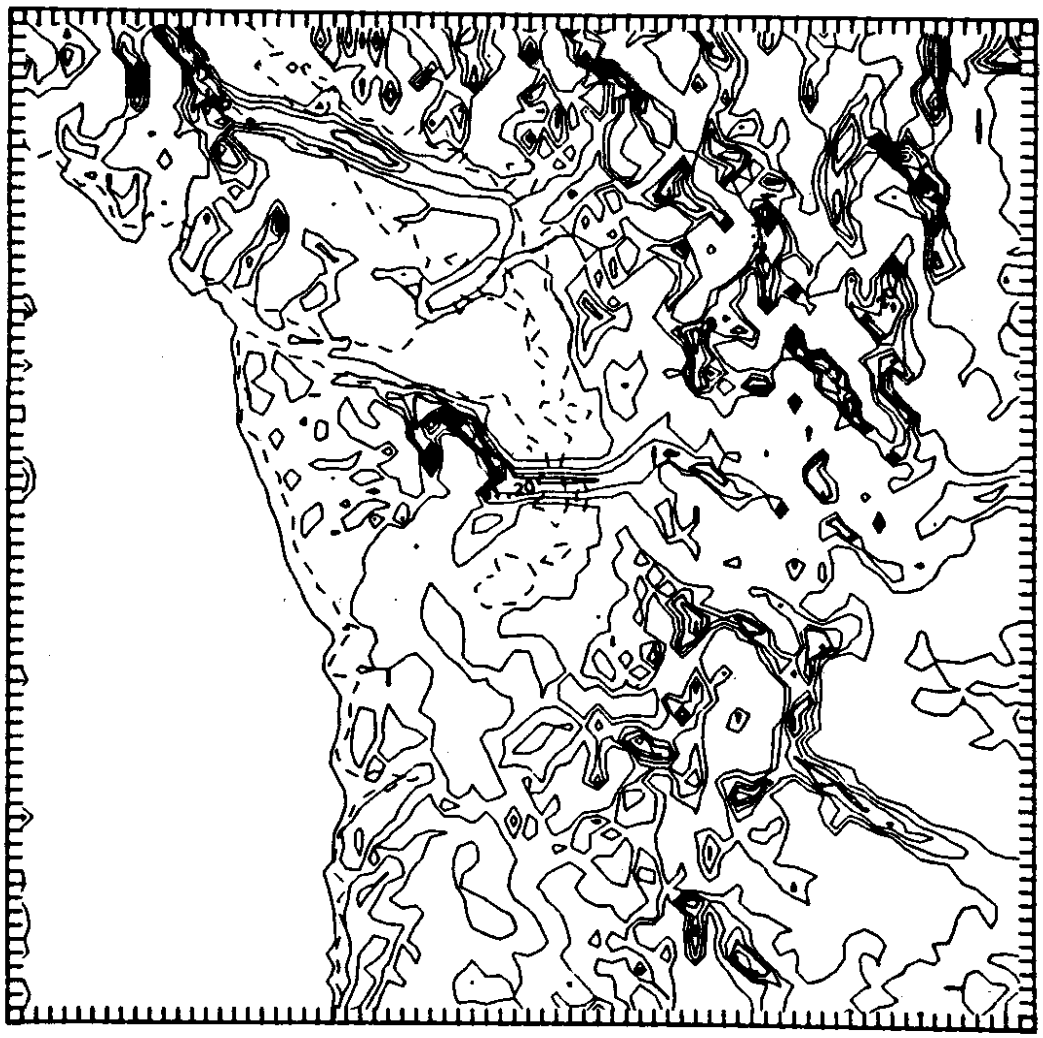

Figure 2.6.b Precipitation model run for a general northwesterly flow. Contour interval is .3 inches of water equivalent.

BIBLIOGRAPHY

Anthes, R.A., and T.T. Warner (1978). Development of hydrodynamic models suitable for air pollution and other mesometeorological studies. Mon. Wea. Rev., 106, 1045-1078.

R.L. Armstrong, and K. Williams (1981). Snowfall Forecasting in the Colorado Mountains. Second Conference on Mountain Meteorology, 386-390.

Bergeron, T., (1965). On the low-level redistribution of atmospheric water caused by orography. Supplement Proceedings of the International Conference on Cloud Physics, Tokyo, 96-100.

Collier, C.G. (1977). The effect of model grid length and orographic rainfall 'efficiency' on computed surface rainfall. Quart. J. R. Met. Soc., 103, 247-253.

Court, A. (1960). Reliability of houry precipitation data. J. Geophys. Res., 65, 4017-4024.

Danard, M.B., (1971). A simple method for computing the variation of annual precipitation over mountainous terrain. Boundary-layer Met., 2, 188-206.

Danard, M.B., (1976). On frictional and orographic effects on precipitation in coastal areas. Boundary-layer Met., 10, 409-422.

Danard, M.B., (1977). A simple model for mesoscale effects of topography on surface winds. Mon. Wea. Rev., 105, 572-581.

Dempsey, D.P., (1985). A one-level mesoscale model for diagnosing surface winds in mountainous and coastal regions. Ph.D. thesis, University of Washington.

Dunn, L.B., (1982). Quantitative and spacial distribution of winter precipitation along Utah's Wasatch Front. Masters thesis, University of Washington.

Elliott, R.D., and R.W. Shaffer, (1962). The development of quantitative relationships between orographic precipitation and airmass parameters for use in forecasting and cloud seeding evaluation. J. Appl. Met., 1, 218.

Fraser, A.B., R.C. Easter, and P.V. Hobbs, (1973). A

theoretical study of the flow of air and fallout of solid precipitation over mountainous terrain, Part 1, Airflow model. J. Atm. Sci., 30(5), 801-812.

Hill, G.E., (1978). Observations of precipitation-forced circulations in winter orographic storms. J. Atms. Sci., 35, 1463-1472.

Hobbs, P.V., R.C. Easter, and A.B. Fraser, (1973). A theoretical study of the flow of air and fallout of solid precipitation over mountainous terrain, Part II, Microphysics. J. Atm. Sci., 30, 813-823.

Lavoie, R.L., (1972). A mesoscale numerical model of lake-effect storms. J. Atm. Sci., 29, 1025-1040.

Lavoie, R.L., (1974). A numerical model of trade wind weather on Oahu. Mon. Wea. Rev., 102. 630-637.

Mahrer, Y., and R. Pielke, (1976). Numerical simulation of the airflow over Barbados. Mon. Wea. Rev., 104, 1392-1402.

Marriott, R.T., and M.B. Moore, (1984). Weather and snow observations for avalanche forecasting: an evaluation of errors in measurement and interpretation. Proceedings International Snow Science Workshop.

Mass, C.F., (1981). Topographically forced convergence in western Washington State. Mon. Wea. Rev., 109, 1335-1347.

Mass, C.F., and D.P. Dempsey, (1985). A one-level, mesoscale model for diagnosing surface winds in mountainous and coastal regions. Mon. Wea. Rev., 113, 1211-1227.

Nickerson, E.C., and E.L. Magaziner, (1976). A three-dimensional simulation of winds and non-precipitating orographic clouds over Hawaii. NOAA TR ERL 377-APCL-39, 29pp.

Overland, J.E., M.H. Hitchman, and Y.J. Han, (1979). A regional surface wind model for mountainous coastal areas. NOAA TR ERL 407-PMEL 32. 34 pp.

Pielke, R., (1974). A three-dimensional numerical model of the sea-breeze over Florida. Mon. Wea. Rev., 102, 115-139.

Rasmussen, L.A., and W.V. Tangborn, (1976). Hydrology of the North Cascades region, Washington 1. Runoff, Precipitation, and Storage Characteristics. Water Resour. Res., 12(2), 187-202.

Rhea, J.O., (1978). Orographic Precipitation Model for hydrometeorological use. Ph. D. thesis, Colorado State University.

Sarker, R.P., (1966). A dynamical model of orographic rainfall. Mon. Wea. Rev., 94, 555-572.

Sarker, R.P., (1967). Some modifications in a dynamical model of orographic rainfall. Mon. Wea. Rev., 95, 673-684.

Schermerhorn, V.P., (1967). Relations between topography and annual precipitation in western Oregon and Washington. Water. Resour. Res., 3(3), 707-711.

Spreen, W.C., (1947). A determination of the effect of topography upon precipitation. Americal Geophysical Union Trans., 28(2), 285-290.

Storr, D., and H.L. Ferguson, (1972). The distribution of precipitation in some mountainous Canadian watersheds. Distribution of Precipitation in Mountainous Areas, 2, WMO/OMM No. 326, 243-263.

Wantz, J.W., C.M. Feris, and N.S. Larsen, (1983). Fifteen year average precipitation patterns as revealed by the Portland, Oregon mesoscale precipitation network. Bonneville Power Administration publication. 15pp.

Wilson, J.W., and M.A. Atwater, (1972). Storm rainfall variability over Connecticut. J. Geophys. Res., 77(21), 3950-3956.

APPENDIX A: PRECIPITATION GAUGE SITES USED IN CHAPTER 1.

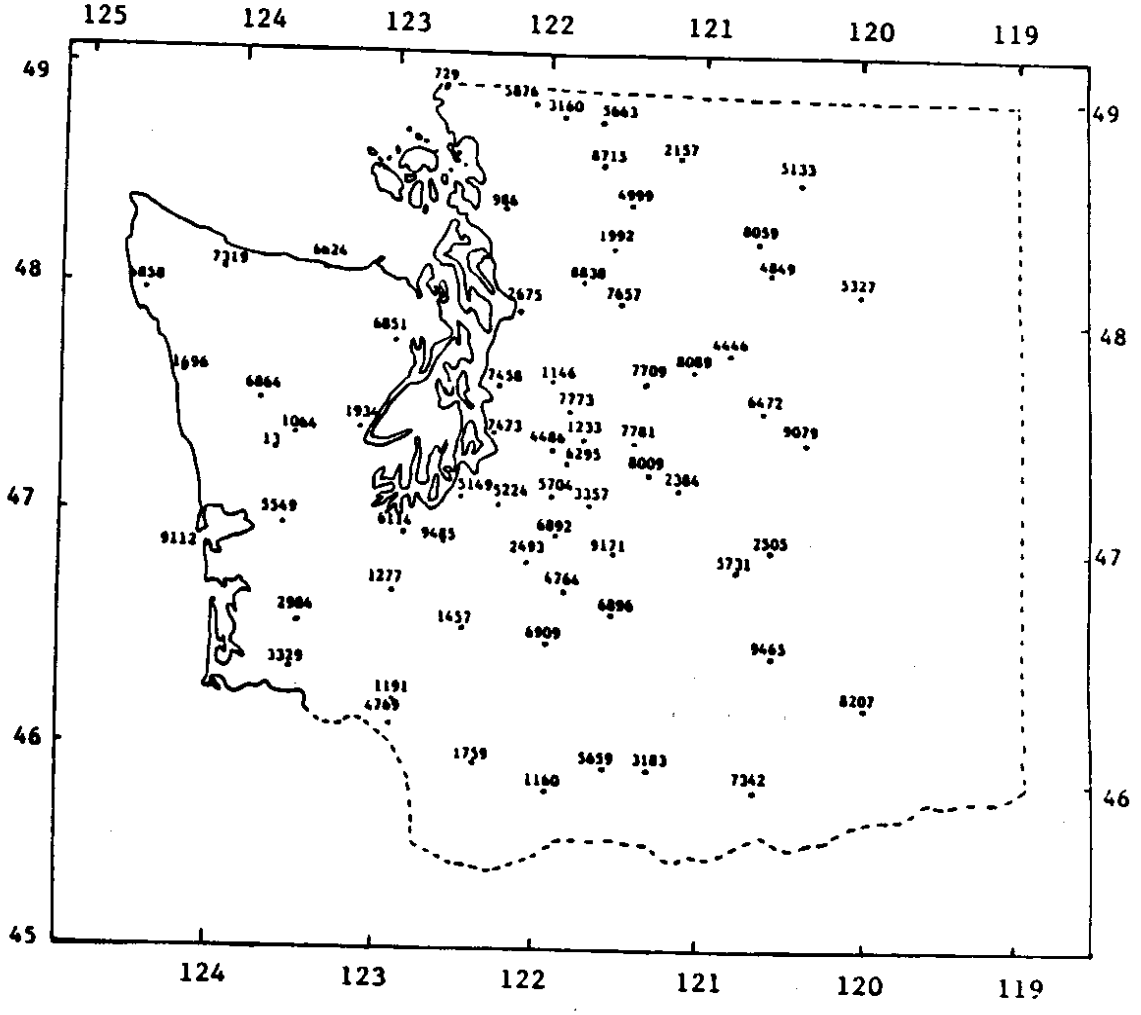

Figure A.1. Locations of the precipitation gauges used for the precipitation analysis in Chapter 1. Numbers refer to the station ID's given in Table A.1..

Table A.1. Precipitation gauge sites used in Chapter 1.

ID	STATION NAME	LAT	LONG	ELEV
0013	ABERDEEN 20 NNE	47 16	123 42	435
0729	BLAINE 1 ENE	49 00	122 44	80
0986	BURLINGTON	48 28	122 19	30
1064	CAMP GRISDALE	47 22	123 36	820
1146	CARNATION 4 NW	47 41	121 59	50
1160	CARSON FISH HATCHERY	45 54	121 57	1134
1191	CASTLE ROCK	46 16	122 55	43
1233	CEDAR LAKE	47 25	121 44	1560
1277	CENTRALIA 1 W	46 43	122 59	185
1457	CINEBAR	46 36	122 30	1000
1496	CLEARWATER	47 35	124 18	75
1759	COUGAR 4 SW	46 01	122 21	520
1934	CUSHMAN DAM	47 25	123 13	760
1992	DARRINGTON RS	48 15	121 36	550
2157	DIABLO DAM	48 43	121 09	891
2384	EASTON	47 15	121 11	2170
2493	ELECTRON HEADWORKS	46 54	122 02	1730
2505	ELLENSBURG	46 59	120 32	1520
2675	EVERETT	47 59	122 11	60
2984	FRANCES	46 33	123 30	231
3160	GLACIER RS	48 53	121 57	935
3183	GLENWOOD	46 01	121 17	1896
3329	GRAYS RIVER	46 22	123 34	50
3357	GREENWATER	47 08	121 38	1730
4446	LAKE WENATCHEE	47 50	120 48	2005
4486	LANDSBURG	47 23	121 58	535
4764	LONGMIRE RAINIER	46 45	121 49	2762
4769	LONGVIEW	46 09	122 55	12
4849	LUCERNE 1 N	48 14	120 36	1200
4999	MARBLEMOUNT RS	48 32	121 27	348
5133	MAZAMA	48 37	120 24	2150
5149	MC CHORD AFB	47 09	122 29	292
5224	MC MILLIN RES	47 08	122 16	579
5327	METHOW	48 08	120 01	1165
5549	MONTESANO 3 NW	47 01	123 39	40
5659	MT ADAMS RS	46 00	121 32	1960
5663	MT BAKER LODGE	48 52	121 40	4150
5704	MUD MT DAM	47 09	121 56	1308
5731	NACHES 10 NW	46 52	120 46	2280
5876	NOOKSACK HATCHERY	48 54	122 09	410
6114	OLYMPIA WSO AP	46 58	122 54	192
6295	PALMER 3 ESE	47 18	121 51	920
6472	PESHASTIN TELEM	47 35	120 37	1050

Table A.1. (continued)

ID	STATION NAME	LAT	LONG	ELEV
6624	PORT ANGELES	48 07	123 26	100
6851	QUILCENE 5 SW DAM	47 47	122 59	1028
6858	QUILLAYUTE WSO AP	47 57	124 33	179
6864	QUINAULT RS	47 28	123 51	220
6892	RAINIER CARBON R E	47 00	121 55	1735
6896	RAINIER OHANAPECOSH	46 44	121 34	1950
6909	RANDLE 1 E	46 32	121 56	900
7319	SAPPHO 8 E	48 04	124 07	760
7342	SATUS PASS 2 SSW	45 57	120 39	2610
7458	SEATTLE EMSU WSO	47 39	122 18	19
7473	SEATAC WSO AP	47 27	122 18	450
7657	SILVERTON	48 04	121 34	1475
7709	SKYKOMISH 1 ENE	47 42	121 22	1030
7773	SNOQUALMIE FALLS	47 33	121 51	440
7781	SNOQUALMIE PASS	47 25	121 25	3020
8009	STAMPEDE PASS WSMO	47 17	121 20	3958
8059	STEHEKIN 4 NW	48 21	120 43	1270
8089	STEVENS PASS	47 44	121 05	4070
8207	SUNNYSIDE	46 19	120 00	747
8715	UPPER BAKER DAM	48 39	121 41	690
8838	VERLOT	48 06	121 47	975
9079	WENATCHEE EXP STA	47 26	120 21	806
9112	WESTPORT 2 N USCG	46 54	124 05	10
9171	WHITE RIVER RS	46 54	121 33	3500
9465	YAKIMA WSO AP	46 34	120 32	1064
9485	YELM	46 57	122 36	350

APPENDIX B: DETAILED COPIES OF THE PRECIPITATION PATTERN MAPS

Figures B1 and B2 show detailed copies of the precipitation pattern maps from Chapter 1 for Hoquiam surface wind direction and Quillayute 850 mb wind direction, respectively. Figure B3 shows E through S and W precipitation maps for Hoquiam surface winds greater than or equal to 15 kts. The precipitation pattern maps for Quillayute 850 mb SE through W and NW winds greater than or equal 25 kts are shown in Figure B4.

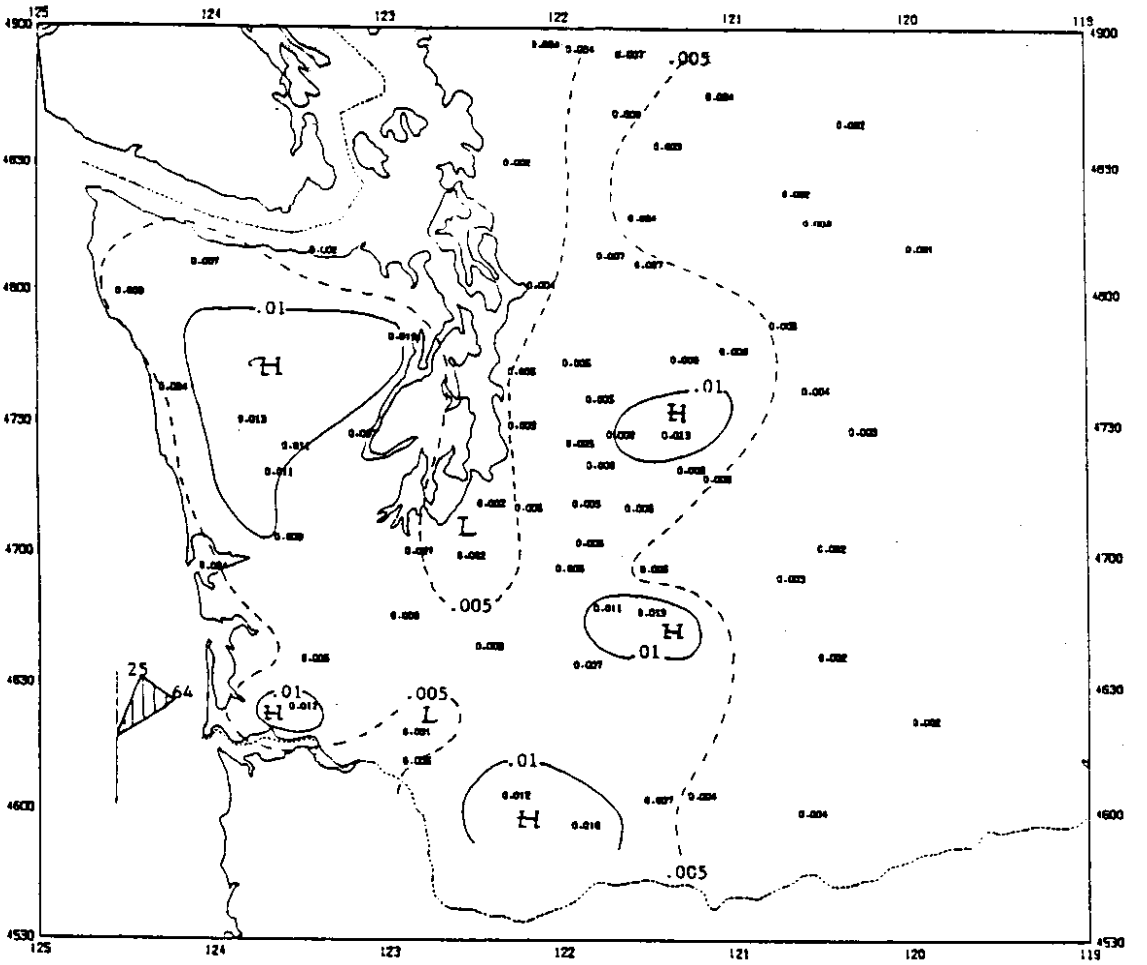

Figure 3.1a Mean hourly precipitation pattern map corresponding to the time period during which the surface wind at Hoquiam blew from the NE. The wind direction is shown by the shaded region of the compass. Precipitation rates are based on 828 hours of data. The solid line contour interval is .01 inches of water equivalent. Dashed line contours are drawn for .005 inch intervals.

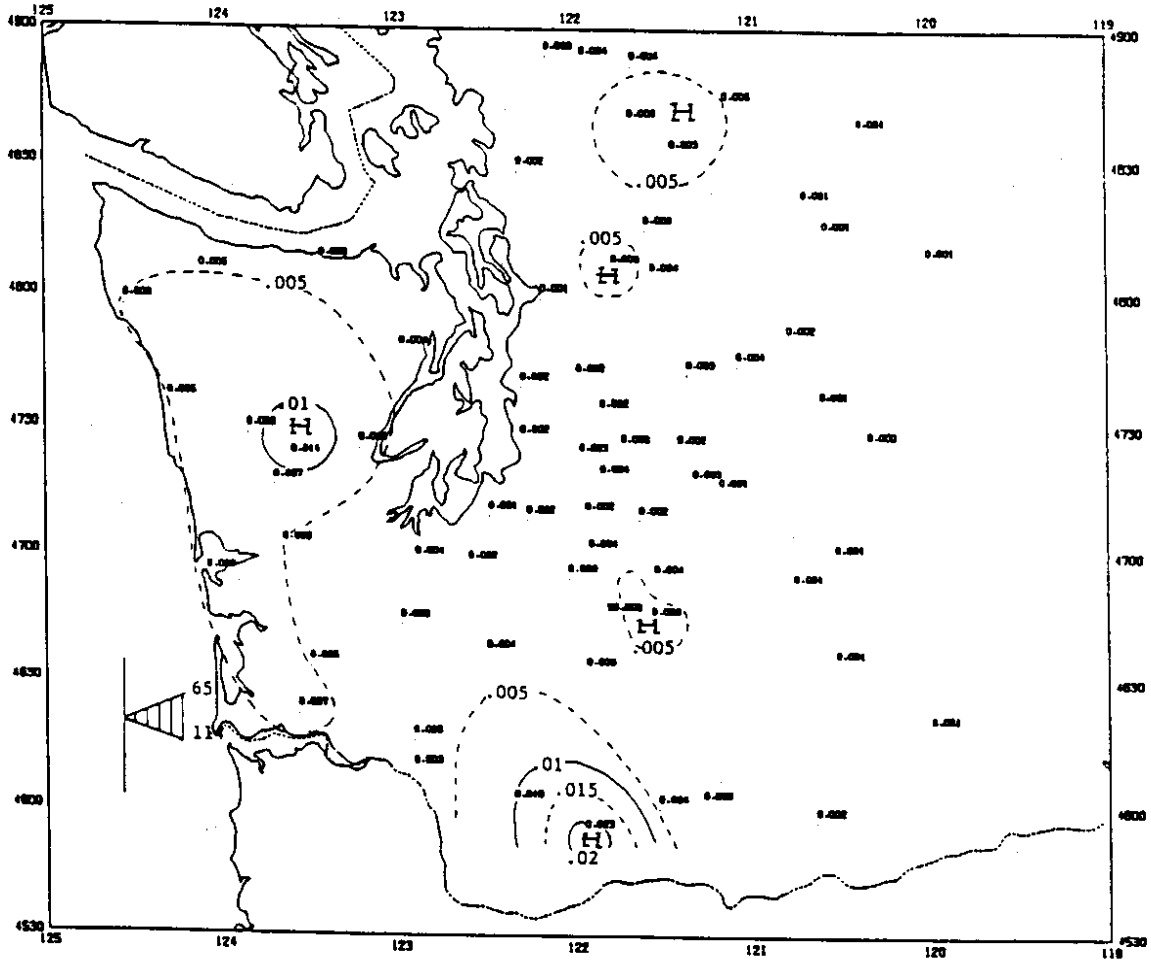

Figure B.1b Mean hourly precipitation pattern map corresponding to the time period during which the surface wind at Hoquiam blew from the E. Precipitation rates are based on 1384 hours of data. Symbols and contour intervals as in Figure B.1a.

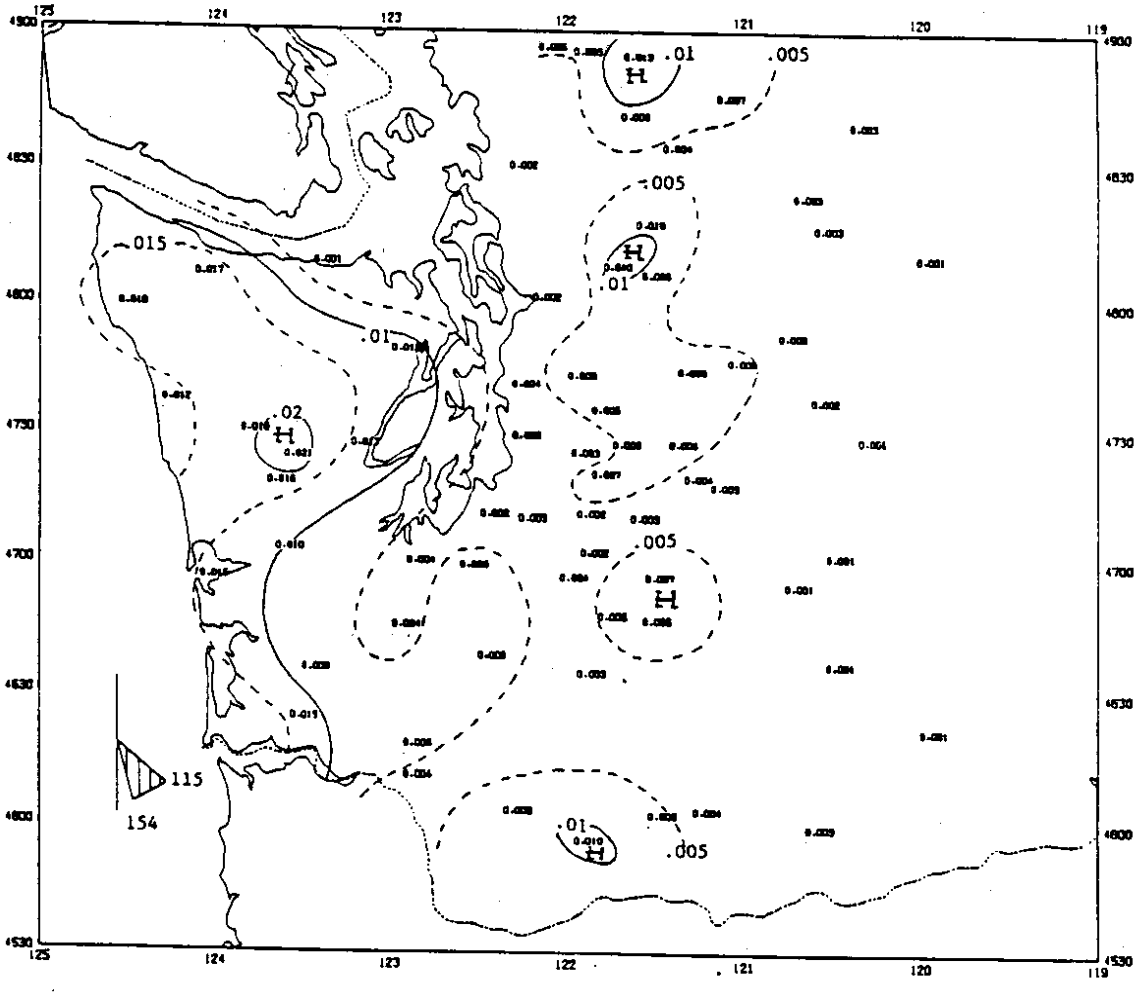

Figure B.1c Mean hourly precipitation pattern map corresponding to the time period during which the surface wind at Hoquiam blew from the SE. Precipitation rates are based on 1390 hours of data. Symbols and contour intervals as in Figure B.1a.

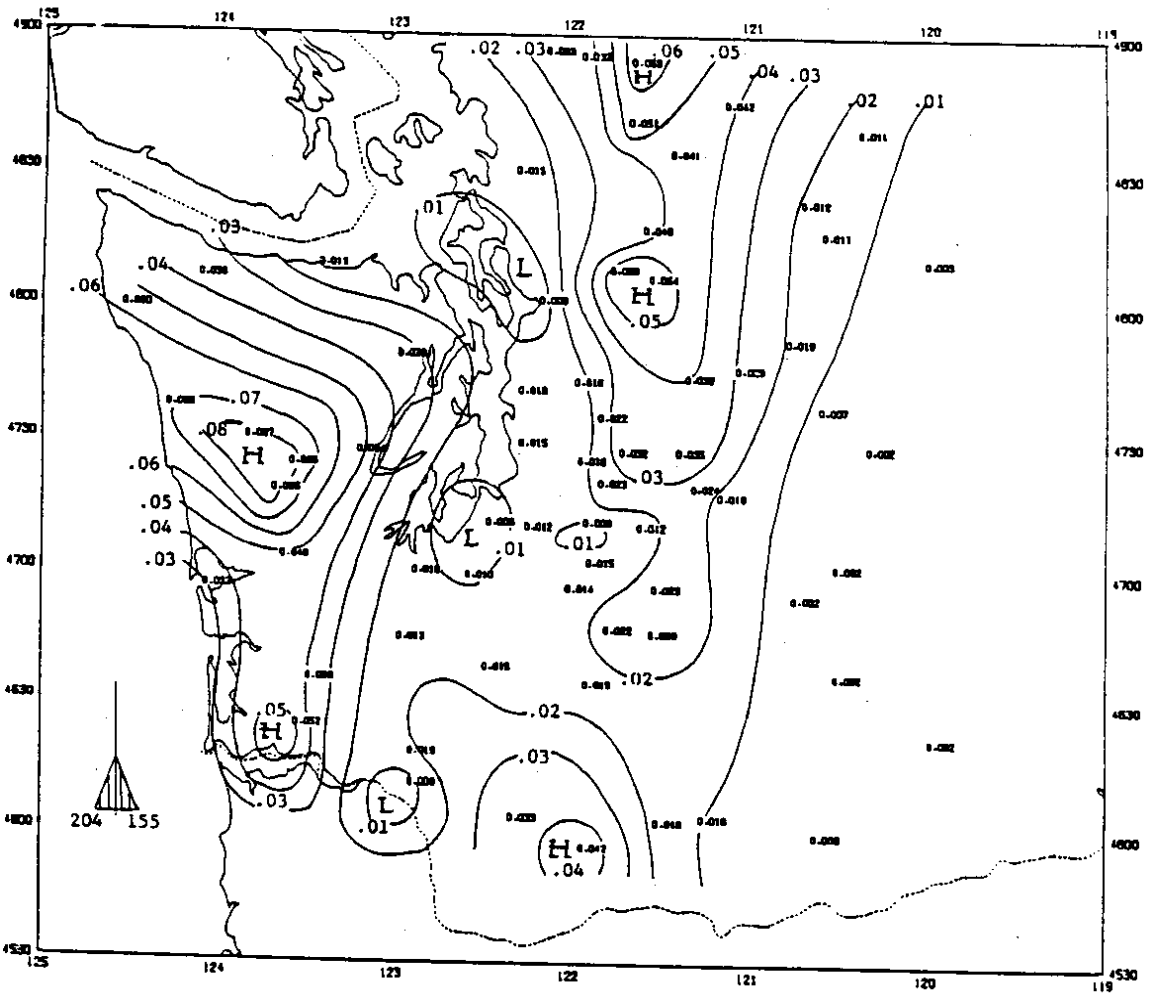

Figure B.1d Mean hourly precipitation pattern map corresponding to the time period during which the surface wind at Hoquiam blew from the S. Precipitation rates are based on 850 hours of data. Symbols and contour intervals as in Figure B.1a.

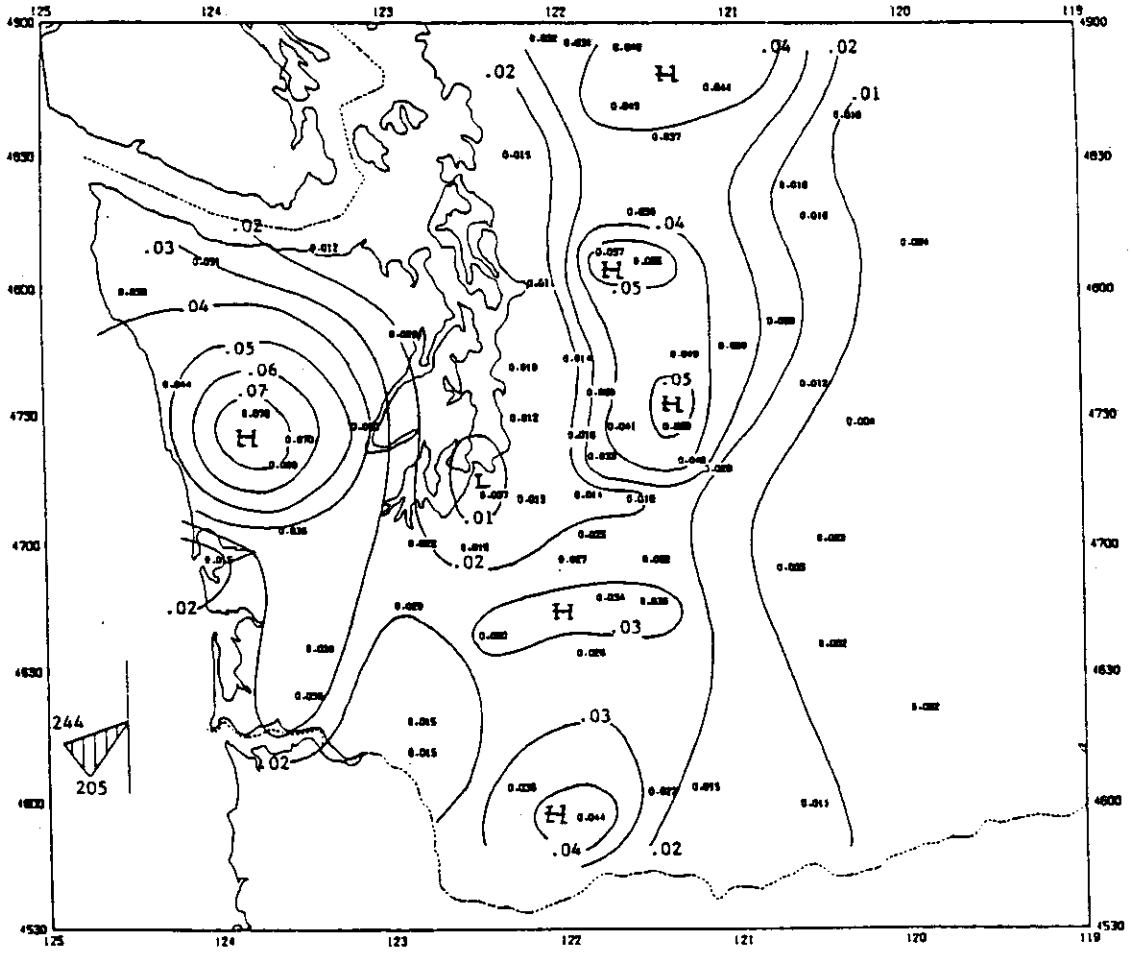

Figure B.1e Mean hourly precipitation pattern map corresponding to the time period during which the surface wind at Hoquiam blew from the SW. Precipitation rates are based on 1207 hours of data. Symbols and contour intervals as in Figure B.1a.

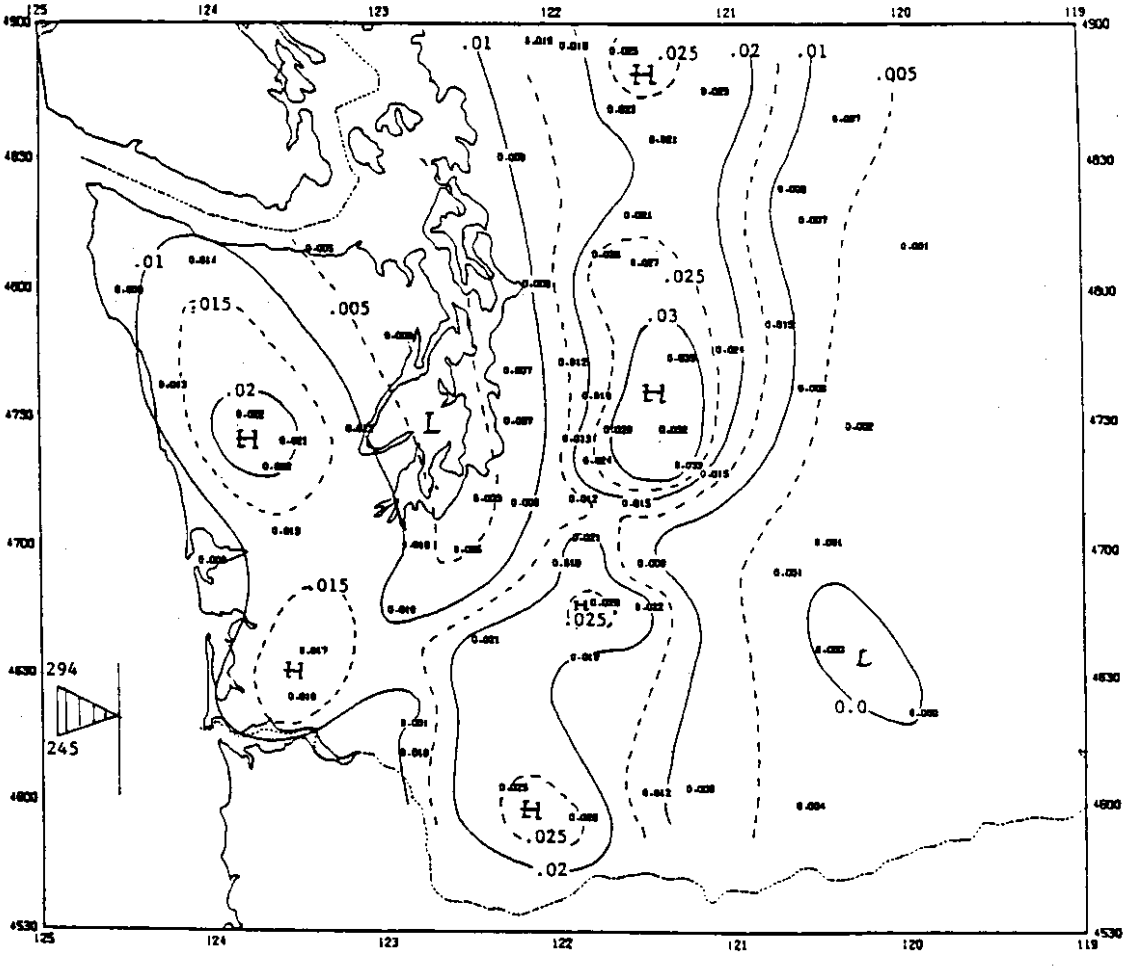

Figure B.1f Mean hourly precipitation pattern map corresponding to the time period during which the surface wind at Hoquiam blew from the W. Precipitation rates are based on 1455 hours of data. Symbols and contour intervals as in Figure B.1a.

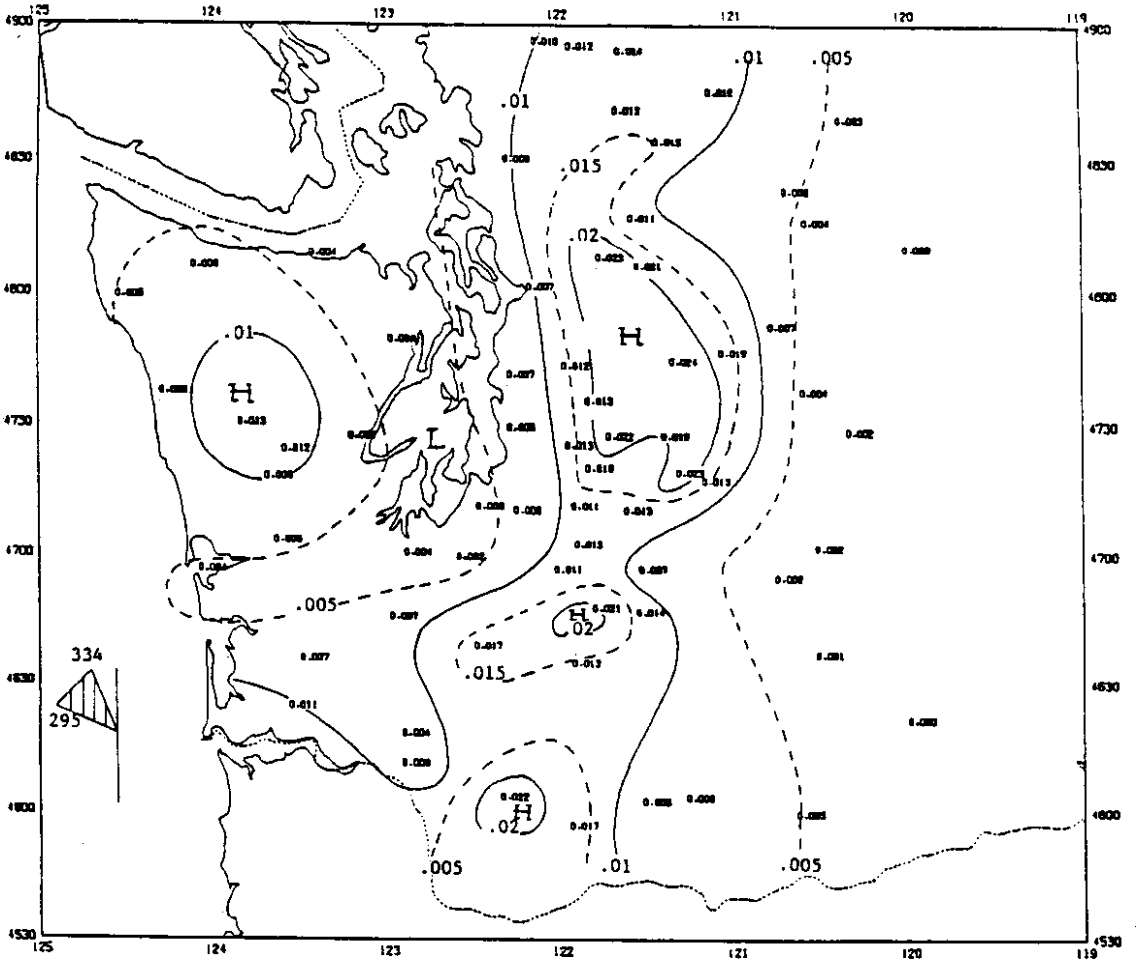

Figure 3.1g Mean hourly precipitation pattern map corresponding to the time period during which the surface wind at Hoquiam blew from the NW. Precipitation rates are based on 859 hours of data. Symbols and contour intervals as in Figure 3.1a.

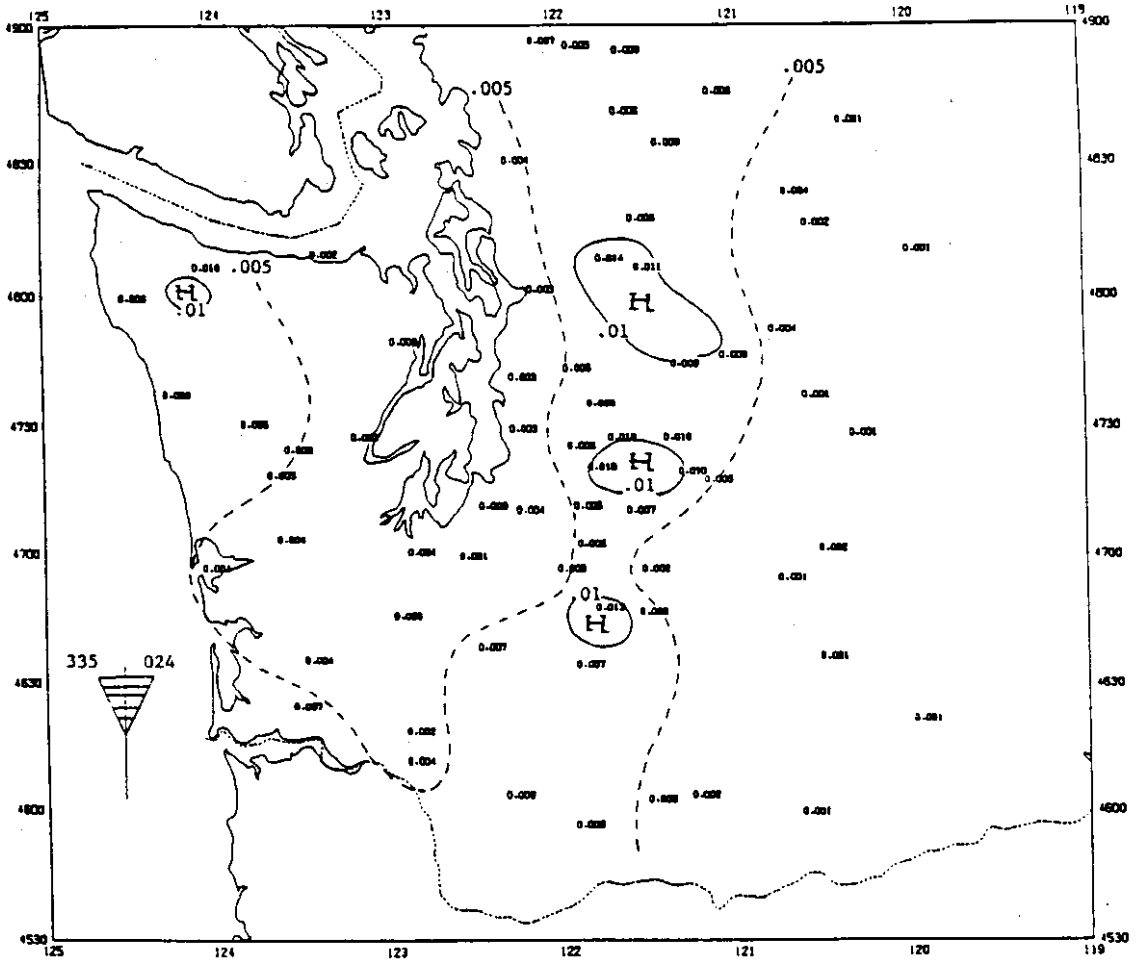

Figure B.1h Mean hourly precipitation pattern map corresponding to the time period during which the surface wind at Hoquiam blew from the N. Precipitation rates are based on 1205 hours of data. Symbols and contour intervals as in Figure B.1a.

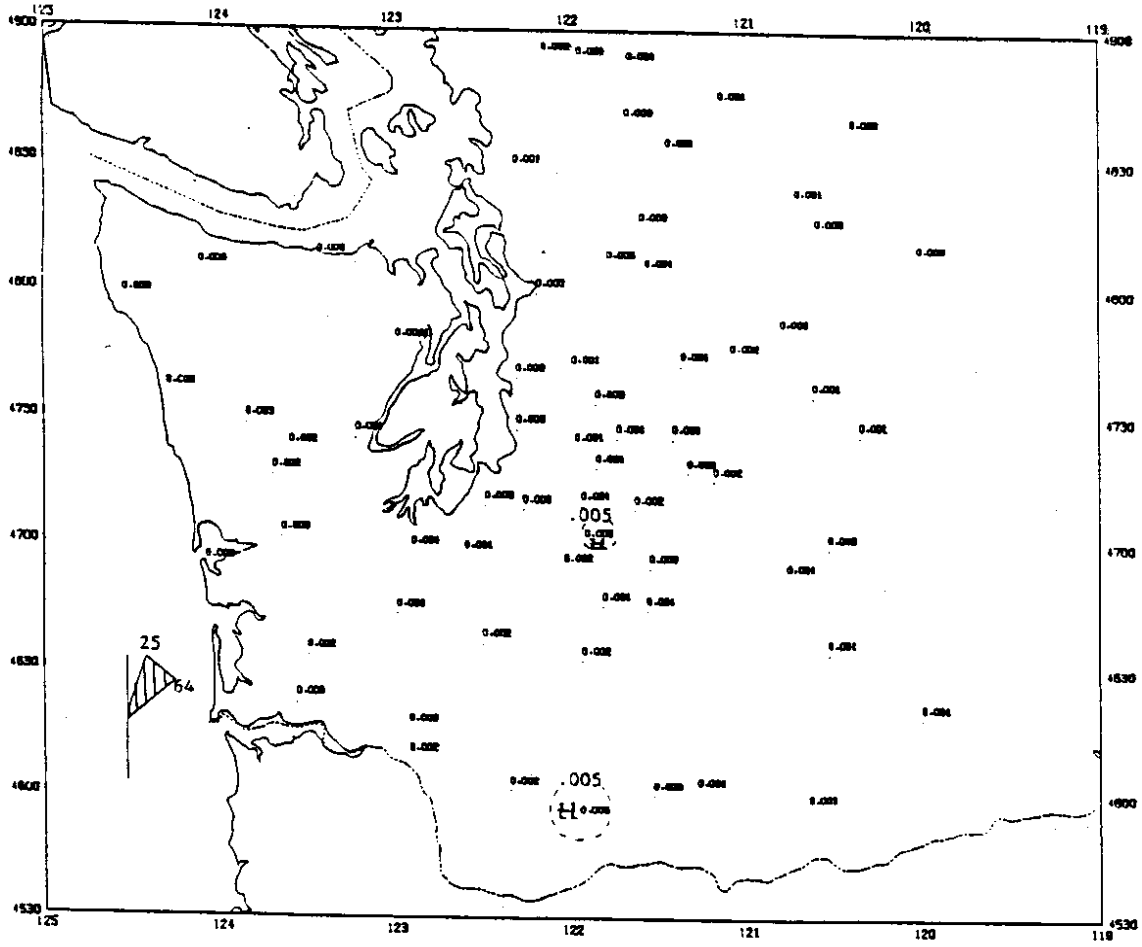

Figure B.2a Mean hourly precipitation pattern map corresponding to the time period during which the 850 mb level wind at Quillayute blew from the NE. The wind direction is shown by the shaded region of the compass. Precipitation rates are based on 230 hours of data. The solid line contour interval is .01 inches of water equivalent. Dashed line contours are drawn for .005 inch intervals.

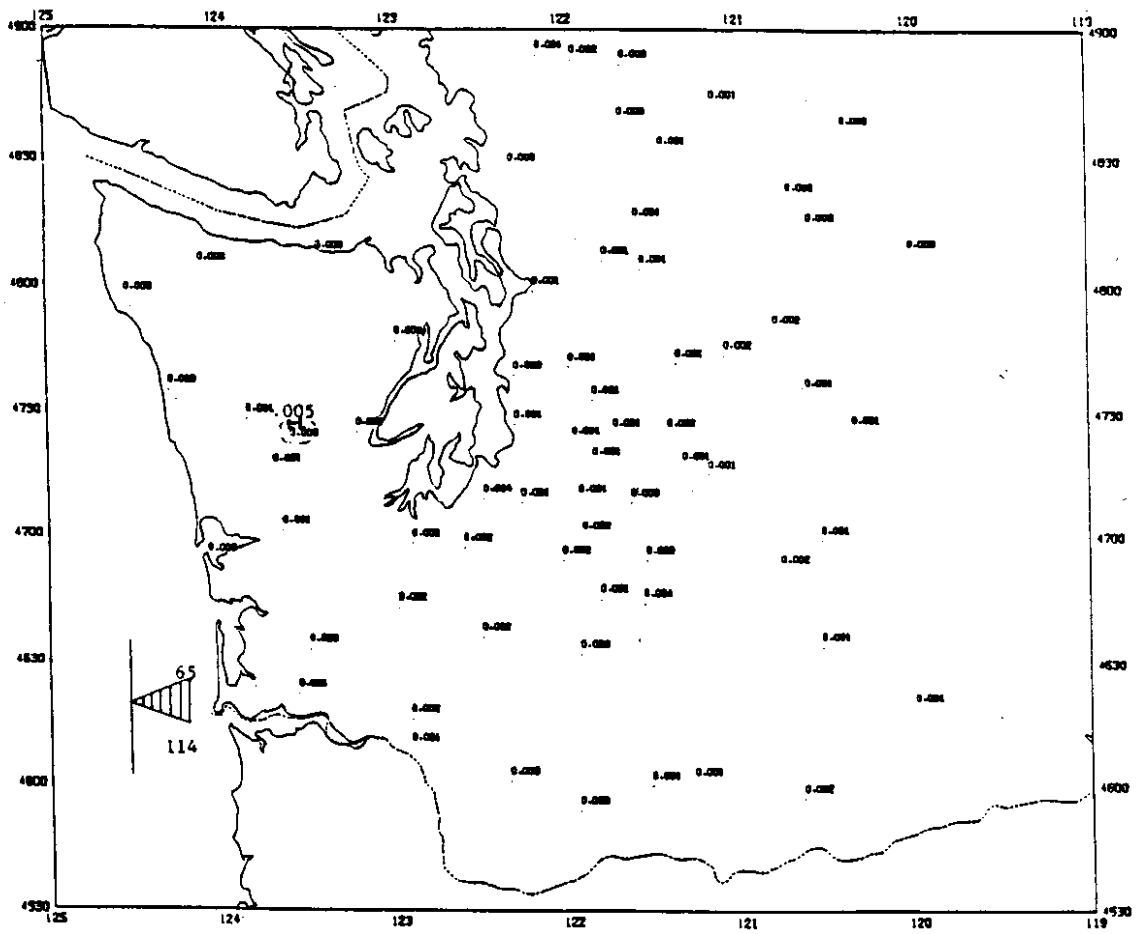

Figure B.2b Mean hourly precipitation pattern map corresponding to the time period during which the 850 mb level wind at Quillayute blew from the E. Precipitation rates are based on 355 hours of data. Symbols and contour intervals as in Figure B.2a.

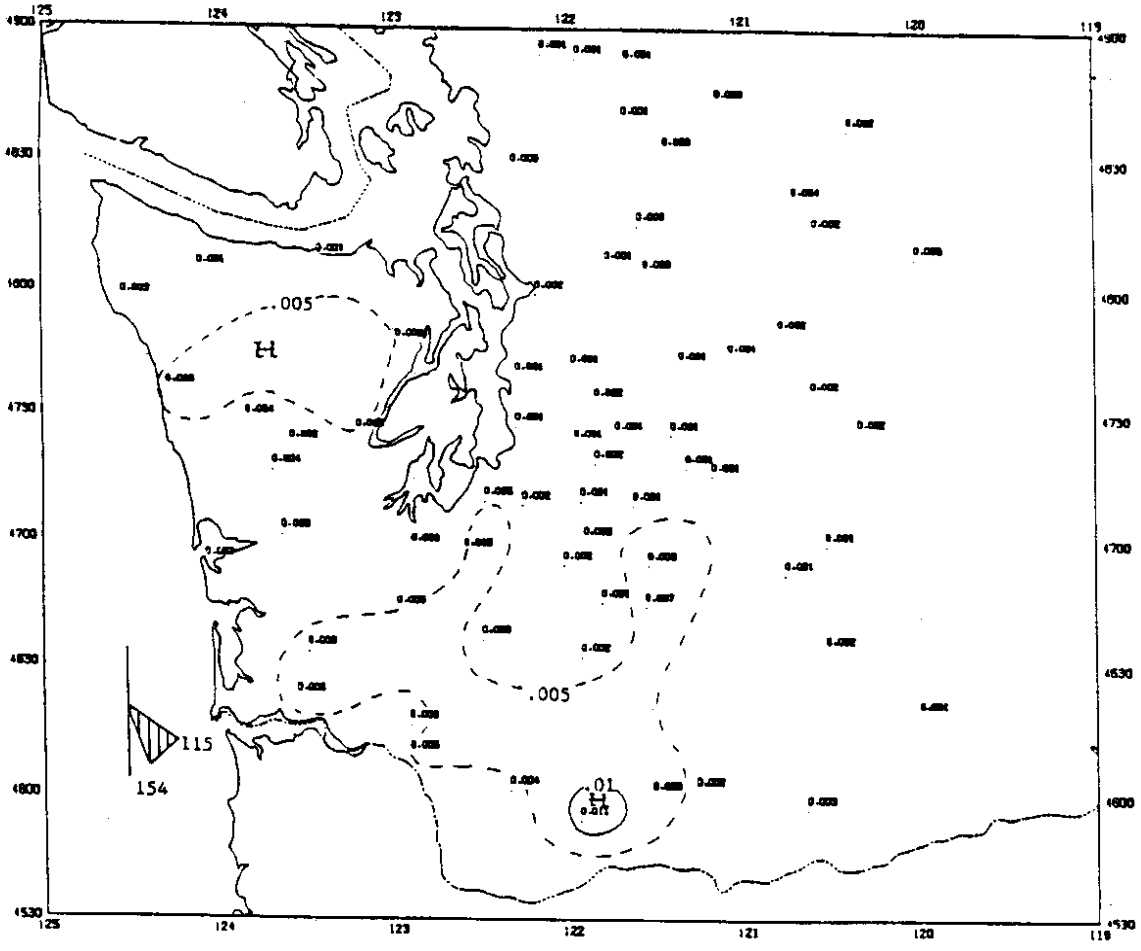

Figure B.2c Mean hourly precipitation pattern map corresponding to the time period during which the 850 mb level wind at Quillayute blew from the SE. Precipitation rates are based on 350 hours of data. Symbols and contour intervals as in Figure B.2a.

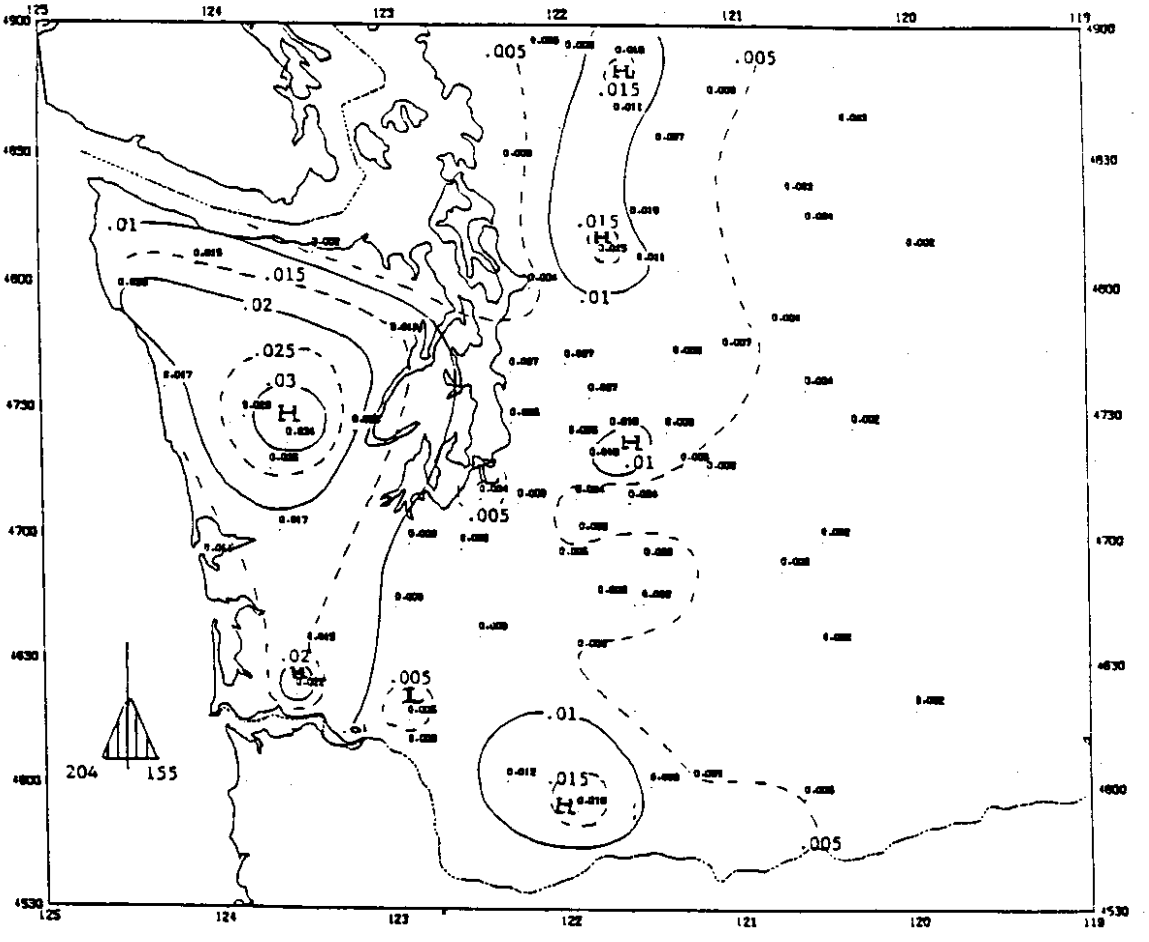

Figure B.2d Mean hourly precipitation pattern map corresponding to the time period during which the 850 mb level wind at Quillayute blew from the S. Precipitation rates are based on 3274 hours of data. Symbols and contour intervals as in Figure B.2a.

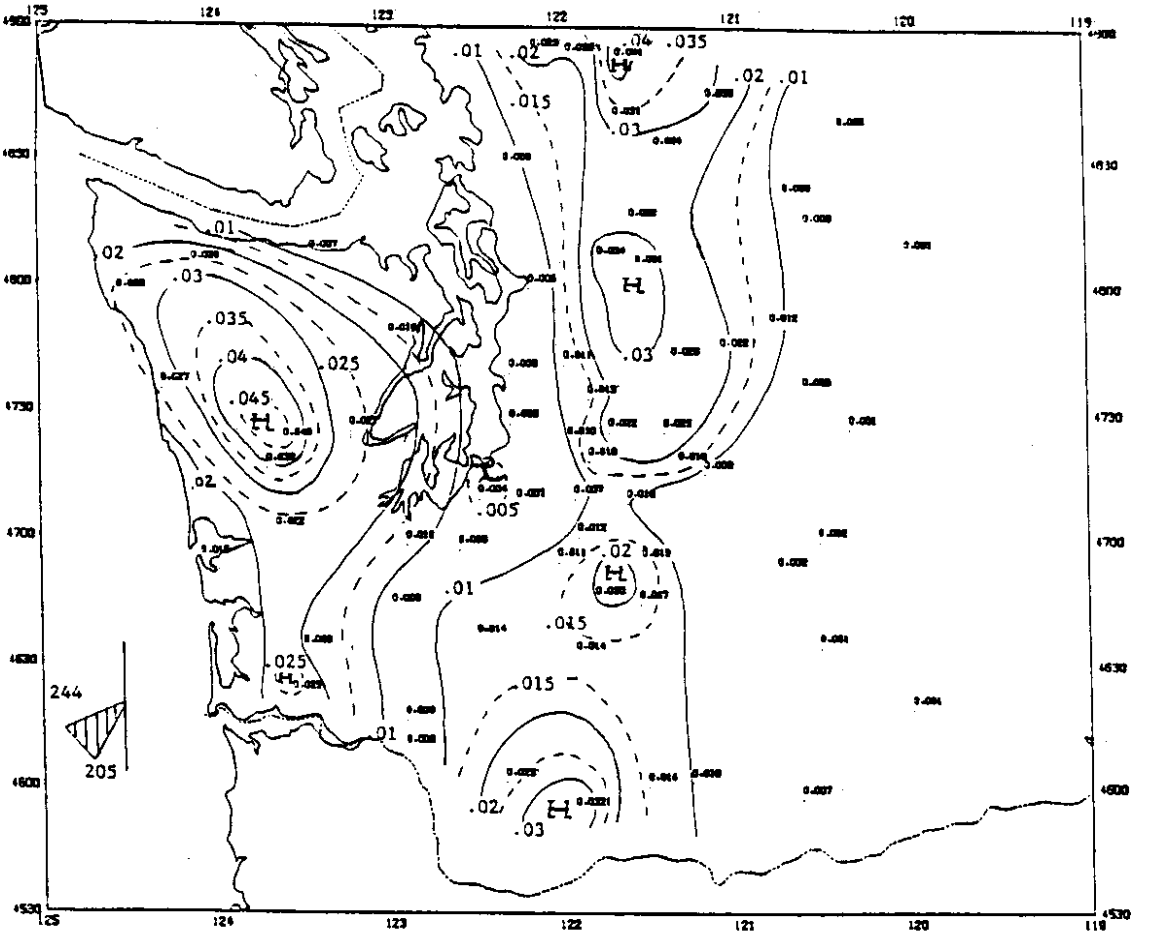

Figure B.2e Mean hourly precipitation pattern map corresponding to the time period during which the 850 mb level wind at Quillayute blew from the SW. Precipitation rates are based on 1577 hours of data. Symbols and contour intervals as in Figure B.2a.

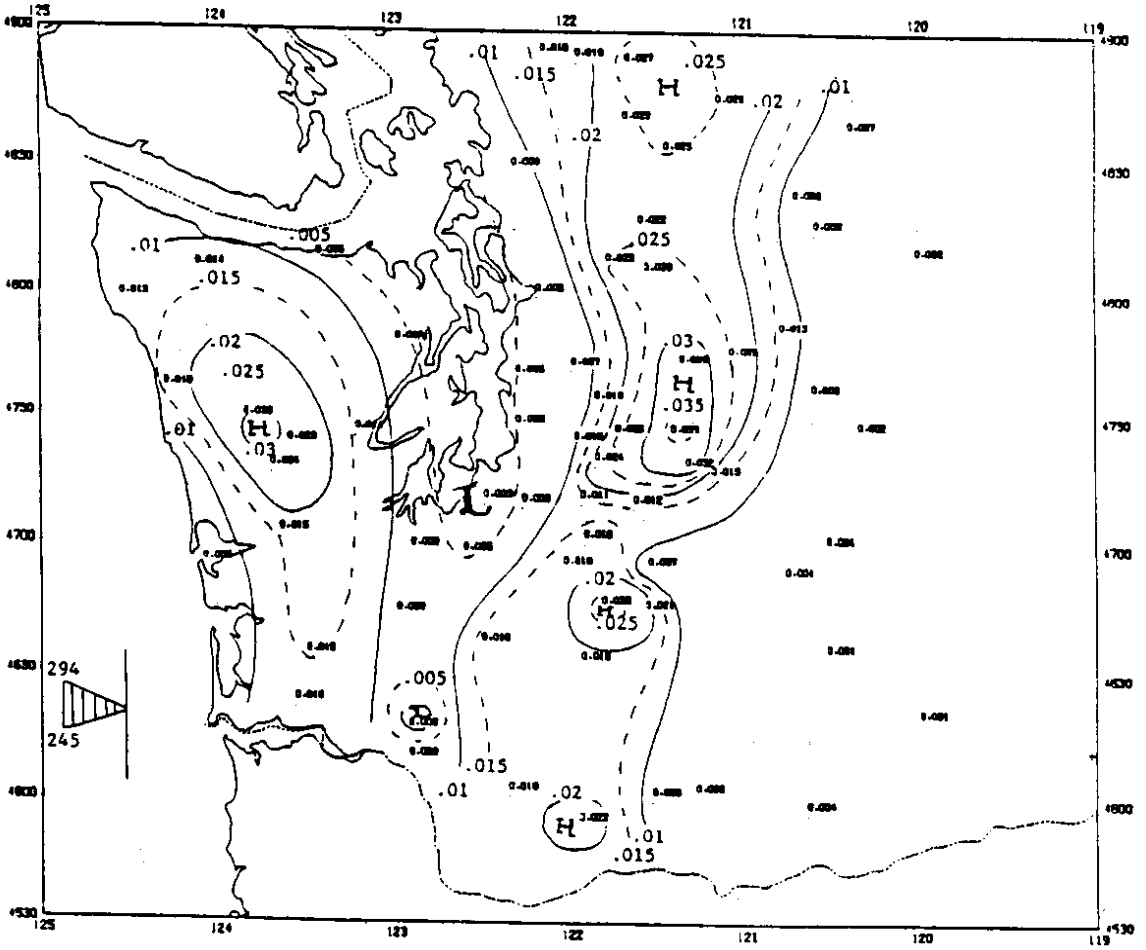

Figure B.2f Mean hourly precipitation pattern map corresponding to the time period during which the 850 mb level wind at Quillayute blew from the W. Precipitation rates are based on 1677 hours of data. Symbols and contour intervals as in Figure B.2a.

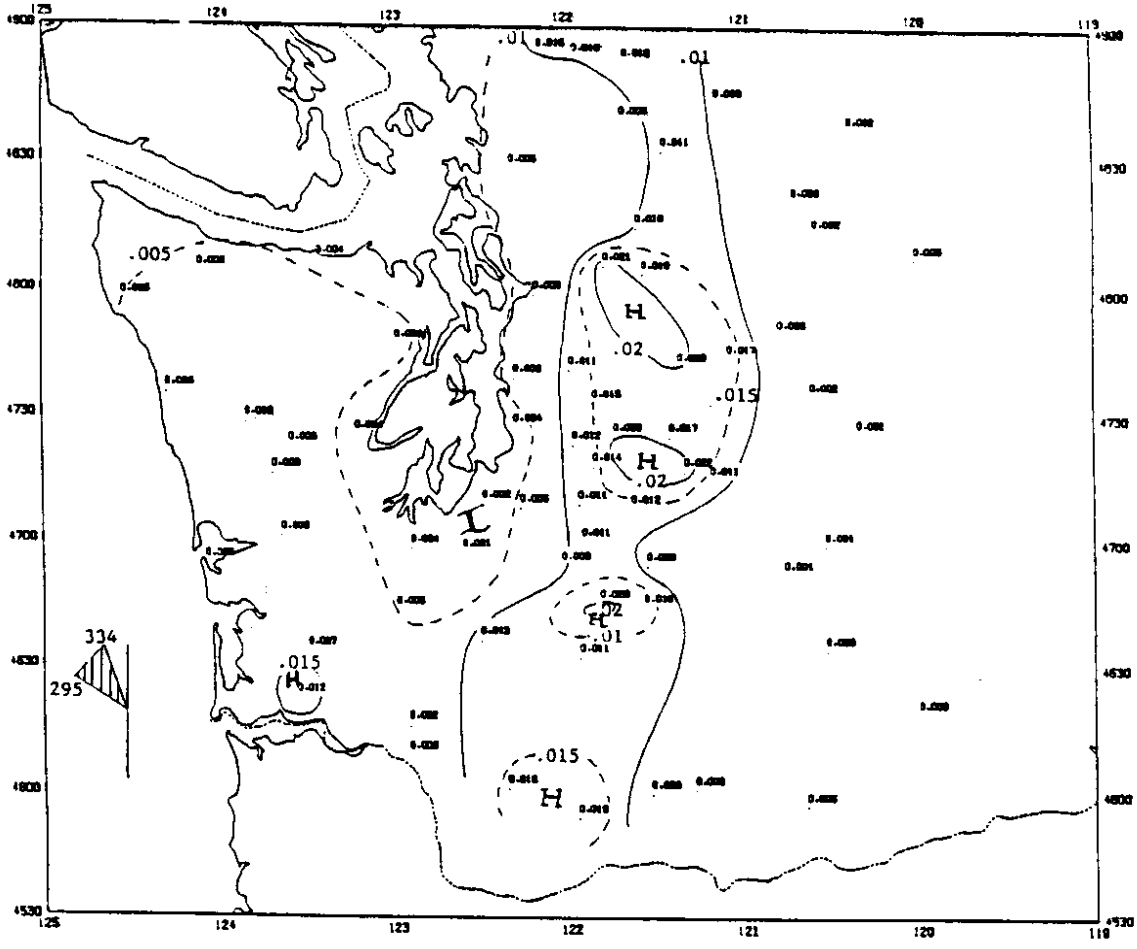

Figure B.2g Mean hourly precipitation pattern map corresponding to the time period during which the 850 mb level wind at Quillayute blew from the NW. Precipitation rates are based on 751 hours of data. Symbols and contour intervals as in Figure B.2a.

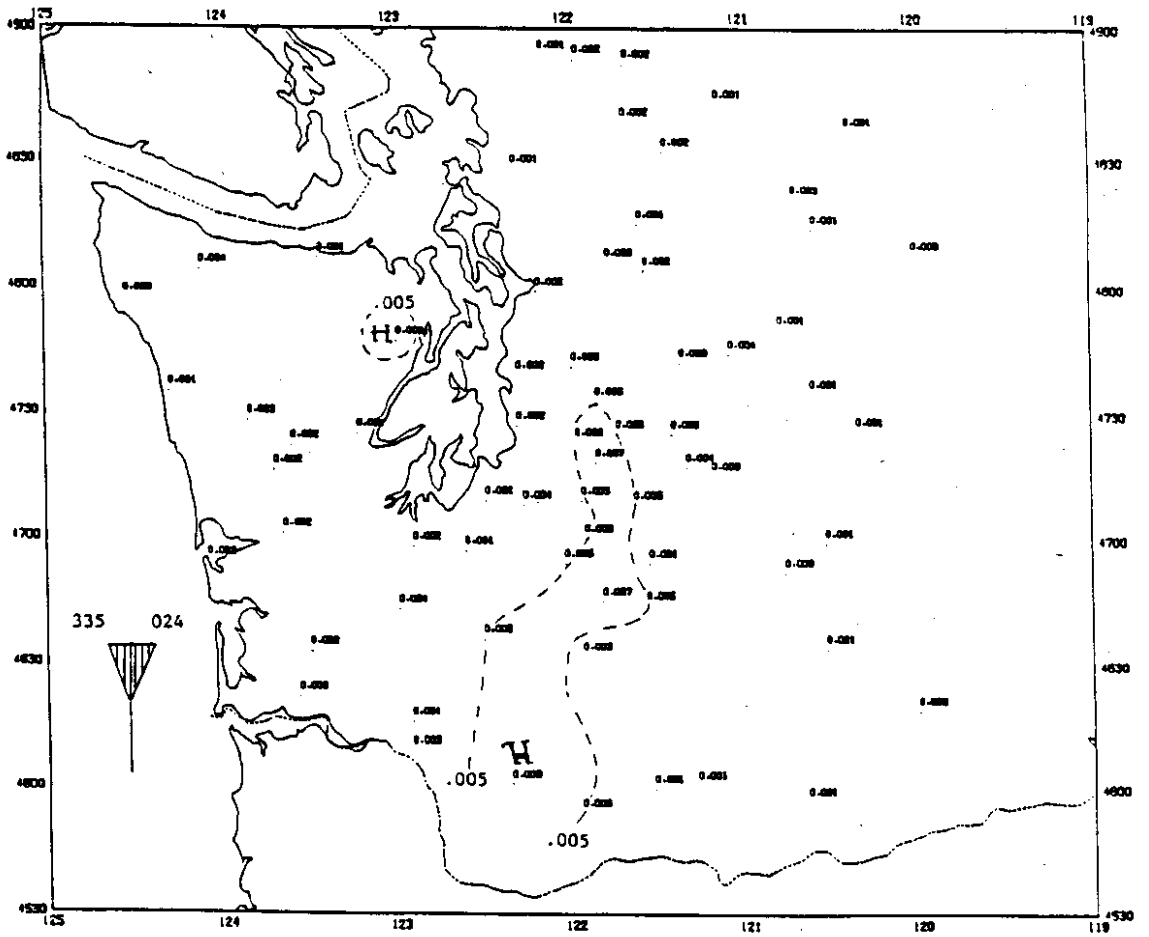

Figure B.2h Mean hourly precipitation pattern map corresponding to the time period during which the 850 mb level wind at Quillayute blew from the N. Precipitation rates are based on 664 hours of data. Symbols and contour intervals as in Figure B.2a.

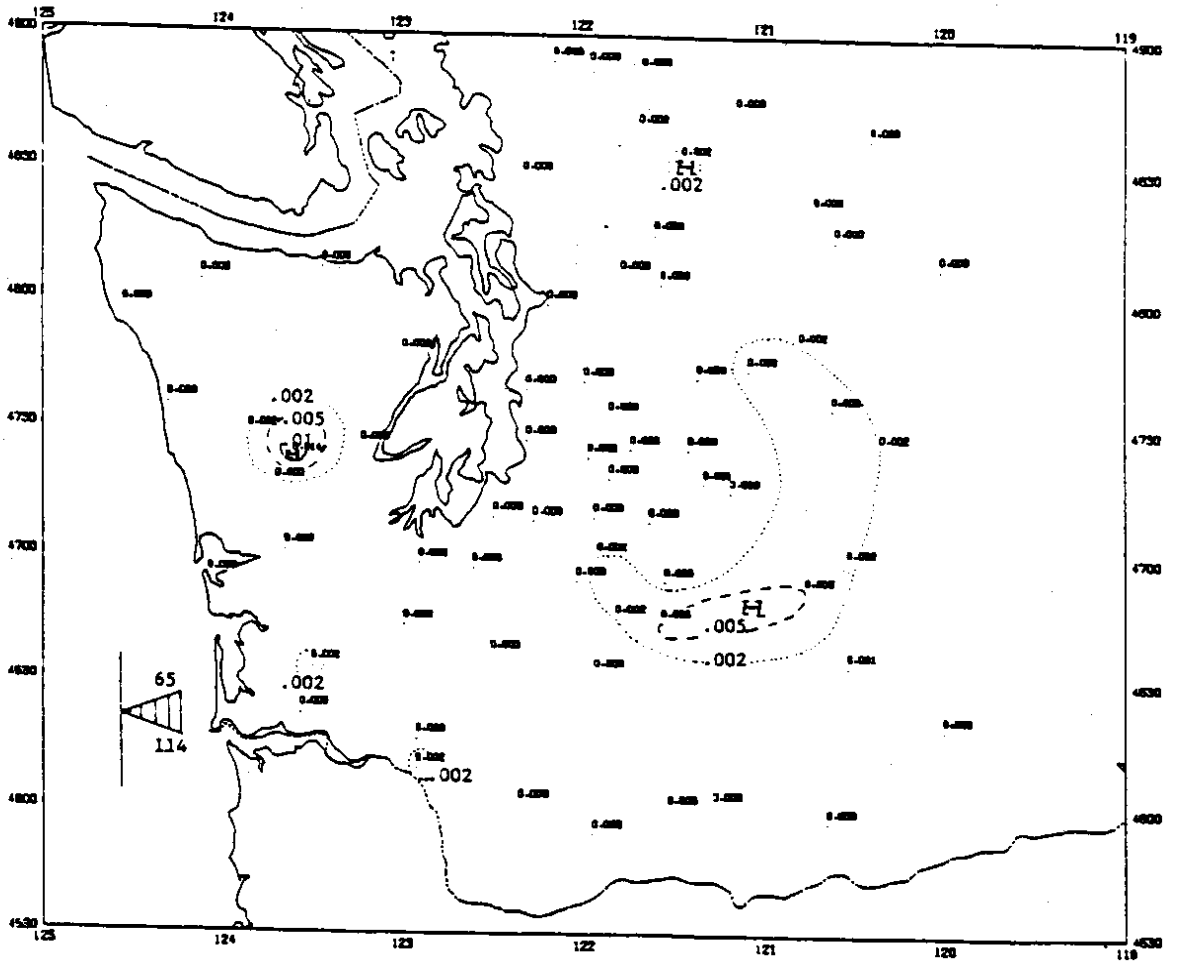

Figure B.3.a. Mean hourly precipitation pattern map corresponding to the time period during which the surface wind at Hoquiam blew 15 kts or greater from the E. The wind direction is shown by the shaded region of the compass. Precipitation rates are based on 66 hours of data. The solid line contour interval is .01 inches of water equivalent. Dashed line contours are drawn for .005 inch intervals. Dotted contours are drawn at .002 inches of water equivalent.

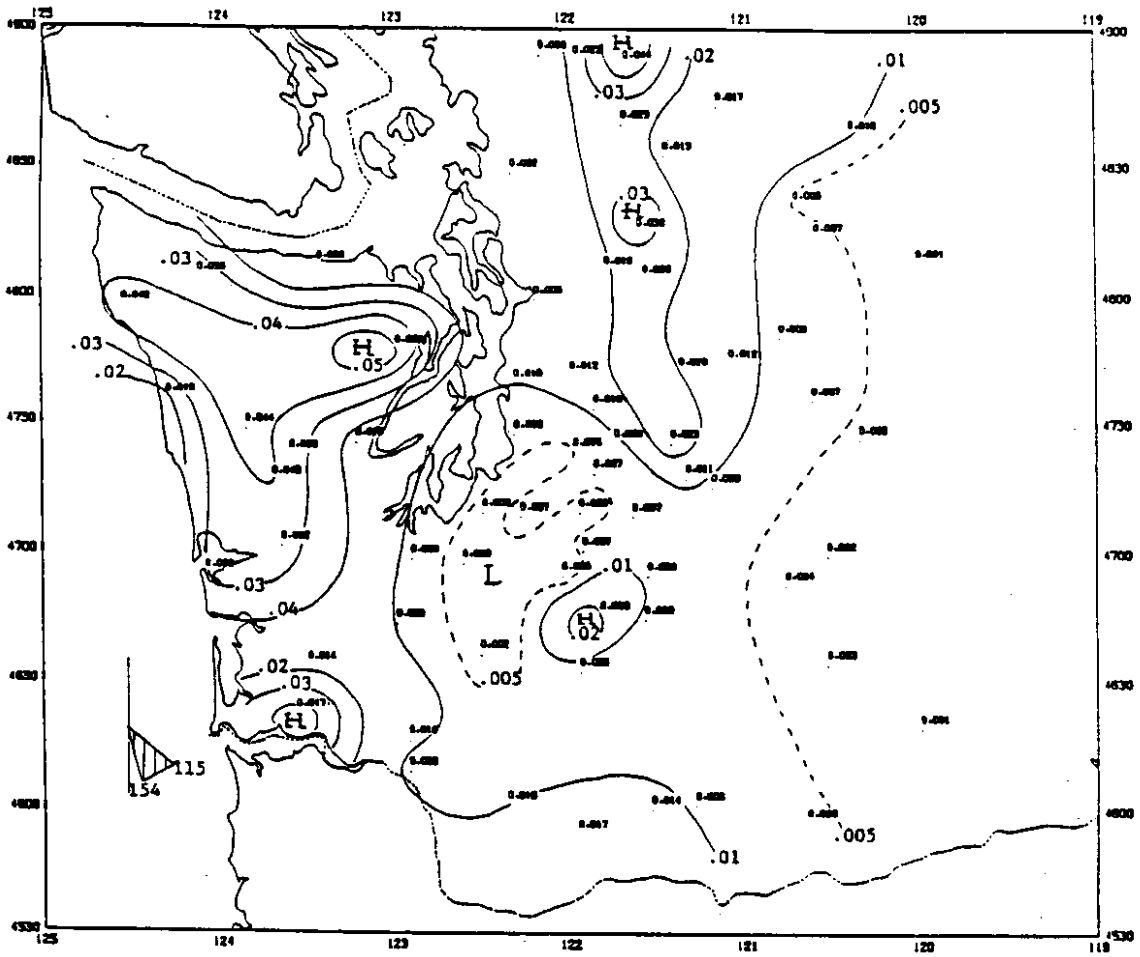

Figure B.3.b. Mean hourly precipitation pattern map corresponding to the time period during which the surface wind at Hoquiam blew 15 kts or greater from the SE. Precipitation rates are based on 102 hours of data. Symbols and contour intervals as in Figure B.3.a.

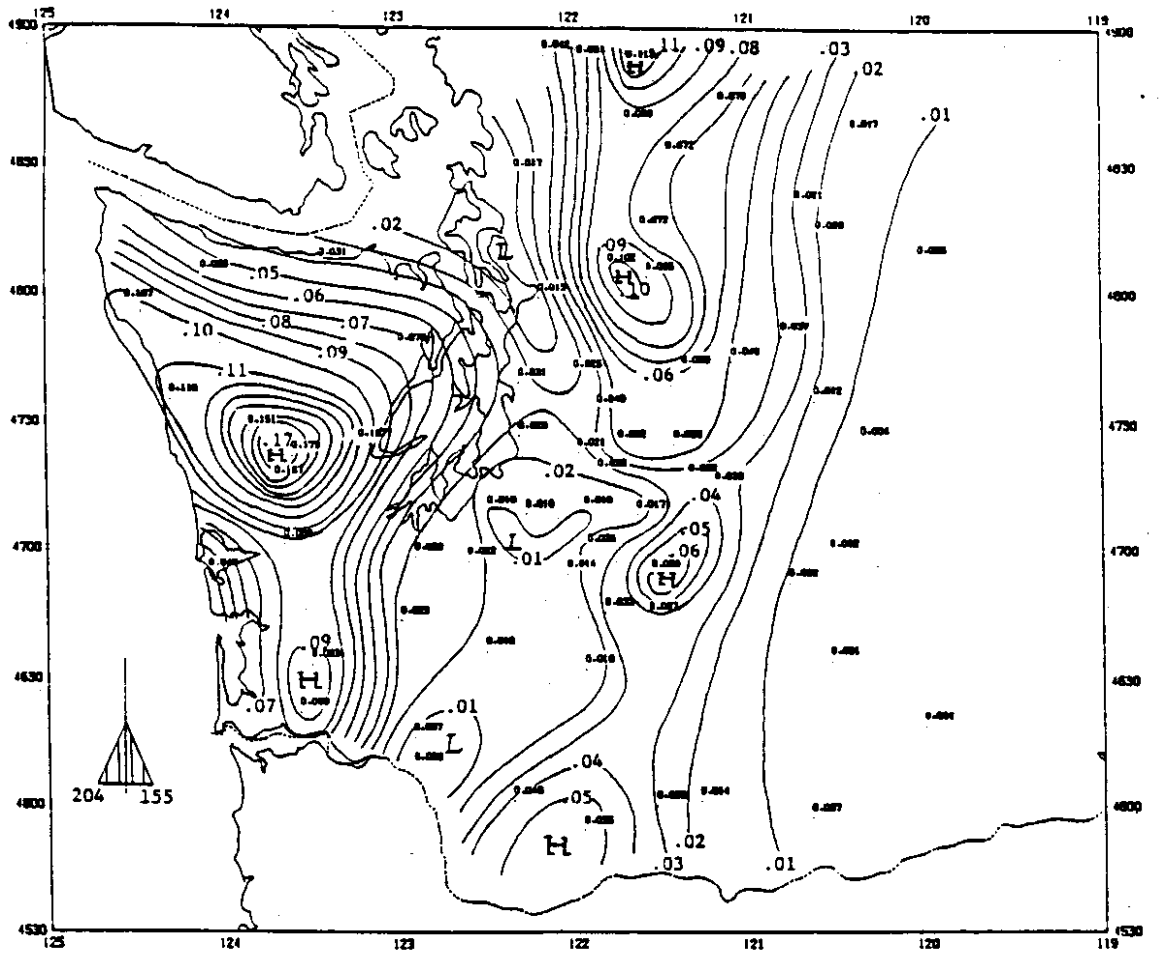

Figure B.3.c. Mean hourly precipitation pattern map corresponding to the time period during which the surface wind at Hoquiam blew 15 kts or greater from the S. Precipitation rates are based on 257 hours of data. Symbols and contour intervals as in Figure B.3.a.

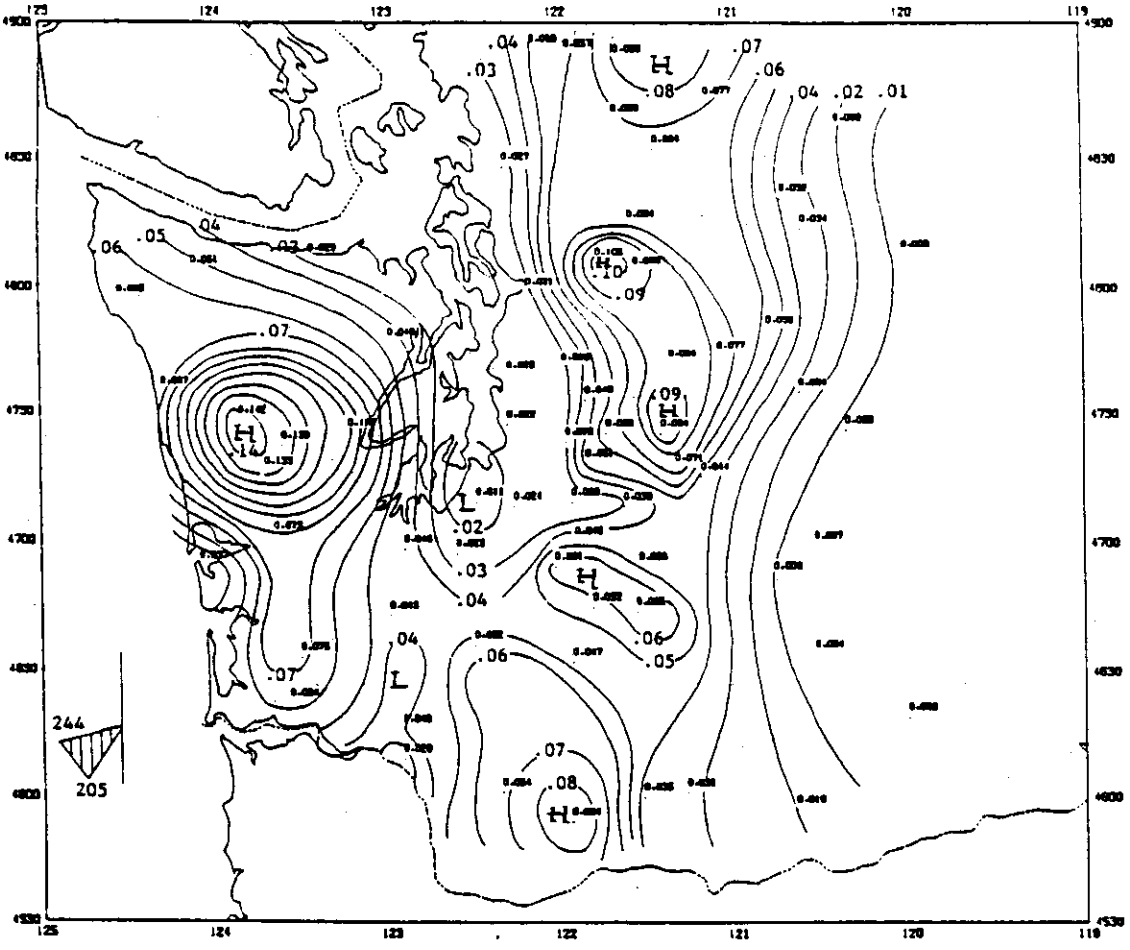

Figure B.3.d. Mean hourly precipitation pattern map corresponding to the time period during which the surface wind at Hoquiam blew 15 kts or greater from the SW. Precipitation rates are based on 386 hours of data. Symbols and contour intervals as in Figure B.3.a.

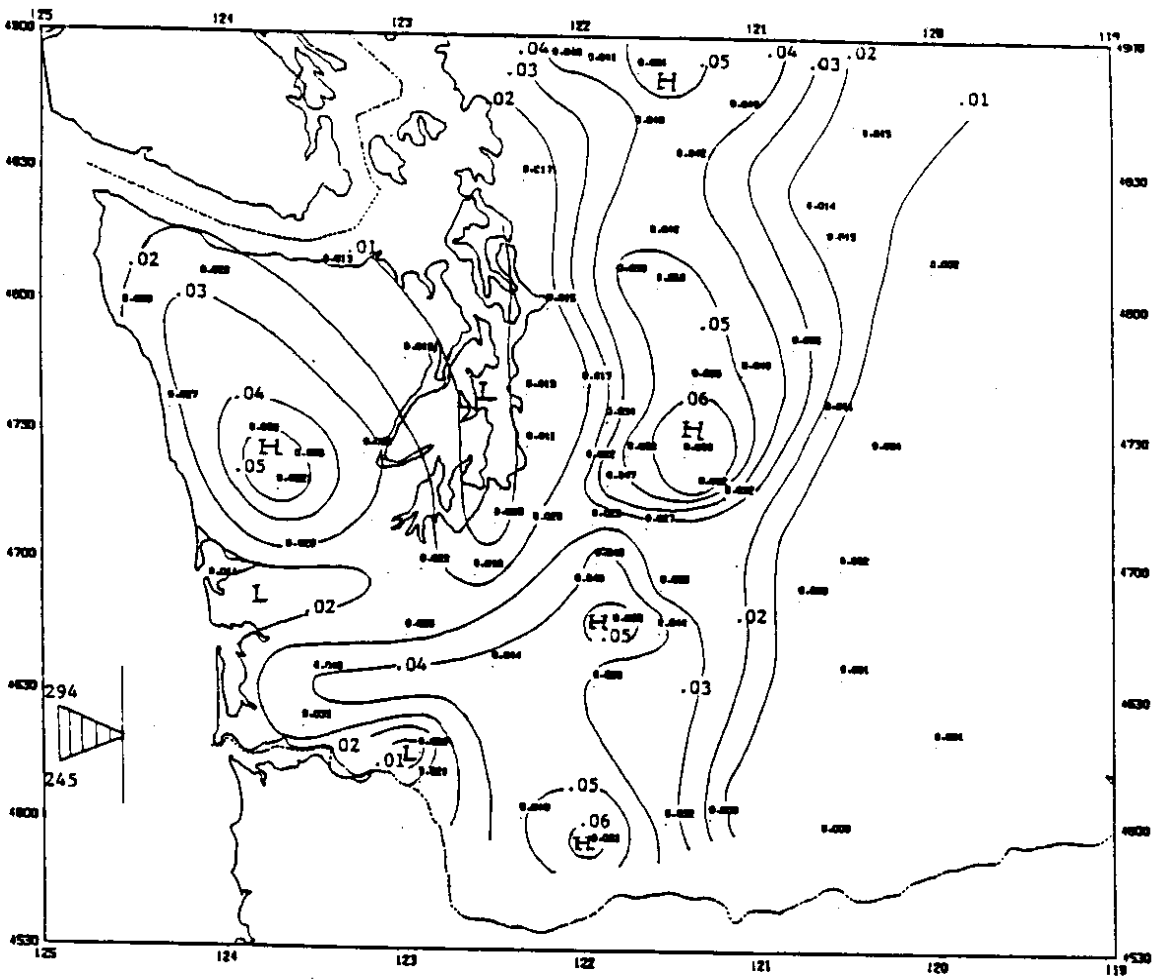

Figure B.3.e. Mean hourly precipitation pattern map corresponding to the time period during which the surface wind at Hoquiam blew 15 kts or greater from the W. Precipitation rates are based on 308 hours of data. Symbols and contour intervals as in Figure B.3.a.

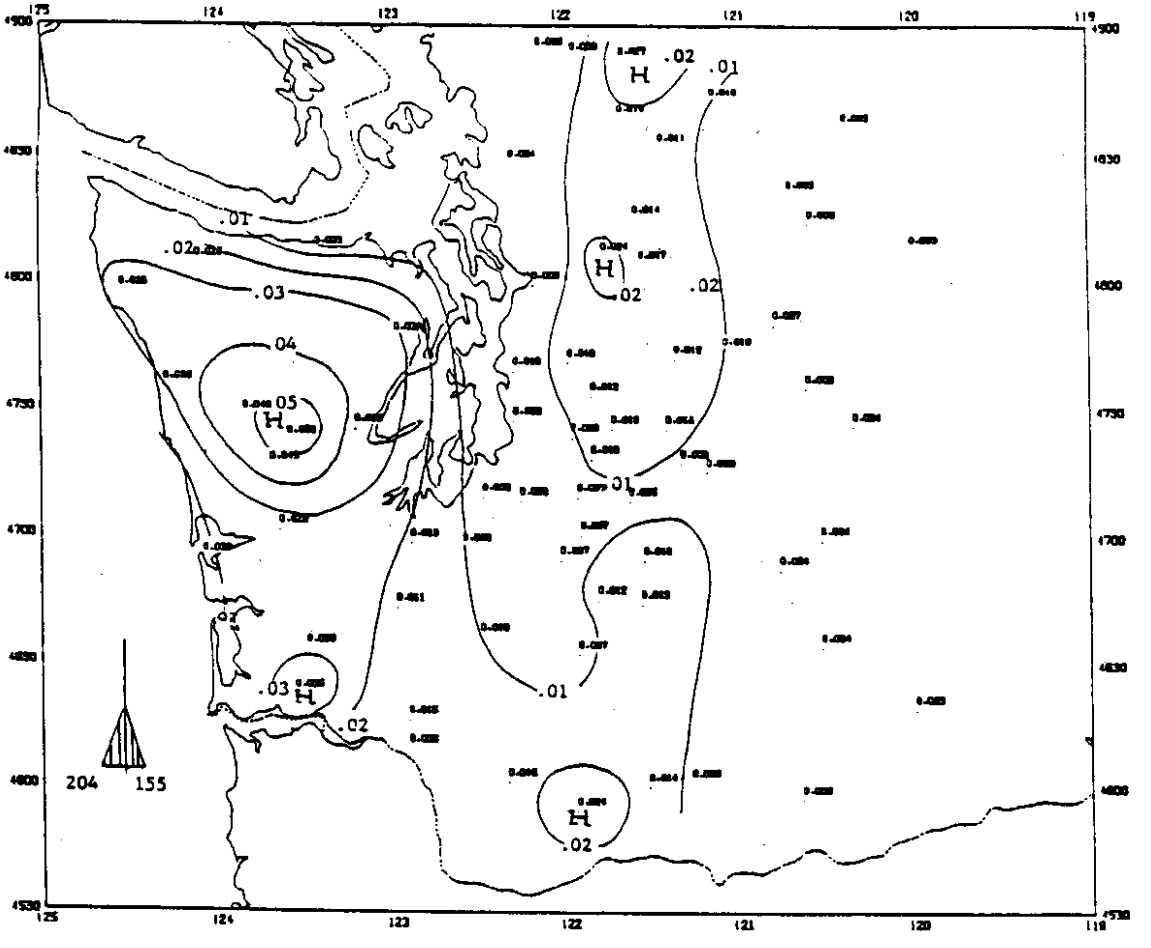

Figure B.4.a. Mean hourly precipitation pattern map corresponding to the time period during which the 850 mb level wind at Quillayute blew 25 kts or greater from the S. The wind direction is shown by the shaded region of the compass. Precipitation rates are based on 1367 hours of data. The solid line contour interval is .01 inches of water equivalent. Dashed line contours are drawn for .005 inch intervals.

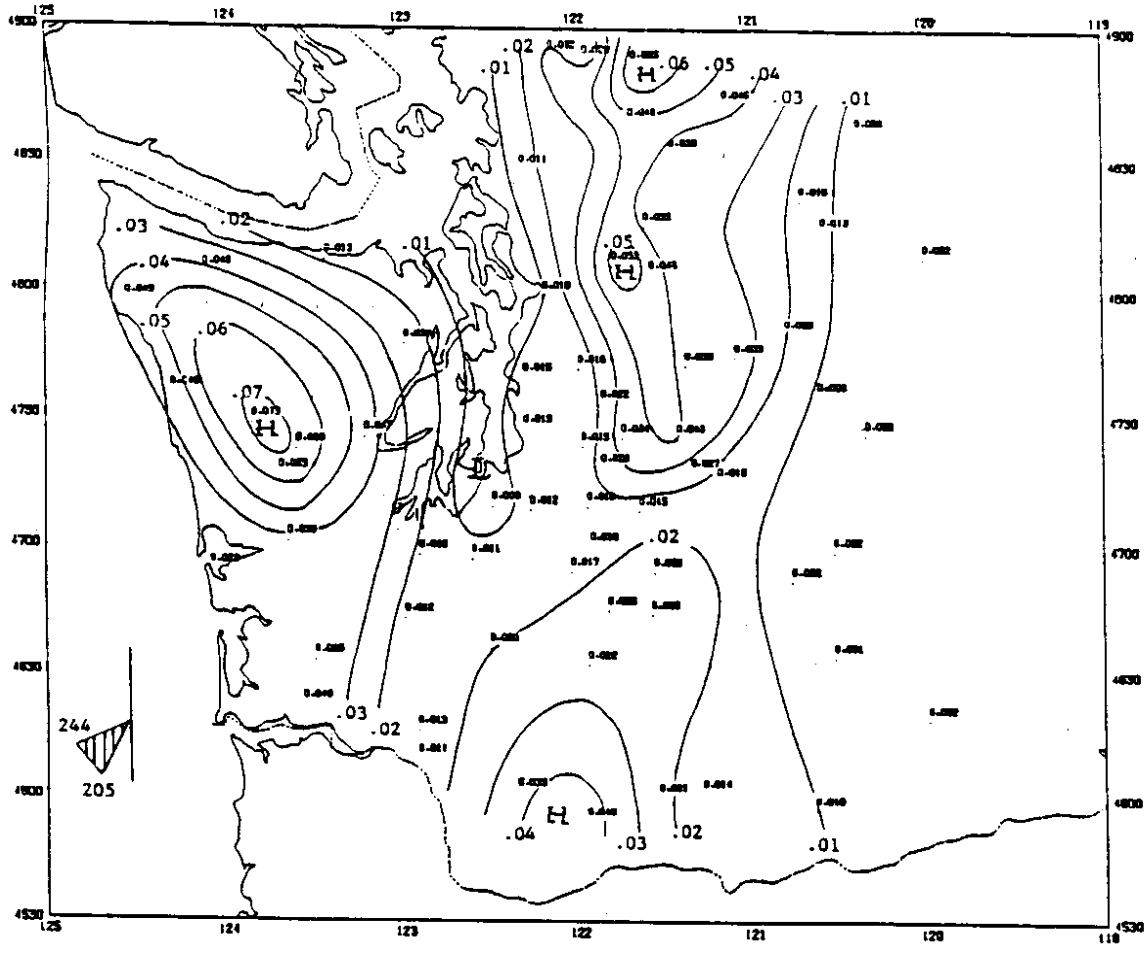

Figure B.4.b. Mean hourly precipitation pattern map corresponding to the time period during which the 850 mb level wind at Quillayute blew 25 kts or greater from the SW. Precipitation rates are based on 810 hours of data. Symbols and contour intervals as in Figure B.4.a.

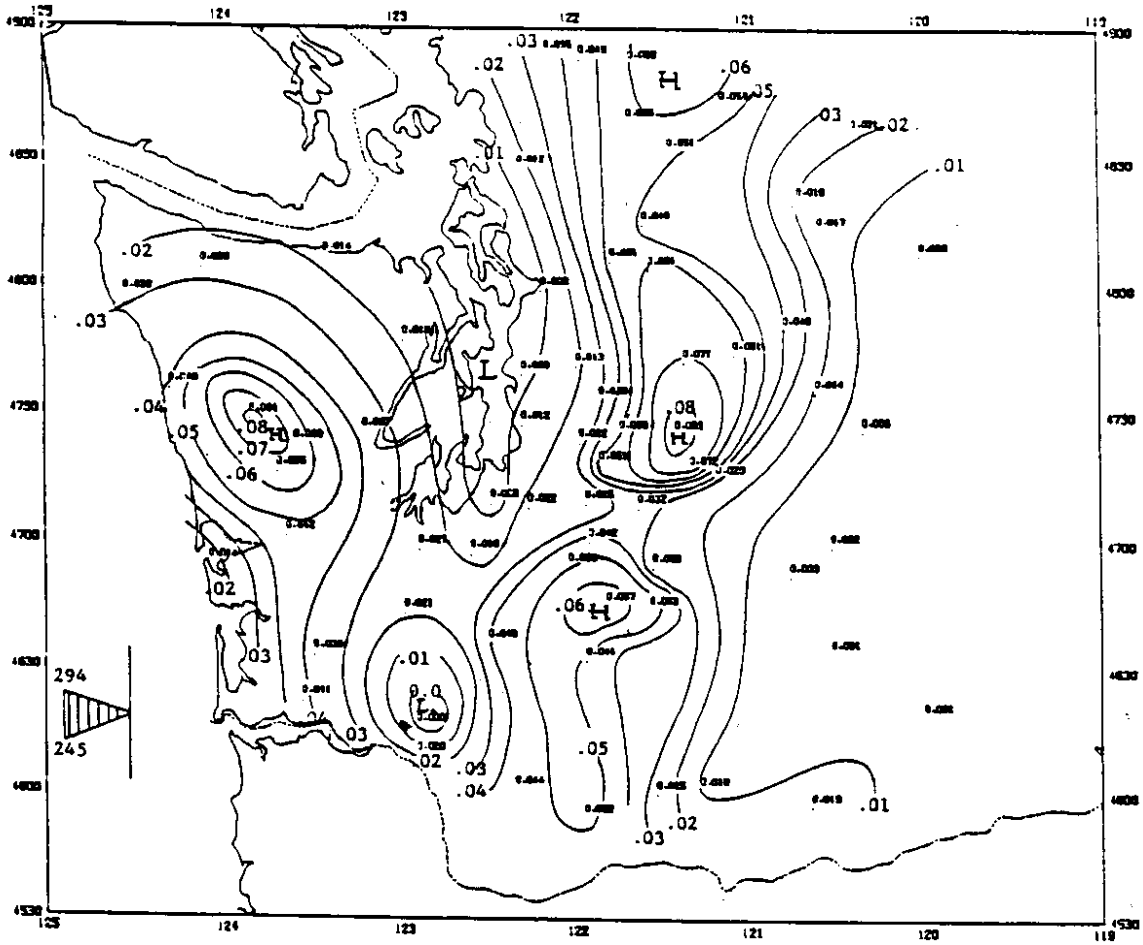

Figure B.4.c. Mean hourly precipitation pattern map corresponding to the time period during which the 850 mb level wind at Quillayute blew 25 kts or greater from the W. Precipitation rates are based on 438 hours of data. Symbols and contour intervals as in Figure B.4.a.

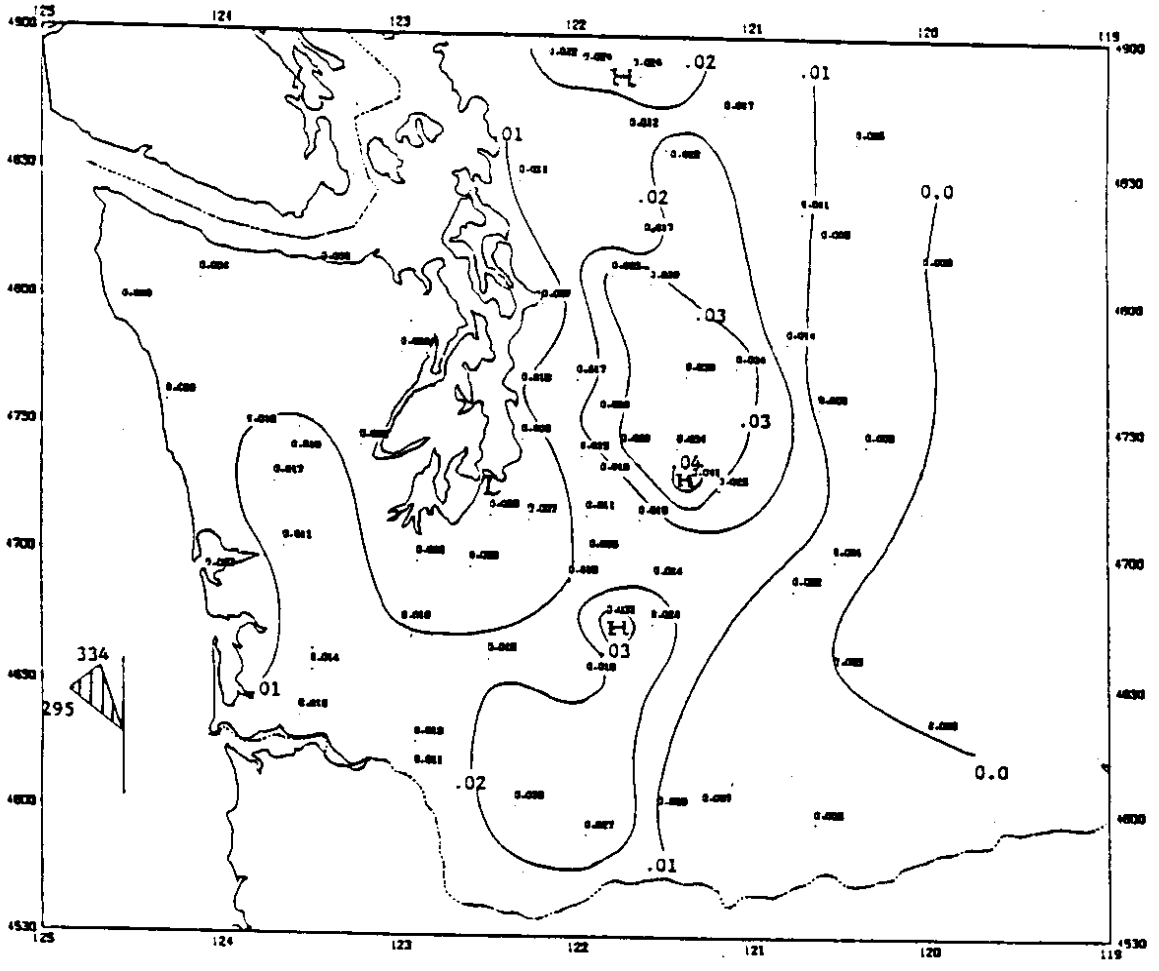

Figure B.4.d. Mean hourly precipitation pattern map corresponding to the time period during which the 850 mb level wind at Quillayute blew 25 kts or greater from the NW. Precipitation rates are based on 223 hours of data. Symbols and contour intervals as in Figure B.4.a.

APPENDIX C: TOPOGRAPHY USED FOR PRECIPITATION MODEL

The smoothed topography shown in Figure 2.3 is based on terrain data from the National Center for Atmospheric Research (NCAR). The original point data, recorded at 30 second intervals, is averaged to produce a 75 by 74 point grid that extends from 45-50 N latitude and 119-126.4 W longitude. The resolution in the east-west direction is 7511 m and in the north-south direction is 7412 m.